UNIVERSITY OF CALIFORNIA
RIVERSIDE

Air Pollution Research in SoCal - From Mobile Laboratory Atmospheric Contaminant Measurements to *In-Vivo* Health Investigations Using a Newly Constructed Environmental Chamber

A Dissertation submitted in partial satisfaction
of the requirements for the degree of

Doctor of Philosophy

in

Chemical & Environmental Engineering

by

Xinze Peng

March 2019

Dissertation Committee:

Dr. David Cocker, Chairperson
Dr. David Lo
Dr. Kelley Barsanti

The Dissertation of Xinze Peng is approved:

Committee Chairperson

University of California, Riverside

Acknowledgments

Dr. David Cocker has been my biggest support for the past 4 years. My thankfulness to him could not be expressed in words. I will continue to work hard and become his proudest and most successful Ph.D. student. I also want to thank my family from China for all the support. Without them, I will never make it here in the United States.

ABSTRACT OF THE DISSERTATION

Air Pollution Research in SoCal - From Mobile Laboratory Atmospheric Contaminant Measurements to *In-Vivo* Health Investigations Using a Newly Constructed Environmental Chamber

by

Xinze Peng

Doctor of Philosophy, Graduate Program in Chemical & Environmental Engineering
University of California, Riverside, March 2019
Dr. David Cocker, Chairperson

Air pollution is the presence of toxic chemicals or compounds emitted into the air at a level that poses a threat to the environment and human health. This Ph.D. thesis provides construction of two energy self-supported mobile laboratories and an environmental chamber for animal exposure experiments to target on real-time on-road measurement of atmospheric contaminants and in-depth health investigations of multiple air pollutants.

Concern has been raised that select atmospheric pollutants might adversely impact the performance of Honda's fuel cell car due to the heavy air pollution in Southern California. Ammonium (NH_4^+) and sodium (Na^+) cations may displace hydrogen ions (H^+) in the fuel cell's Proton Exchange Membrane (PEM), while SO_2 and NO_2 may react with the platinum anode. Ammonia (NH_3) may attack the cathode directly and can be a potential source of additional ammonium cations. A short-period intensive study was performed to identify transient and average exposure levels to these species in Southern California and to compare these values to the closest local air monitoring station data. We found highly

elevated NO_2 and SO_2 concentration in the industrial areas and similar concentration range for other target contaminants when comparing with available data from SCAQMD.

The negative impact of air pollution also prompts the development of health research. Most *in-vivo* health studies conducted regarding air pollutants have been either through traditional medical intranasal treatment or using a tiny chamber, which limit animal activities. In this study, we designed and tested a large, whole-body, multiple animal exposure chamber that simultaneously controls particle size distribution and PM mass concentration. We demonstrate that the chamber system provides well controlled and characterized whole animal exposures, where dosage is by inhalation of particulate matter. We found inhalation exposure to a natural fungal allergen sufficient to induce lung inflammation and surprisingly caused reductions in baseline expression of select innate immune molecules in the region of the CNS controlling respiration.

Contents

List of Figures

List of Tables

Chapter 1

Thesis Introduction

Targeting on real-time on-road measurement of atmospheric contaminants and in-depth health investigations of multiple air pollutants, this Ph.D. thesis provides construction of two energy self-supported mobile laboratories and an environmental chamber for animal exposure experiments.

Problems with energy consumption and production are related not only to global warming, but also to such environmental concerns, particularly air pollution (Dincer, 2000). Air pollution problems prompt the development of renewable energy as clean sources of energy and optimal use of these resources minimize environmental impacts and produce minimum secondary pollution (Panwar et al., 2011; Ehsani et al., 2018). Chapter 2 of this thesis presents the investigation of real-time on-road measurement of air contaminants that could potentially cause damage to a special vehicle using renewable energy-the Honda Fuel Cell Vehicles (FCV). Honda's Fuel Cell Vehicles (FCV) use hydrogen to generate electricity, which is either used to drive the vehicle or stored in an energy storage device, such as bat-

tery pack or ultracapacitors (Chan, 2007). Since fuel cells generate electricity from chemical reaction (isothermal), they do not need to burn fossil fuels like the Internal Combustion Engines (ICE) and therefore do not produce multiple pollutants. Water is the only byproduct of a hydrogen fuel cell from the FCV. While the FCV does not produce any air contaminants, concern had been raised that the serious polluted atmospheric environment in the Los Angeles area might have an adverse impact on the heart of this zero emission vehicle. Ammonium (NH_4^+) and sodium (Na^+) cations may displace hydrogen ions (H^+) in the fuel cell's Proton Exchange Membrane (PEM), while SO_2 and NO_x may react with the platinum anode. Ammonia (NH_3) may attack the cathode directly and can be a potential source of additional ammonium cations. Although the South Coast Air Quality Management District (SCAQMD) provides us the concentrations of all these pollutants (COAST, 2014), it is possible that these concentrations are considerably higher on the road. Therefore, a short-period intensive study was performed to identify transient and average exposure levels to these species on Southern California roadways and to compare these values to the closest local air monitoring station data available.

Air pollution can not only cause damage to the natural environment or even artificial products, it also continues to pose a significant threat to the environment and human health. Most in-vivo health studies conducted regarding air pollutants, including particulate matter (PM) and gas phase pollutants, have been either through traditional medical intranasal treatment or using a tiny chamber, which limit animal activities. In our study presented in Chapter 3, we designed and tested a large, whole-body, multiple animal exposure chamber with uniform dispersion and exposure stability for animal studies.

The chamber simultaneously controls particle size distribution and PM mass concentration. Two different methods were used to generate aerosol suspension through either soluble material (*Alternaria* extract), liquid particle suspension (Nanosilica solution) or dry powder (silica powder). We demonstrate that the chamber system provides well controlled and characterized whole animal exposures, where dosage is by inhalation of particulate matter.

The exciting establishment and characterization of our multi-purpose large animal exposure chamber paves the way for investigating health effects. In Chapter 4 of this thesis, our research discovered that continuous exposure to aerosolized fine (particle size < 2.5 µm) and ultrafine (particle size < 0.1 µm) particulates can trigger innate inflammatory responses in the lung and brain depending on particle composition. Most studies of manmade toxicants use inhalation exposure routes while most studies of allergens use soluble solutions administered via intranasal or injection routes. Here, we tested whether continuous inhalation exposure to aerosolized Alternaria alternata particulates (a common fungal allergen associated with asthma), would induce innate inflammatory responses in the lung and brain. By designing a new environmental chamber able to control particle size distribution and mass concentration, we continuously exposed adult mice to aerosolized ultrafine Alternaria particulates for 96 hours. Despite induction of innate immune responses in the lung, induction of innate immune responses in whole brain samples was not detected by qPCR or flow cytometry. However, exposure did trigger decreases in Arginase 1, INOS, and TNFα mRNA in the brainstem samples containing the CNS respiratory circuit (the dorsal and ventral respiratory groups, the pre-Botzinger and Botzinger complexes). Additionally, a significant decrease in the percentage of TLR2-expressing brainstem microglia

was detected by flow cytometry. Histologic analysis revealed a significant decrease in Iba1 but not GFAP immunoreactivity in both the brainstem and the hippocampus. Together these data indicate that inhalation exposure to a natural fungal allergen under conditions sufficient to induce lung inflammation, surprisingly causes reductions in baseline expression of select innate immune molecules (similar to that observed during endotoxin tolerance) in the region of the CNS controlling respiration

Chapter 2

Real-time Field Tests with Mobile Laboratories

2.1 Introduction

The introduction of particulates, chemicals or biological materials into the atmosphere results in air pollution and it could cause damage to human health and natural environment. One of the largest sources of air pollution comes from energy consumption and production (Hari et al., 1986; Bollen et al., 2010). Problems with energy consumption and production are related not only to global warming, but also to such environmental concerns, particularly air pollution (Dincer, 2000). Air pollution problems prompt the development of renewable energy as clean sources of energy and optimal use of these resources minimize environmental impacts and produce minimum secondary pollution (Panwar et al., 2011; Ehsani et al., 2018). As one of the cleanest renewable energy, hydrogen energy, particularly

fuel cell technology, has become increasingly important and more widely used.

Honda's Fuel Cell Vehicles (FCV) use hydrogen to generate electricity, which is either used to drive the vehicle or stored in an energy storage device, such as battery pack or ultracapacitors (Chan, 2007). Since fuel cells generate electricity from chemical reaction (isothermal), they do not need to burn fossil fuels like the Internal Combustion Engines (ICE) and therefore do not produce multiple pollutants. Water is the only byproduct of a hydrogen fuel cell from the FCV. While the FCV does not produce any air contaminants, concern had been raised that the serious polluted atmospheric environment in the Los Angeles area might have an adverse impact on the heart of this zero emission vehicle. Ammonium (NH_4^+) and sodium (Na^+) cations may displace hydrogen ions (H^+) in the fuel cell's Proton Exchange Membrane (PEM), while SO_2 and NO_x may react with the platinum anode. Ammonia (NH_3) may attack the cathode directly and can be a potential source of additional ammonium cations. Although the South Coast Air Quality Management District (SCAQMD) provides us the concentrations of all these pollutants (COAST, 2014), it is possible that these concentrations are considerably higher on the road. Therefore, a short-period intensive study was performed to identify transient and average exposure levels to these species on Southern California roadways and to compare these values to the closest local air monitoring station data available.

2.2 Target Atmospheric Contaminants

Sodium (Na^+) cations could be a displacement of hydrogen ions in the fuel cell PEM and reduce its efficiency. Formed through wave breaking at the surface of the ocean,

sea spray aerosol particles contribute to natural aerosol particle concentrations and could also impact the gas-particle partitioning in coastal environments (Bertram et al., 2018). As a major ion of the chemical composition of the sea spray aerosol, sodium aerosol in sub-micron form could increase in downwind situation (Gantt et al., 2015; Jourdain and Legrand, 2002).

Ammonium (NH_4^+) coming from mostly ammonium nitrate and ammonium sulfate may also displace H^+ in the fuel cell's PEM. In a polluted urban environment, especially in California, ammonium nitrate consists of 35% of the total mass concentration of submicron aerosol (PM1) (Young et al., 2016). While sea spray aerosol could be a major source of ammonium salt near coastal areas (Guo et al., 2018), in some densely populated urban locations, over 10 years of quality aerosol data also show that ammonium sulfate (up to 31%) was one of the main PM2.5 constituents (Snider et al., 2016). The highly elevated PM concentration, mainly due to high ammonium salt concentration (Aksoyoglu et al., 2017), could be a potential risk of both human health and industrial products like the fuel cells.

Nitrogen Dioxide (NO_2) is one of a group of highly reactive gases known as oxides of nitrogen (NO_x) and it was primarily emitted from the exhaust gas of internal combustion engines (ICE). Although Sulfur Dioxide (SO_2) also comes from the combustion of fossil fuels, the sulfur content of diesel fuel has been cut down to ultra low levels by the Environmental Protection Agency to improve air quality. Some marine fuels still contain relatively high level of sulfur, resulting in a high level of SO_x and NO_x emissions (Vutukuru and Dabdub, 2008). While the state of California's sulfur limit for on-road diesel is only 15 ppm, SO_2 concentration could be elevated near the Port of Long Beach and Port of Los Angeles

areas (Bishop et al., 2011). Despite their health effects that irritate airways in the human respiratory system, NO_2 and SO_2 can also interact with water and oxygen and directly react with the fuel cell platinum anode.

Ammonia (NH_3) is one of the most abundant nitrogen-containing compounds in the atmosphere. Exposure to high concentrations of ammonia in air causes immediate burning of the nose, throat and respiratory tract (New York State Department of Health, 2004). Recognized as an environmental issue in the early 1980s, the major source of NH_3 emissions to the atmosphere is the volatilization from decomposing livestock waste, with the second major source being losses from agricultural plant canopies such as N fertilizers (Sutton et al., 2000; Anderson et al., 2003; Amon et al., 2006; Velthof et al., 2012). Ammonia may attack the cathode directly and it reacts with oxides of nitrogen and sulfur to form fine particles and becomes another potential contaminant to the fuel cell: Ammonium cations.

Data acquisition of Hydrogen Sulfide (H_2S) concentration near the agriculture areas in Southern California was also requested from Honda R&D of North America. Although the reason behind this data request was not provided by Honda, hazardous H_2S levels can be generated in swine confinement buildings during the pulling of manure pit plugs, manure agitation and pump out, operation and maintenance of manure handling equipment and drainage lines, and power washing (Christianson et al., 2004). The presence of H_2S at high levels can also be corrosive to the reinforced concrete that are often used in swine barn construction (Assaad et al., 2003).

2.3 Research Approach

A mobile sensing platform was built for high time resolution sensing of roadway NH_4^+), Na^+, SO_2, NO_x, H_2S and ammonia, coupled with video and GPS to identify transient and average levels of these species identified on Southern California roadways. This platform was equipped with an Aerodyne Aerosol Mass Spectrometer, a Selected Ion Flow Tube Mass Spectrometer, NO_x analyzers, ammonia, H_2S, SO_2 and H_2S analyzers. A 2-dimensional map was created to show the location and concentrations of observed species at select locations within Southern California by linking GPS location to observed species. Also, video graphic recordings allowed identification of vehicles and estimated following distances during major transients for each of the species. Three different routes were selected for different purposes.

2.3.1 Road-map Information

The first route is from Seal Beach to Newport Beach on the Pacific Coast Highway (PCH). On this route Na^+ is the main target atmospheric pollutant for the fuel cell car since shorelines will maximize marine aerosol infiltration.

Starting from 1101 Pacific Coast Highway, Seal Beach (Figure 2.1), the test vehicle headed south on PCH towards 3199 W Balboa Blvd, Newport Beach. Then a U-turn was made and the test vehicle would head back to the starting point. The vehicle speed was set to follow the traffic flow.

The second route is on Western Riverside County roadways for agricultural emissions. It is anticipated that major increases in NH_4^+ will be observed as we drive east

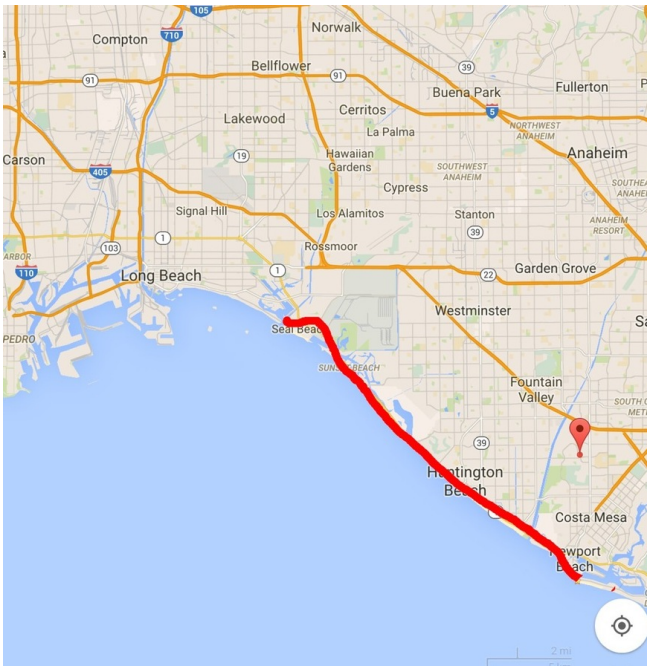

Figure 2.1: Route 1 on Pacific Coast Highway

of diamond bar after photochemical aged air mass (nitric acid) crosses major agricultural emissions (e.g., Chino). Ammonia and H_2S will be the two atmospheric pollutants focused on for on this route.

Starting from Exit 38 of S Achibald Ave on CA 60 Freeway, the test vehicle drove through the highlighted route as shown in Figure 2.2. This loop encircled some major agricultural (dairy farming) operations.

The third route is at the Long Beach industrial area around Terminal Island. On this route there are numerous sources associated with goods movement including heavy heavy duty diesel trucks (HHDDTs) and marine engines operating in the shipping channel. Therefore, ammonia (SCR slip), SO_2, and NO_x are the three major atmospheric pollutants on this route.

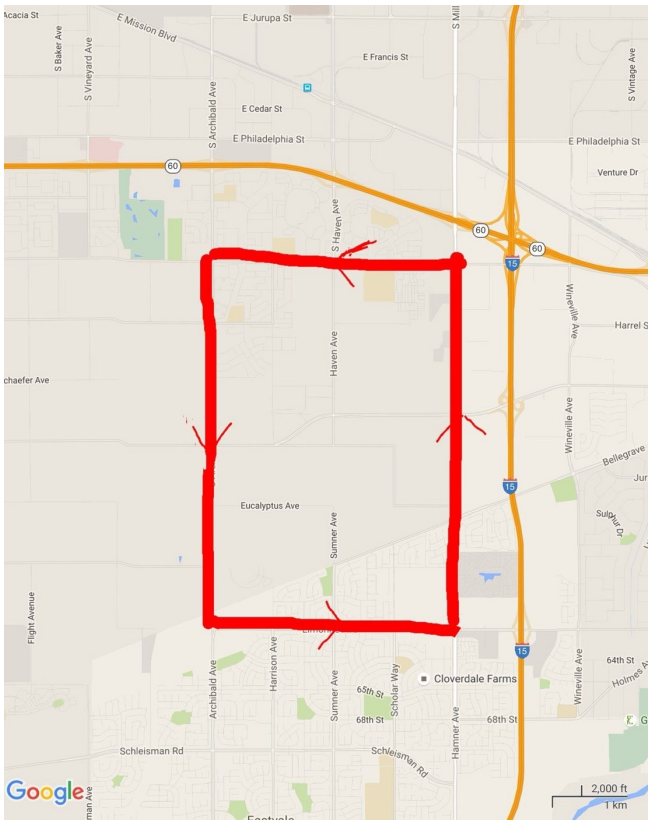

Figure 2.2: Route 2 near Diary Farms

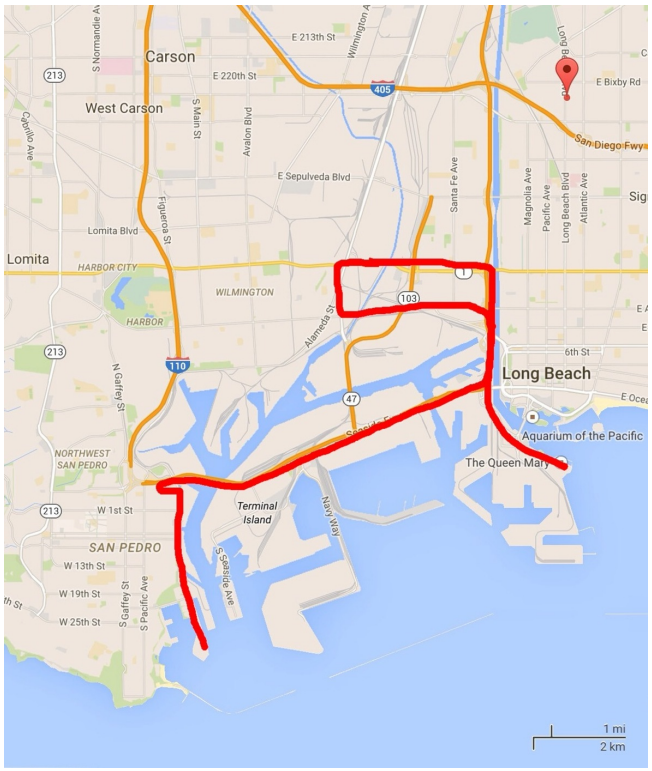

Figure 2.3: Route 3 in Long Beach industrial areas

Starting from the intersection of the Pacific Coast Highway and I-710 freeway, the test vehicle drove through the highlighted route as shown in Figure 2.3. The vehicle speed was set to follow the traffic flow.

2.3.2 Instrumentation

High Resolution Time-of-Flight Aerosol Mass Spectrometer (HR-ToF-AMS). Cation analysis was performed using an Aerodyne High Resolution Time-of-Flight Aerosol Mass Spectrometer (HR-ToF-AMS) operating in "V" mode (Figure 2.4). The HR-ToF-AMS is a real-time chemical aerosol analyzer capable of quantitatively sampling, sizing and chemically analyzing aerosol with fast time resolution and sufficient mass spectral reso-

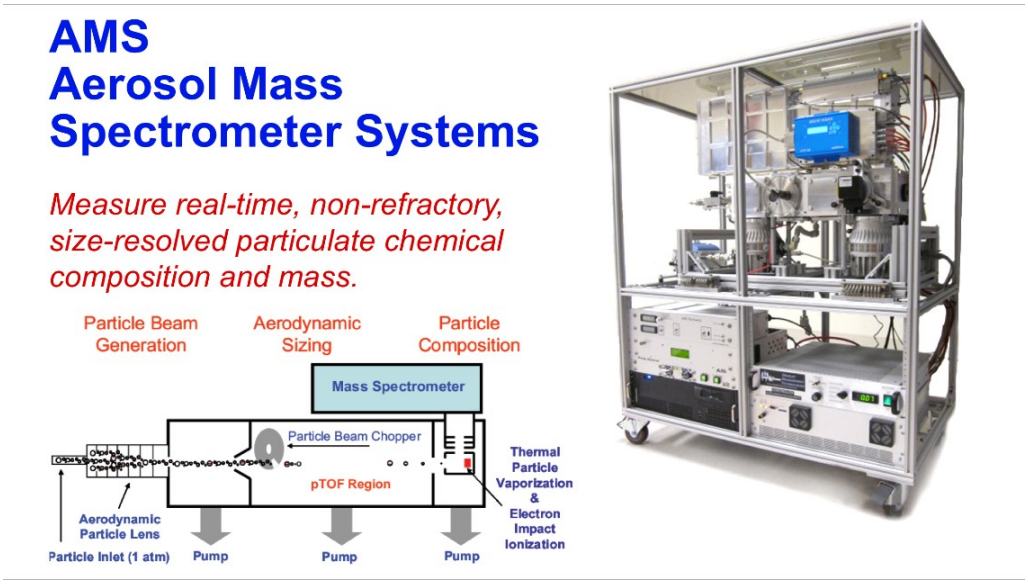

Figure 2.4: Aerodyne AMS

lution to directly distinguish elemental composition of ions having the same mass (DeCarlo et al., 2006). The V-mode offers high sensitivity (0.04 µg/m^3) for all species with mass to charge (m/z) resolving power of approximately 2100 (the W-mode offers sensitivity of 0.4 µg/m^3 for all species with m/z resolving powers approaching 5000). The HR-ToF-AMS is especially suited for quantification of key aerosol species including Sodium and Ammonium (Ovadnevaite et al., 2012).

NO_2 and SO_2 Analyzers. NO_2 and SO_2 was collected using a chemilumenescent TECO model 42 NO_x analyzer (<1 ppb sensitivity, 5 sec average time) and TECO model 43i fluorescent SO_2 analyzer (∼1 ppb sensitivity, 5 second average time), respectively. These instruments are commercially available (Figure 2.5 & 2.6) and stable for mobile platform deployment.

Figure 2.5: TECO model 42 NO_x Analyzer

Figure 2.6: TECO model 43i fluorescent SO_2 Analyzer

Figure 2.7: H_2S Analyzer

Ammonia Analyzer. A stainless steel tube thermal oxidizer (650°C) was used to convert Ammonia to NO and was subsequently sampled using the NO_x channel of a TECO Model 42C NO_x box. Another split sample line was connected to the NO channel of the NO_x box. The difference between these two values, after calibration, is the NH3 concentration (∼1 ppb sensitivity, 5 second average time).

H_2S Analyzer. The portable Jerome® 631 Hydrogen Sulfide Analyzer (Figure 2.7) provided a sampling range of 0.003-50 ppm for H_2S on a 1 minute time basis. It was operated on survey mode.

Selected Ion Flow Tube-Mass Spectrometry (SIFT-MS). The Selected Ion Flow Tube-Mass Spectrometry (SIFT-MS) (Figure 2.8) is a form of direct mass spectrometry that utilizes precisely controlled chemical ionization reactions to detect and quantify trace amounts of volatile organic compounds (VOCs)(Smith and Španěl, 2005). The SIFT-MS

Figure 2.8: Selected Ion Flow Tube-Mass Spectrometry (SIFT-MS)

Figure 2.9: Interior of Mobile Laboratory I-Test Van

can be used for measurements of NO_2, H_2S and NH_3. Unfortunately, the instrument was damaged during mobile sampling and was only able to provide NO_2 numbers after in-field repair.

2.3.3 Mobile Platform Setup and Test Vehicles

A Ford 12-passenger-van with seats removed was used as the Mobile Laboratory I (Figure 2.9 & 2.10). The mobile platform sampling package (especially MS instruments) was vibration shock mounted to the vehicle to lessen the influence of roadway vibration on measurement accuracy. All analyzers were strap mounted to the test vehicle. The sampling inlet was located at the front of the vehicle approximately 2 feet off the ground to simulate

Figure 2.10: Exterior of Mobile Laboratory I-Test Van

Figure 2.11: Mobile Laboratory II-Pickup Truck

Figure 2.12: System Power for Mobile Laboratory I

Figure 2.13: System Power for Mobile Laboratory II

the air intake position of the fuel cell vehicle.

A Silverado pickup truck was modified as the Mobile Laboratory II (Figure 2.11). SO_2, NO_x, H_2S) and NH_3 analyzers were mounted to the back seats of the vehicle. The sampling inlet was located at the front of the vehicle 2 feet off the ground.

A 13-KW Honda generator was used to distribute power to the mobile platform on Mobile Laboratory I (Figure 2.12). The generator exhaust was directed away from the sampling inlets to prevent self-contamination during the program. Four propane tanks were mounted and towed by the test vehicle in the back to provide up to 16 hours of power supply. A 3.3-KW generator was used for Mobile Laboratory II due to less power usage (Figure 2.13).

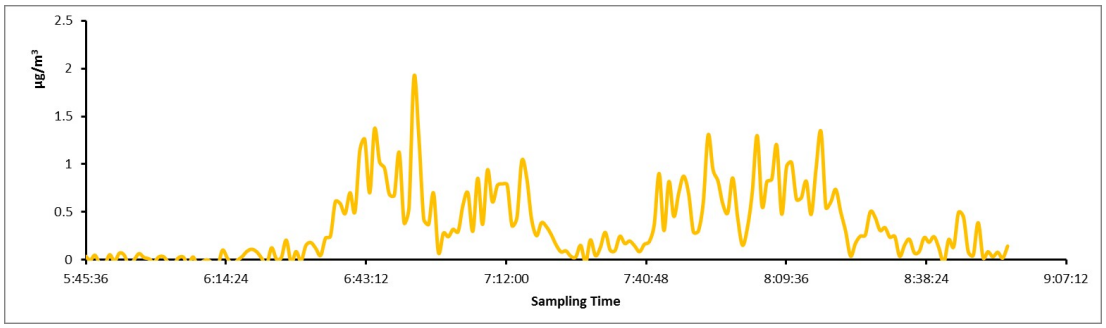

Figure 2.14: Sodium concentration on Route 1(PCH)

2.4 Data Report

2.4.1 Sodium (Na^+)

Route 1 on PCH from 6:30 to 8:30 am. A peak of 1.91 µg/m^3 appeared at W Balboa Blvd, Newport Beach at 6:53 am (Figure 2.14). From 7:53 to 8:16, several peaks also appeared near Huntington Beach. These peaks can be seen in the data mapping graphs (Figure 2.16). According to the wind direction, sea spray aerosols were blowing from the Pacific Ocean and provided the AMS some sodium signals. The overall sodium concentration was within the range (1∼3 µg/m^3) reported by Ovadnevaite(Ovadnevaite et al., 2012) for sea side Na^+ concentrations. A wide range of Na^+ is observed over the test course with the highest levels observed toward the SE of the test track. This is possibly attributed to the relative surf intensity and wind intensity at these locations.

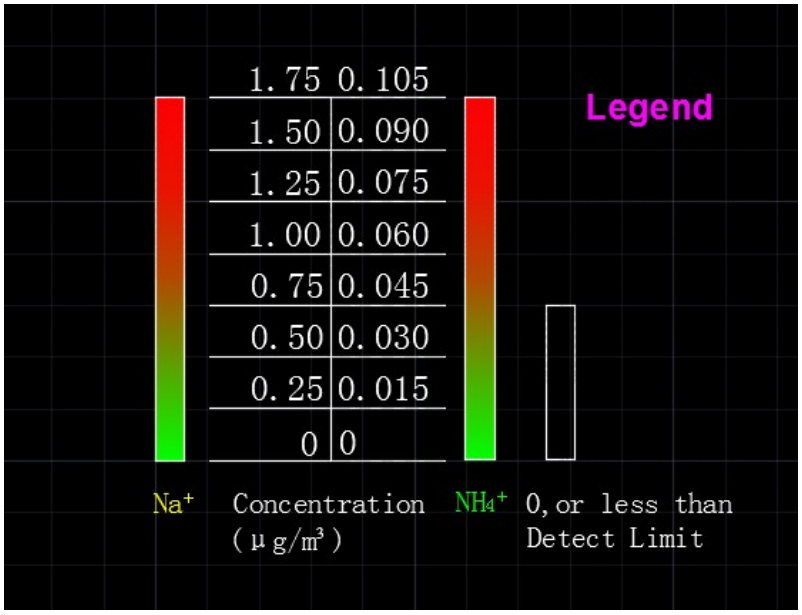

Figure 2.15: Measuring Scale for Sodium

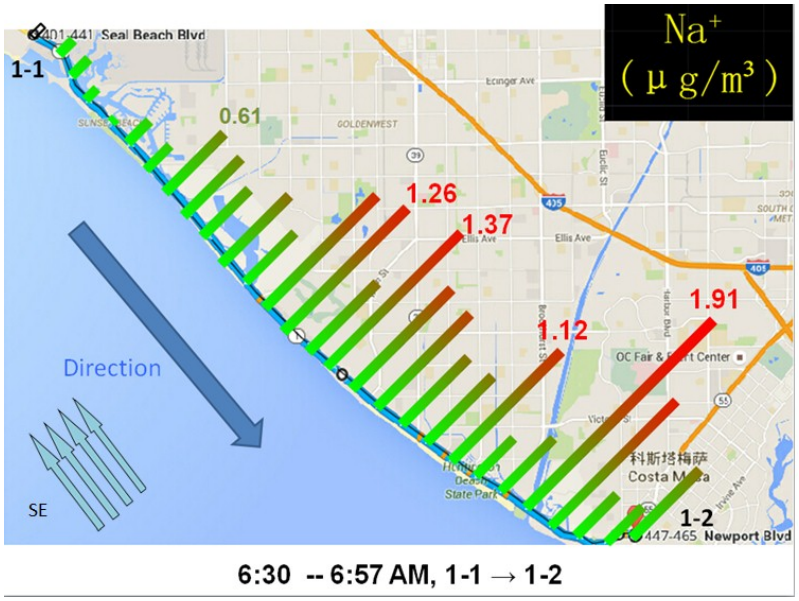

Figure 2.16: Sodium data mapping 2015-09-17

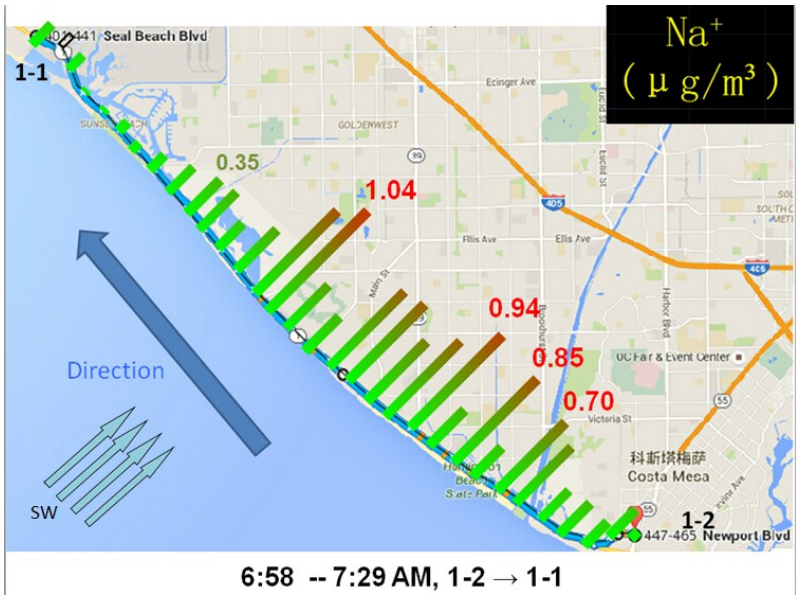

6:58 -- 7:29 AM, 1-2 → 1-1

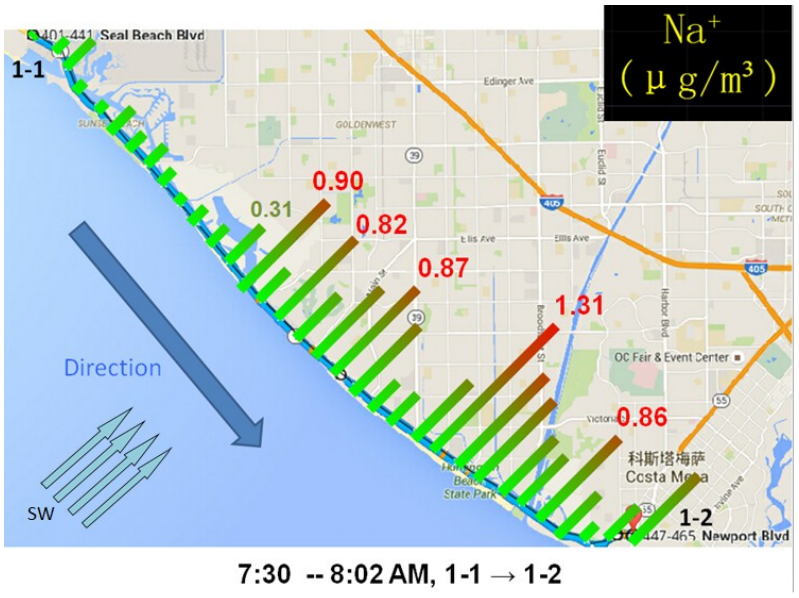

7:30 -- 8:02 AM, 1-1 → 1-2

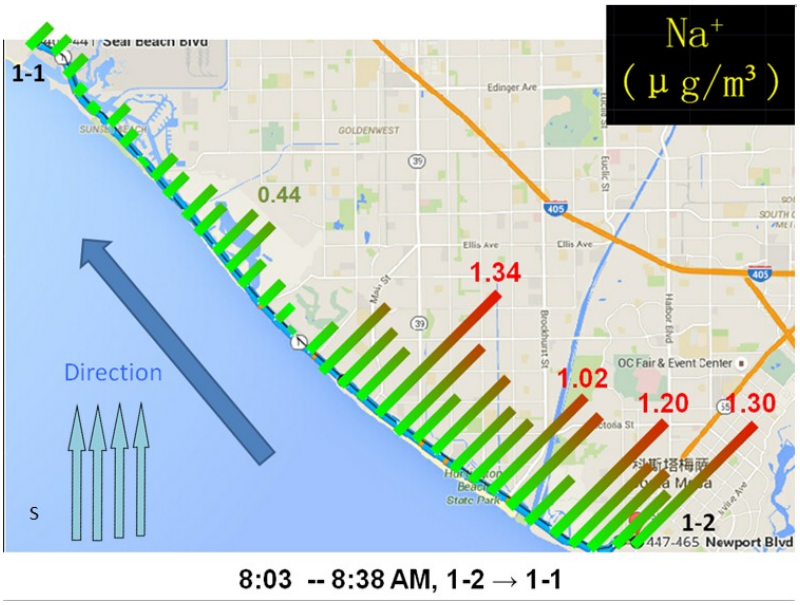

2.4.2 Ammonium (NH_4^+)

The average concentration of ammonium on the farm route was 0.047 µg/m^3. The two major peaks (Figure 2.17) appeared right next to the dairy farm and the highest peak was 0.136 µg/m^3.

The relatively lower ammonium concentration could be caused by highly elevated temperature on the road ways and ammonium nitrate/sulfate particles were vaporized into the air and could not be captured by the Aerosol Mass Spectrometer.

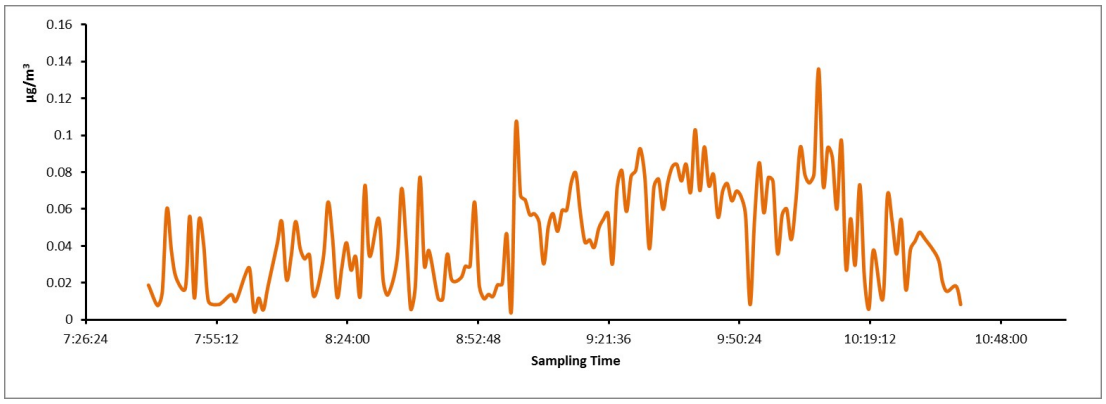

Figure 2.17: Ammonium concentration on Route 1(PCH)

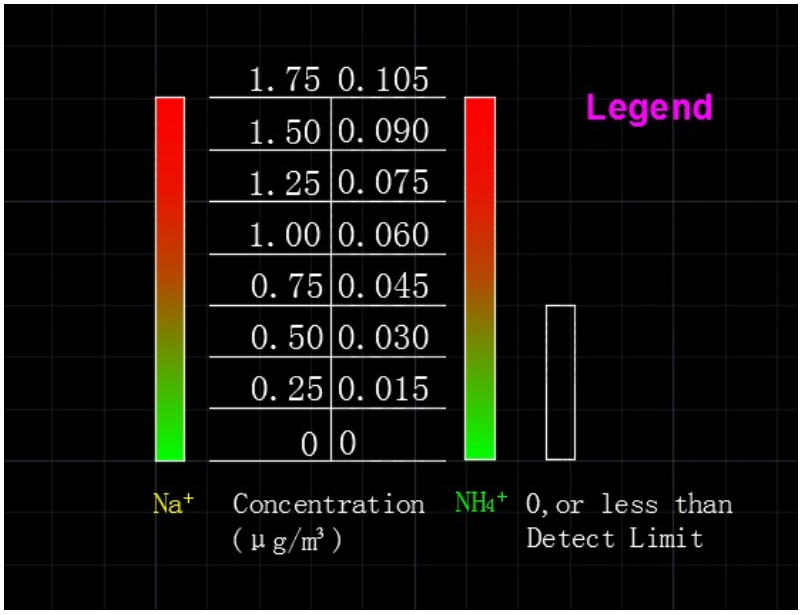

Figure 2.18: Measuring Scale for Ammonium

Figure 2.19: Ammonium data mapping 2015-09-17

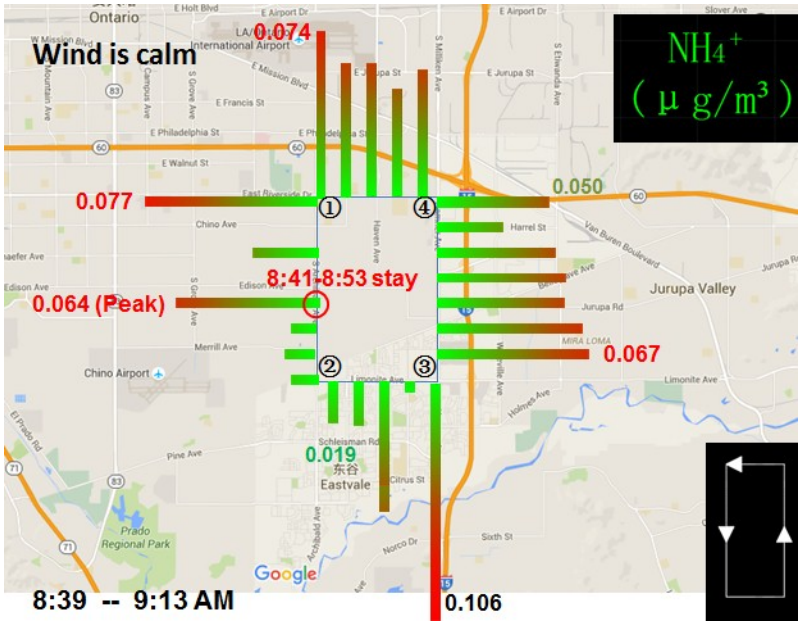

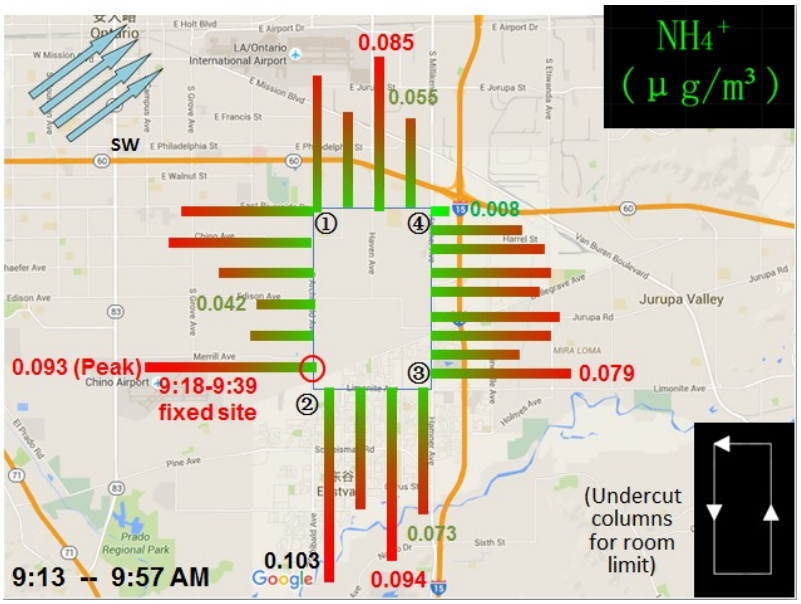
NH4+ (μg/m3)
SW
0.085
0.055
0.008
0.042
0.093 (Peak)
9:18-9:39
fixed site
0.079
0.073
0.103
0.094
(Undercut columns for room limit)
9:13 -- 9:57 AM
Ontario
LA/Ontario International Airport
Jurupa Valley
Chino Airport
Prado Regional Park

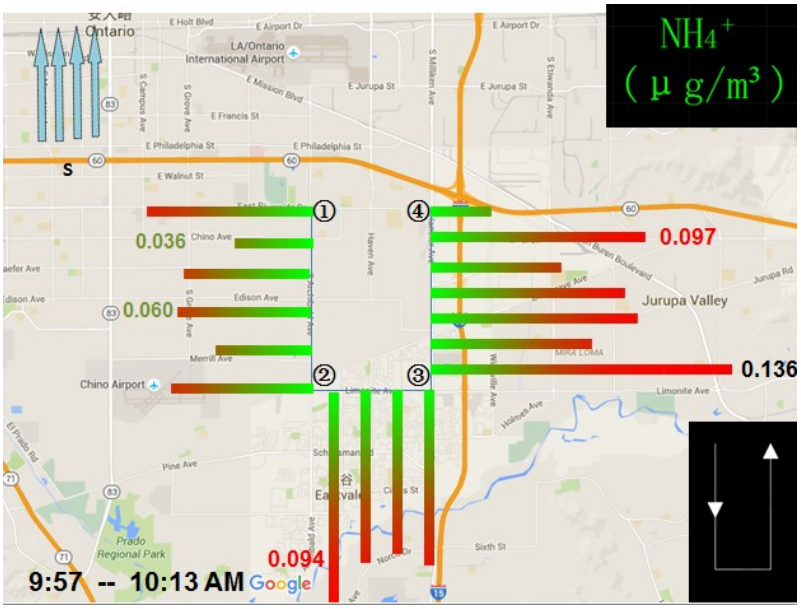
NH4+ (μg/m3)
S
0.036
0.060
0.097
0.136
0.094
9:57 -- 10:13 AM
Ontario
LA/Ontario International Airport
Jurupa Valley
Chino Airport
Prado Regional Park

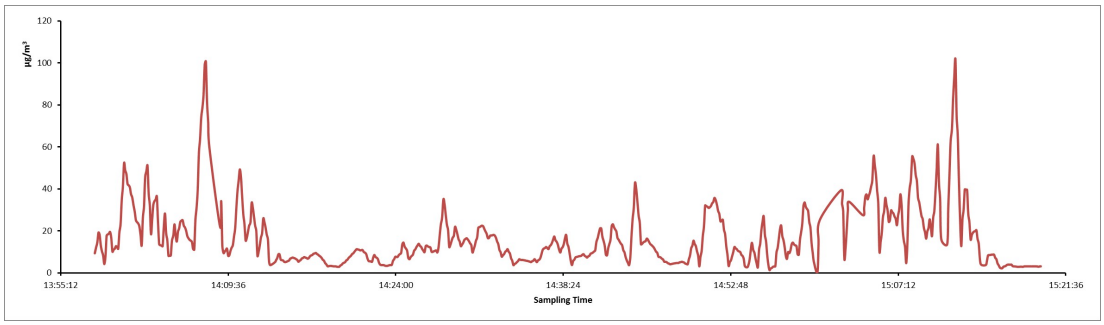

Figure 2.20: NO_2 concentration on freeways 2015-09-08

2.4.3 Nitrogen Dioxide (NO_2)

The average NO_2 concentration on freeways was 16.8 ppb. Peaks in NO_2 were observed when following semi-trucks and driving past the intersection of two freeways. The highest peak observed was around 100 ppb.

The average concentration on Route 3 is relatively higher than the freeway average. The highest concentration of 84.1 ppb was captured near the intersection of I-710 freeway and the Pacific Coast Highway.

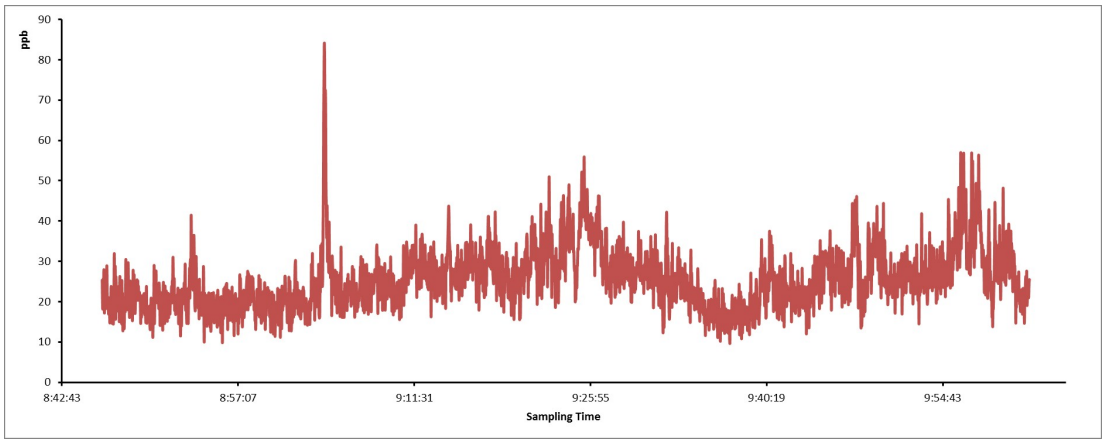

Figure 2.21: NO_2 concentration on freeways 2015-09-11

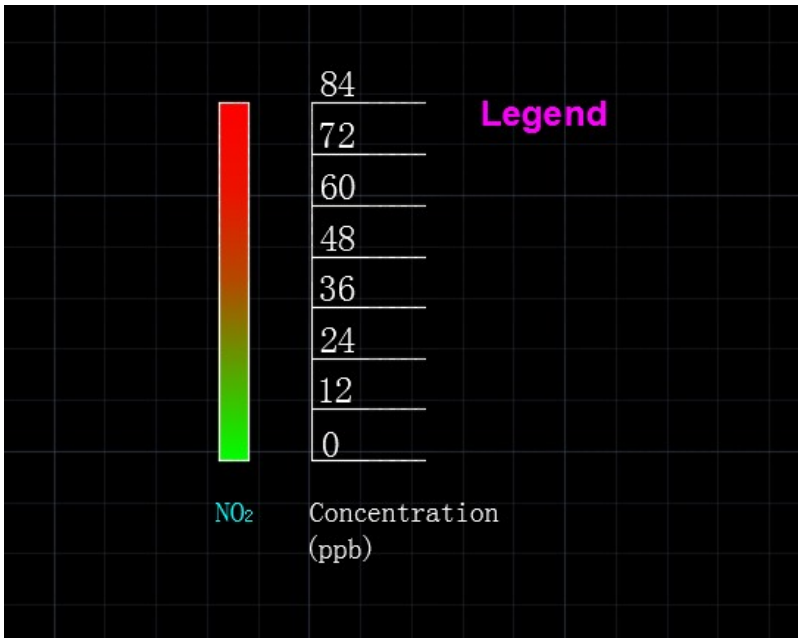

Figure 2.22: Measuring Scale for NO_2

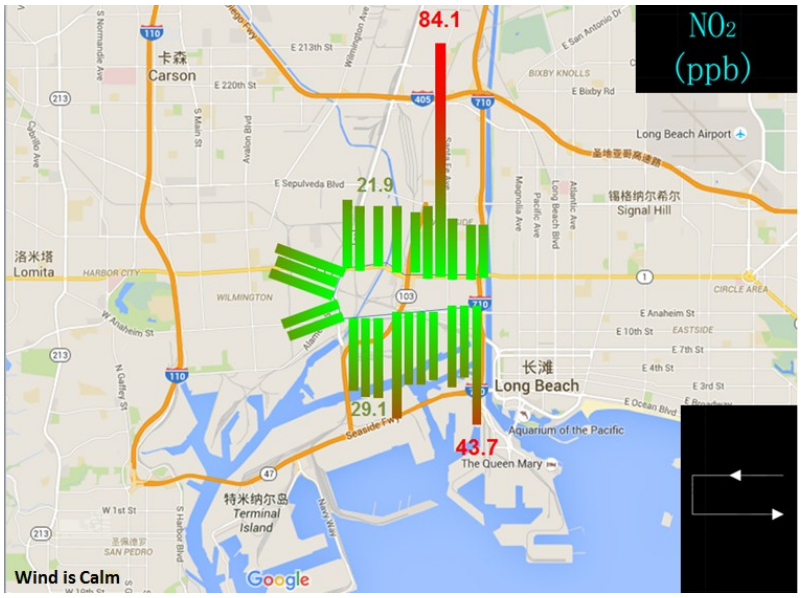

Figure 2.23: NO_2 data mapping 2015-09-11

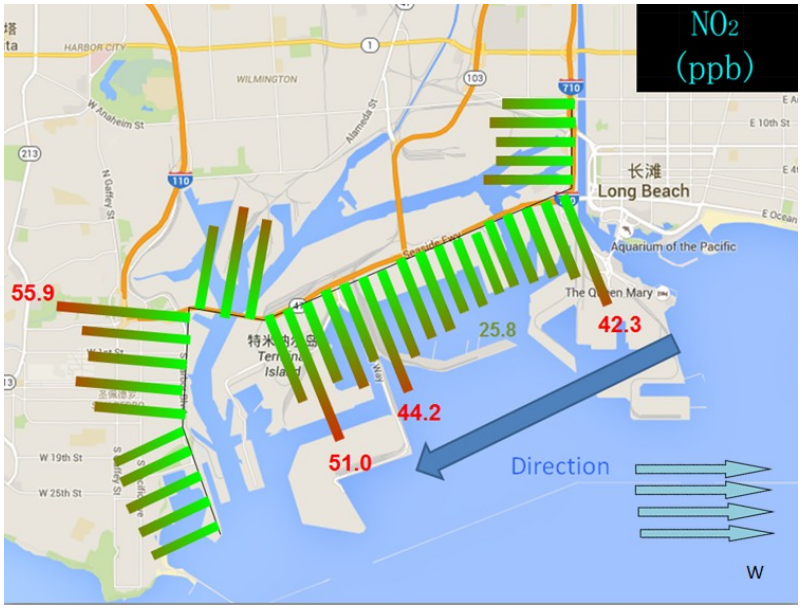

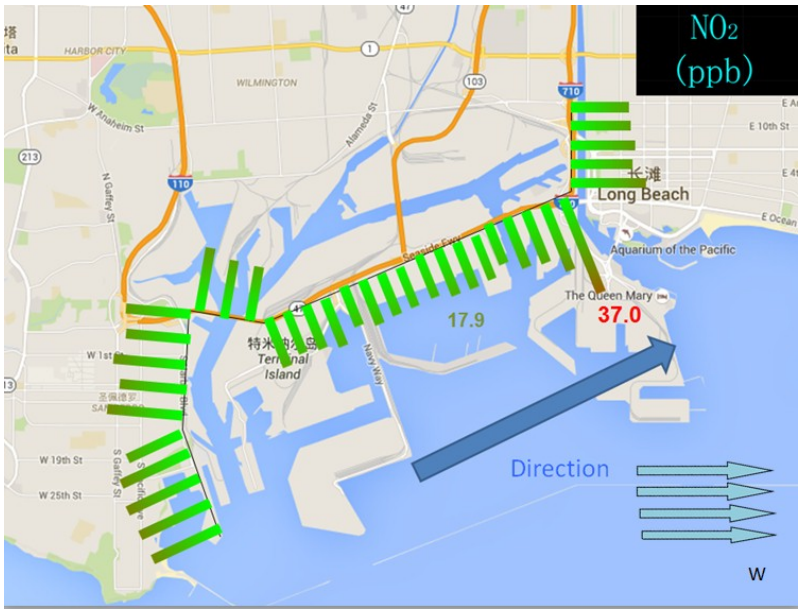
NO2
(ppb)
HARBOR CITY
WILMINGTON
W Anaheim St
Alameda St
N Gaffey St
213
110
103
710
E 10th St
长滩
Long Beach
E Ocean
Aquarium of the Pacific
The Queen Mary
37.0
17.9
Seaside Fwy
W 1st St
Navy Way
W 19th St
W 25th St
S Gaffey St
Direction
W

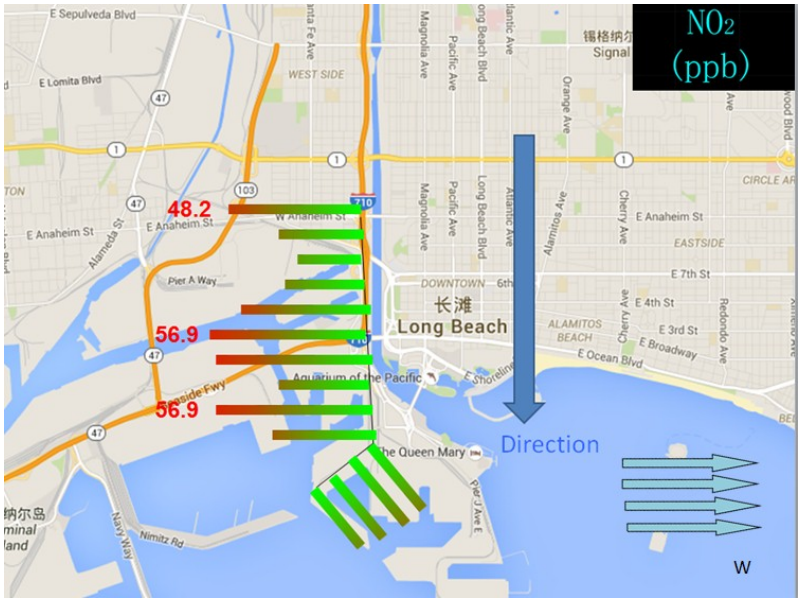
NO2
(ppb)
E Sepulveda Blvd
E Lomita Blvd
WEST SIDE
Santa Fe Ave
Magnolia Ave
Pacific Ave
Long Beach Blvd
Atlantic Ave
Orange Ave
Alamitos Ave
Cherry Ave
CIRCLE AR
47
1
103
710
48.2
E Anaheim St
W Anaheim St
Alameda St
Pier A Way
56.9
56.9
DOWNTOWN
6th
长滩
Long Beach
EASTSIDE
E 7th St
E 4th St
E 3rd St
E Broadway
E Ocean Blvd
ALAMITOS
BEACH
Redondo Ave
Aquarium of the Pacific
Seaside Fwy
The Queen Mary
Direction
Navy Way
Nimitz Rd
W

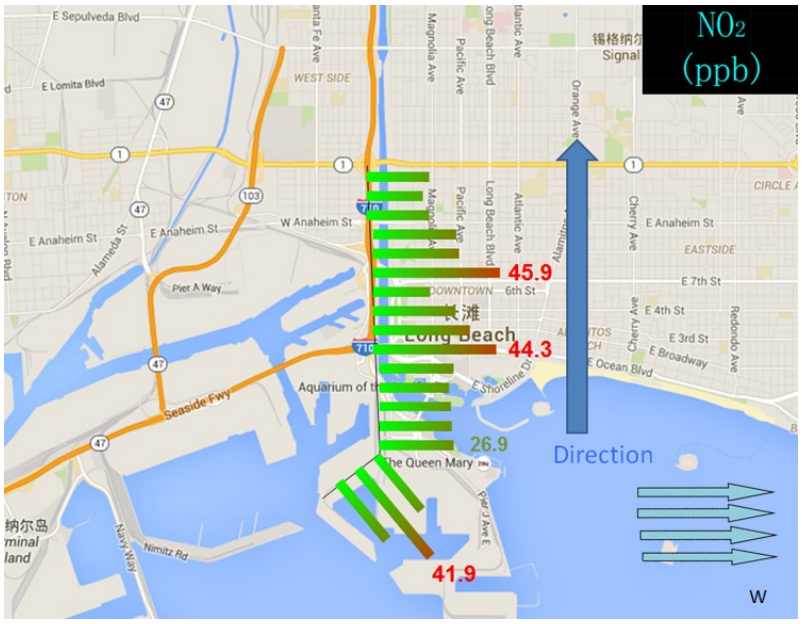
NO2
(ppb)
45.9
44.3
26.9
41.9
Direction
W
E Sepulveda Blvd
E Lomita Blvd
WEST SIDE
Pacific Ave
Long Beach Blvd
Atlantic Ave
Signal
W Anaheim St
E Anaheim St
Alameda St
Pier A Way
DOWNTOWN
6th St
Long Beach
Cherry Ave
EASTSIDE
E 7th St
E 4th St
E 3rd St
E Broadway
E Ocean Blvd
Seaside Fwy
Aquarium of t
Shoreline Dr
he Queen Mary
Pier J Ave E
Nimitz Rd
Navy Way
CIRCLE
Redondo Ave

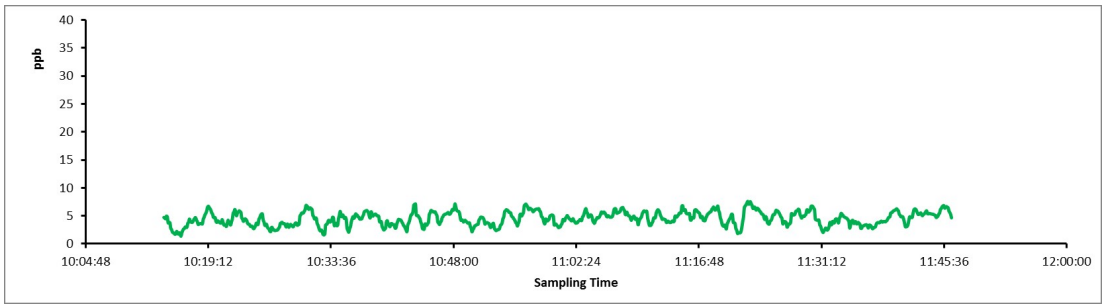

Figure 2.24: SO_2 concentration on freeways 2016-01-21

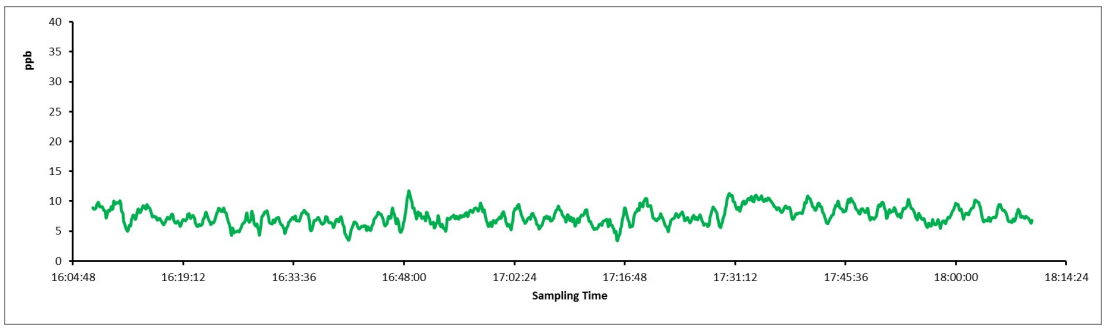

Figure 2.25: SO_2 concentration on Dairy Farm Route 2016-01-22

2.4.4 Sulfur Dioxide (SO_2)

SO_2 concentration was low on Southern California freeways with an average of 4.5 ppb. No significant on-road peak concentrations of SO_2 were observed during freeway sampling (Figure 2.24).

SO_2 concentration was relatively higher on the Dairy Farm Route with an average of 7.5 ppb and the highest concentration was 11.7 ppb when multiple vehicles at the traffic intersection (Figure 2.25).

Relatively higher SO_2 concentration was observed on Route 3 with an average of 7.8 ppb. Also, a series of peaks appeared on Vincent Thomas Bridge with the highest

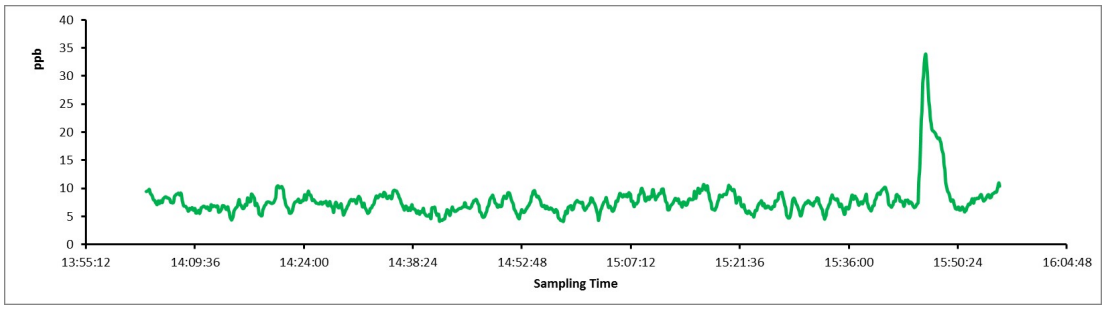

Figure 2.26: SO_2 concentration on Route 3(Long Beach) 2016-01-21

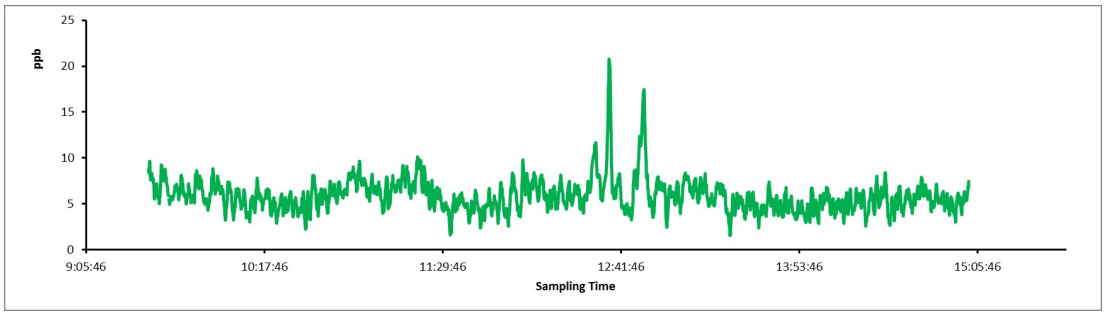

Figure 2.27: SO_2 concentration on Route 3(Long Beach) 2016-01-22

concentration of 33.8 ppb. It is due to the fact that the bridge was built for both vehicle commutes and ships pass through. Marine engine exhausts are one of the major sources for Southern California SO_2 emission. Peaks appeared at the same site (Vincent Thomas Bridge) during the returning sampling visit on 2016-01-22 (Figure 2.27). The average concentration was 6.4 ppb while the highest concentration is 20.8 ppb.

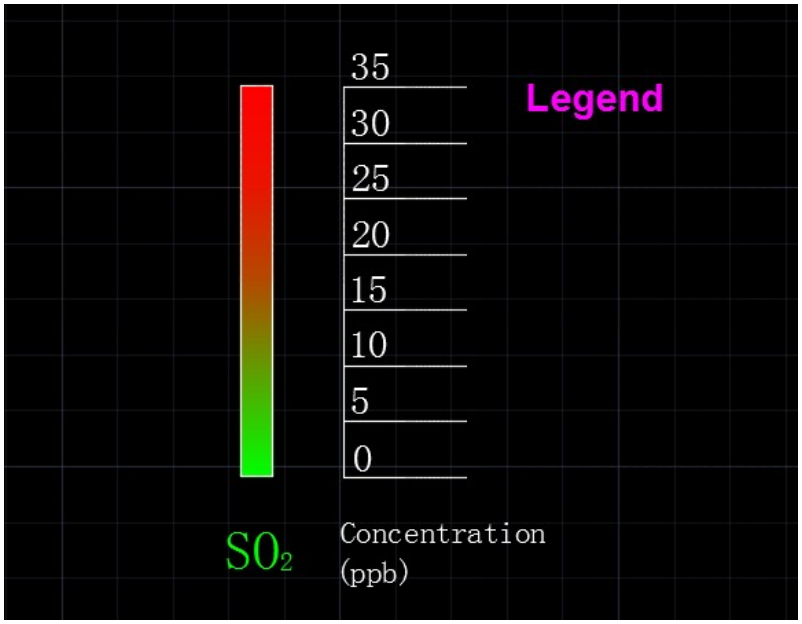

Figure 2.28: Measuring Scale for SO_2

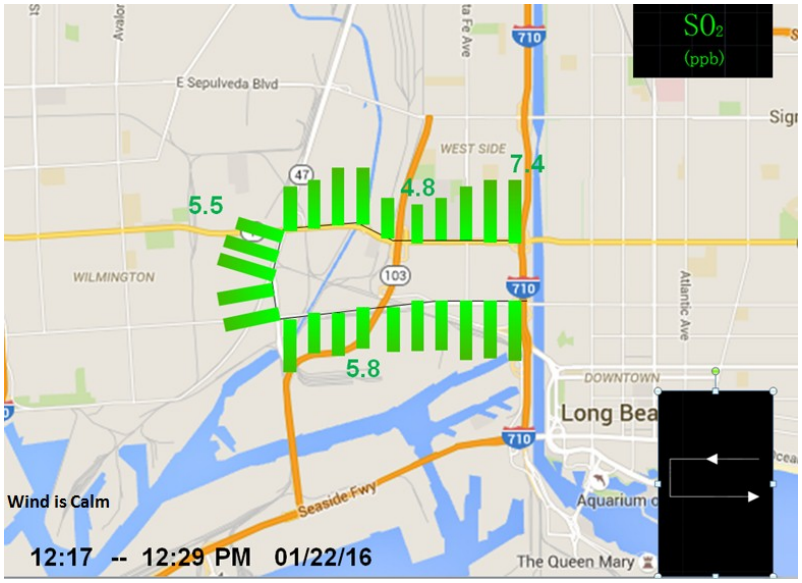

Figure 2.29: SO_2 data mapping 2016-01-22

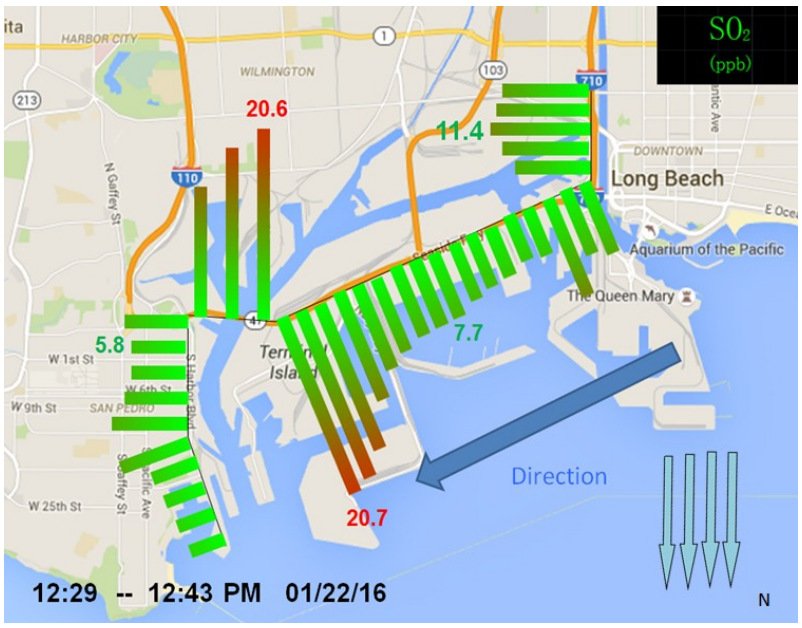
SO2
(ppb)
20.6
11.4
5.8
7.7
20.7
Direction
12:29 -- 12:43 PM 01/22/16
N
HARBOR CITY
WILMINGTON
DOWNTOWN
Long Beach
Aquarium of the Pacific
The Queen Mary
SAN PEDRO
W 1st St
W 9th St
W 25th St
N Gaffey St
S Gaffey St

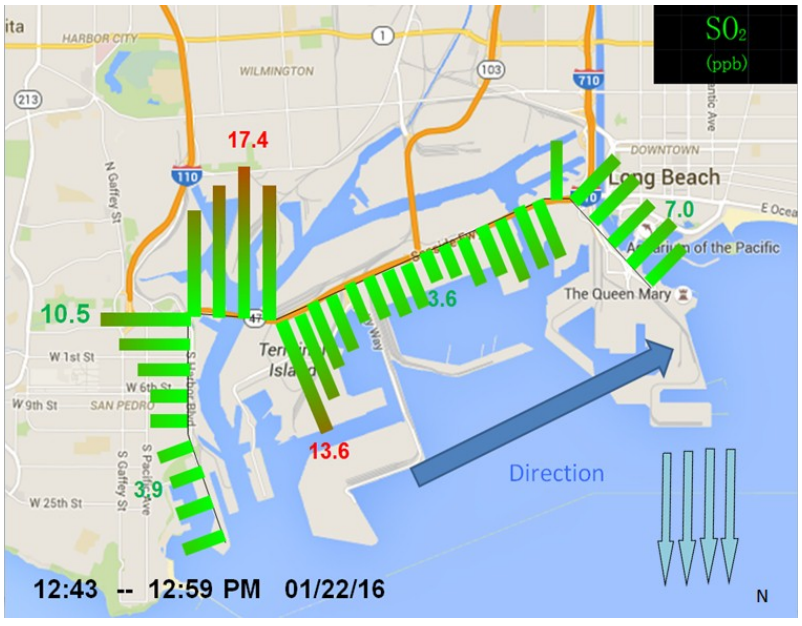
SO2
(ppb)
17.4
7.0
3.6
10.5
13.6
3.9
Direction
12:43 -- 12:59 PM 01/22/16
N
HARBOR CITY
WILMINGTON
DOWNTOWN
Long Beach
The Queen Mary
SAN PEDRO
W 1st St
W 6th St
W 9th St
W 25th St
N Gaffey St
S Gaffey St

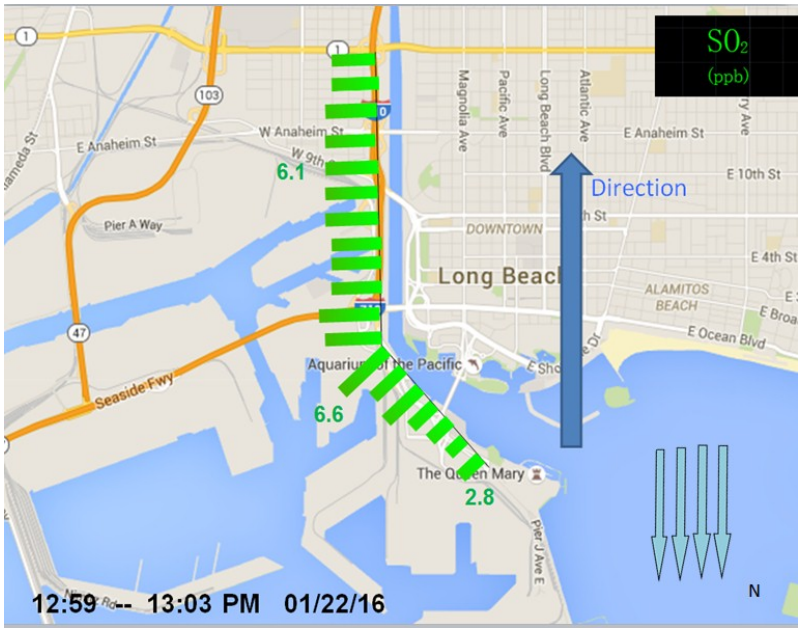
SO2
(ppb)
6.1
6.6
2.8
Direction
Long Beach
DOWNTOWN
ALAMITOS BEACH
Aquarium of the Pacific
The Queen Mary
E Anaheim St
W Anaheim St
E 10th St
E 4th St
E Ocean Blvd
Pier A Way
Seaside Fwy
Magnolia Ave
Pacific Ave
Long Beach Blvd
Atlantic Ave
12:59 -- 13:03 PM 01/22/16
N

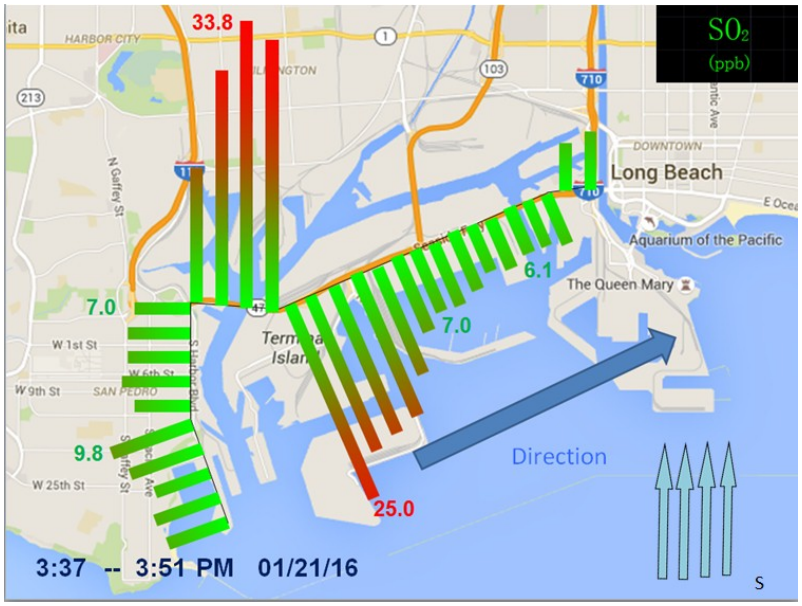
SO2
(ppb)
33.8
7.0
9.8
6.1
7.0
25.0
Direction
Long Beach
DOWNTOWN
Aquarium of the Pacific
The Queen Mary
HARBOR CITY
SAN PEDRO
W 1st St
W 9th St
W 25th St
3:37 -- 3:51 PM 01/21/16
S

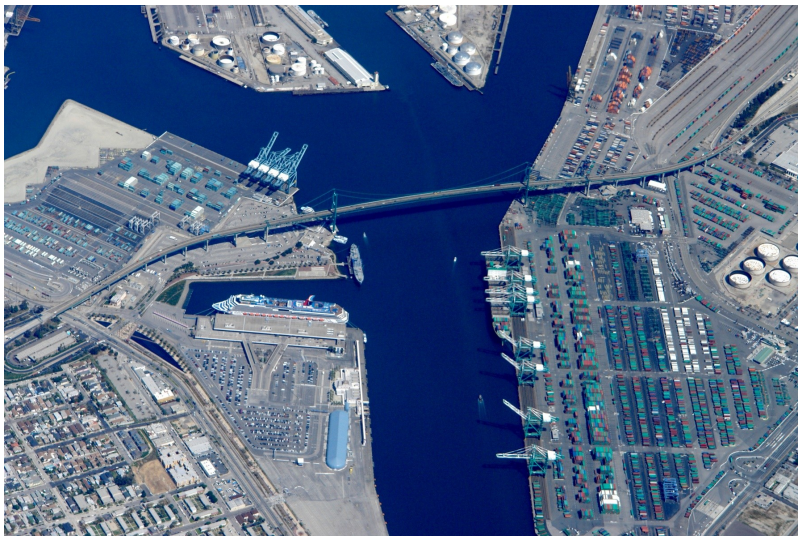

Figure 2.30: Satellite view of Vincent Thomas Bridge

Figure 2.31: Vincent Thomas Bridge

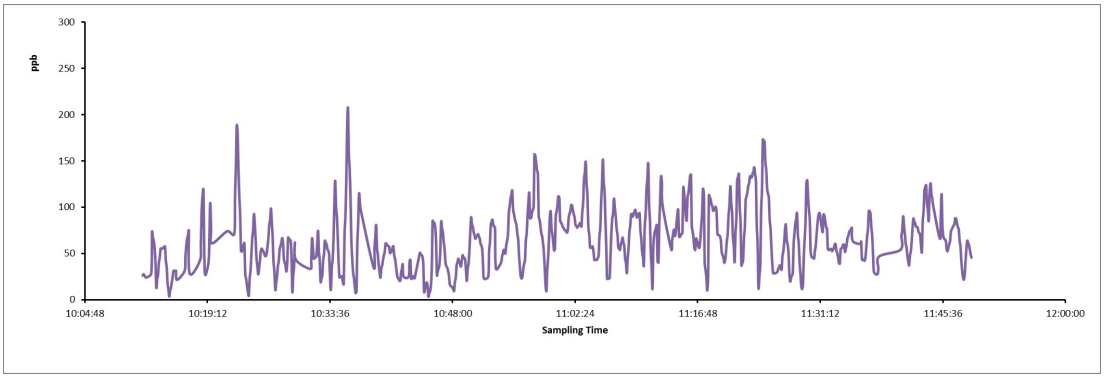

Figure 2.32: NH_3 concentration on Freeways 2016-01-21

2.4.5 Ammonia (NH_3)

A peak of 207.3 ppb at 10:35 am appeared when the test vehicle passed by a freeway construction area on CA 91 Freeway in Corona. There's no obvious event for the earlier peak of 188 ppb near the car dealer center of Riverside. The average concentration of NH_3 on freeways is 65.5 ppb. It is possible that the spikes were attributable to ammonia slip from a malfunctioning SCR system.

A peak of 185.4 ppb appeared next to a heavy duty warehouse where loading and unloading container activity happens. The peak concentration could also be a sign of a malfunctioning SCR system from diesel trucks. However, the average concentration was 67.3 ppb, which was close to the value observed on freeways.

The NH_3 concentration quickly climbed up when the test vehicle was approaching the dairy farms with an average of 204.4 ppb and the highest concentration observed was 1173 ppb. From 4:32 to 4:42 pm the test vehicle pulled over to one of the farms for fixed

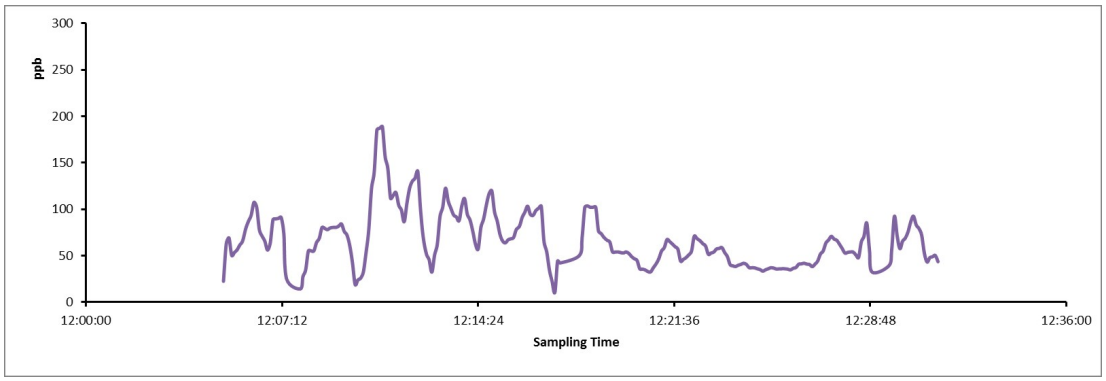

Figure 2.33: NH_3 concentration on Route 3 2016-01-21

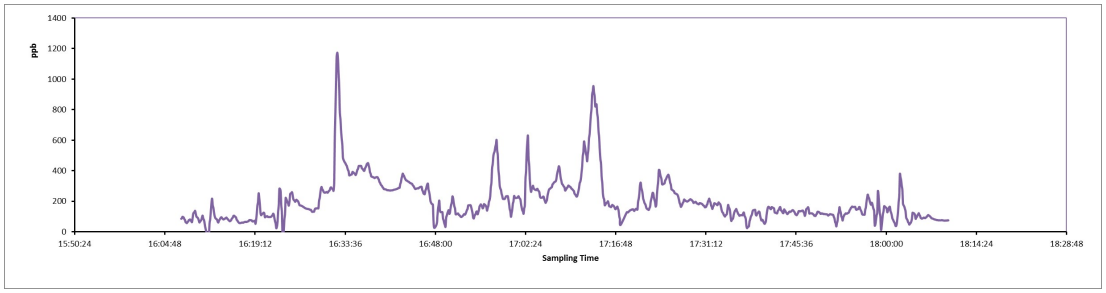

Figure 2.34: NH_3 concentration on Dairy Farm Route 2016-01-22

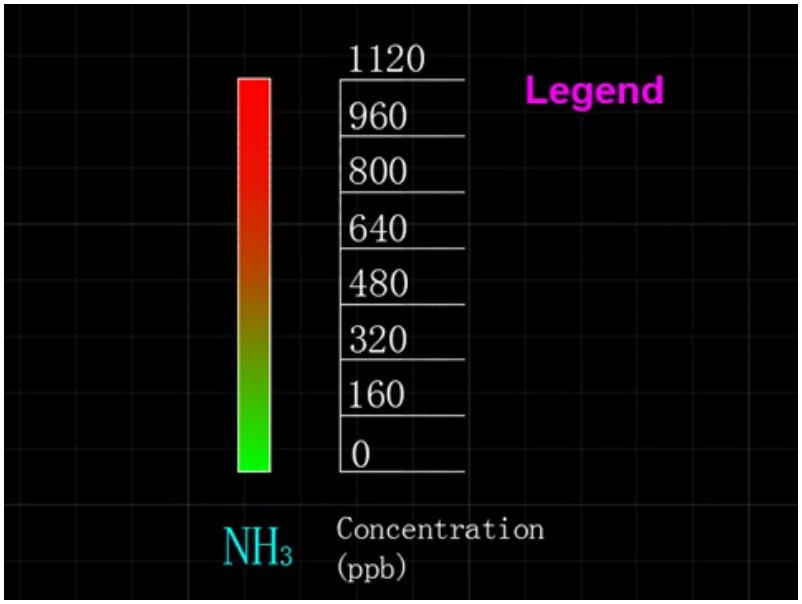

Figure 2.35: Measuring Scale for NH_3

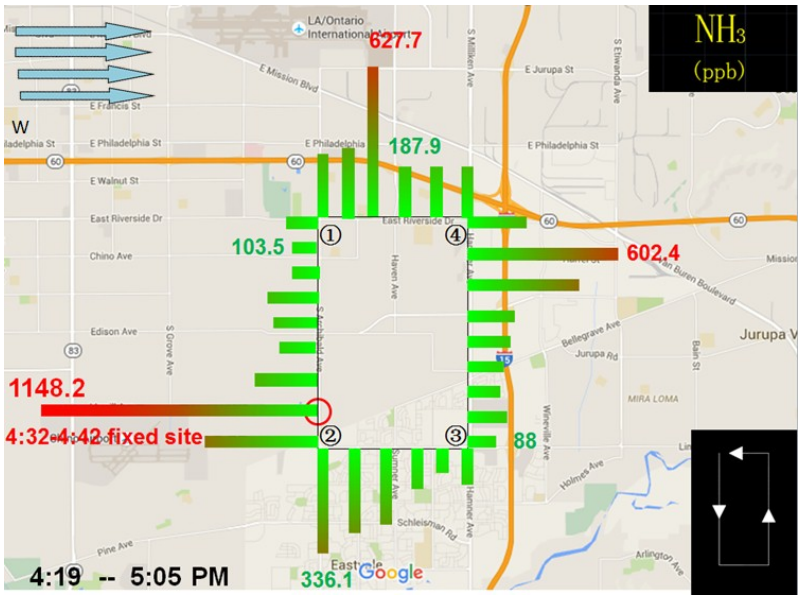

Figure 2.36: NH_3 data mapping 2016-01-22

site sampling. Results can be seen on the data mapping graph of NH_3 (Figure 2.36).

The average concentration of NH_3 climbed up to 407 ppb at the fixed site 10 feet away from the dairy fenceline and the highest concentration of 1173 ppb was also observed. The test vehicle stayed downwind of the dairy farm during the fixed site sampling.

Figure 2.37: Fixed Site Satellite Map

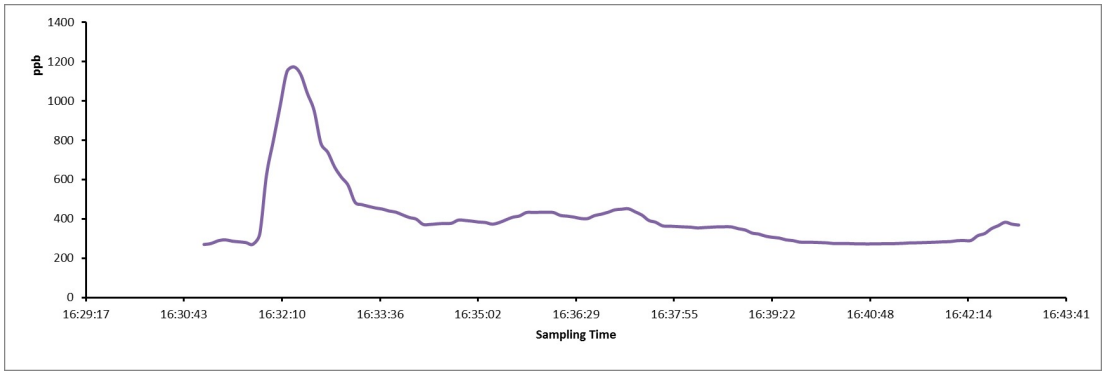

Figure 2.38: NH_3 concentration at the Fixed Site

Figure 2.39: Cows at the Fixed Site

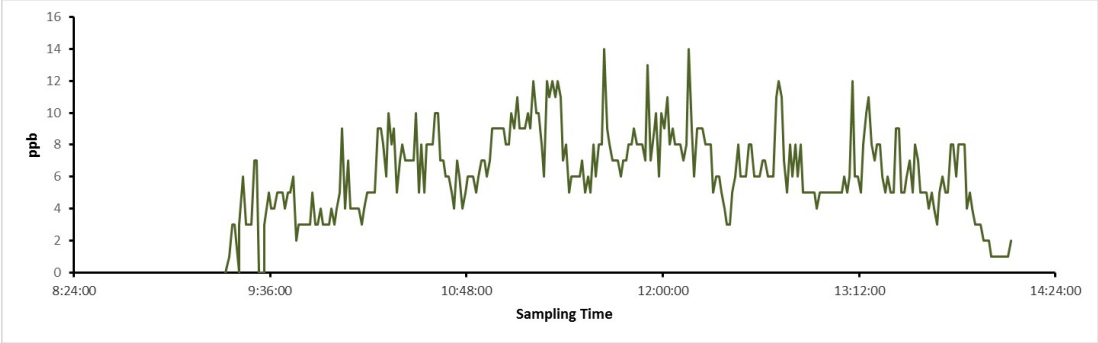

Figure 2.40: H_2S concentration on freeways and Route 3 01-21-2016

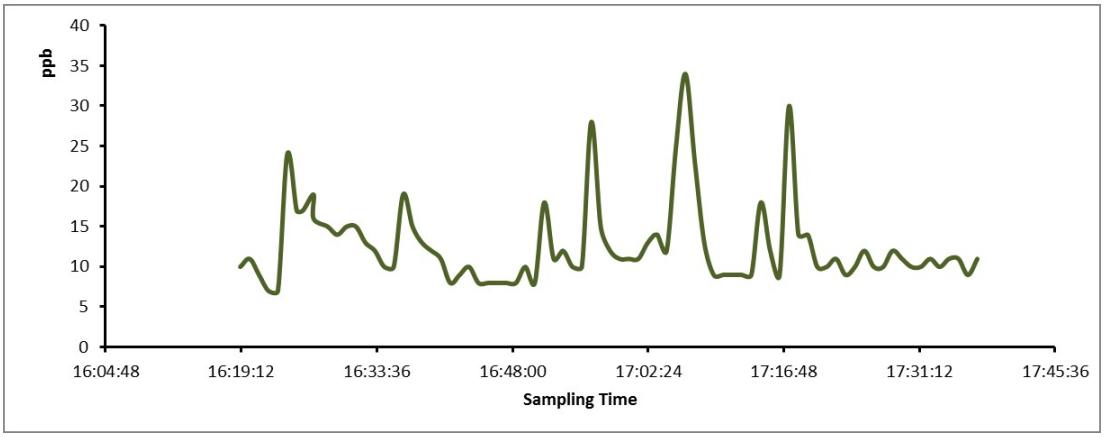

Figure 2.41: H_2S concentration on Dairy Farm 01-22-2016

2.4.6 Hydrogen Sulfide (H_2S)

The average concentration of H_2S was at a low value of 5 ppb. Multiple peaks of 14 ppb appeared in Long Beach area without obvious events observed.

Peak concentrations of H_2S continued to show up randomly without obvious events observed. However, the average concentration on the dairy farm route was twice higher than the Freeway and Route 3 average with a peak value of 34 ppb.

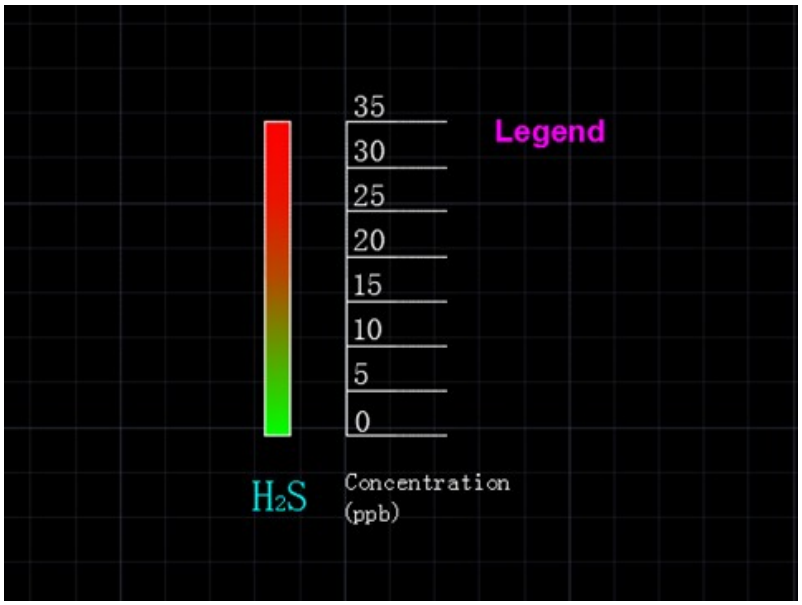

Figure 2.42: Measuring Scale for H_2S

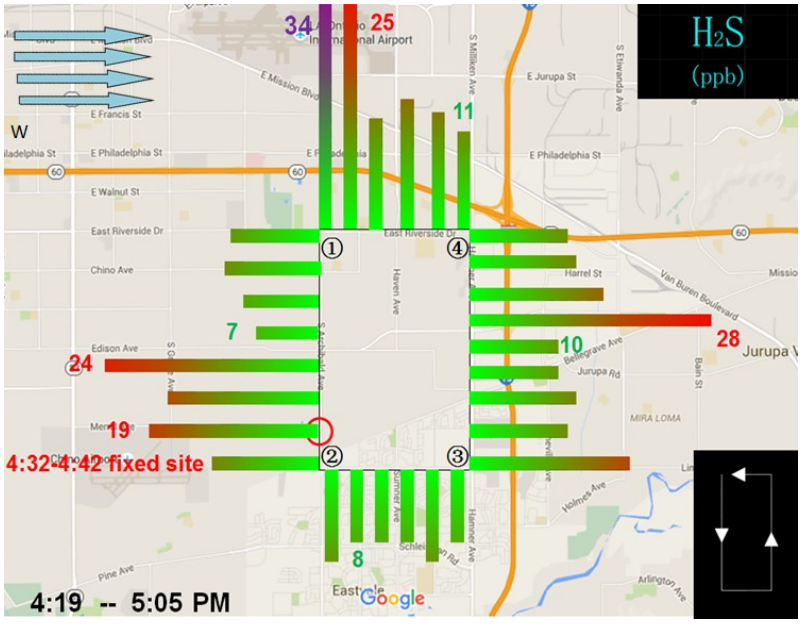

Figure 2.43: H_2S data mapping 2016-01-22

Figure 2.44: Fixed Site Satellite Map

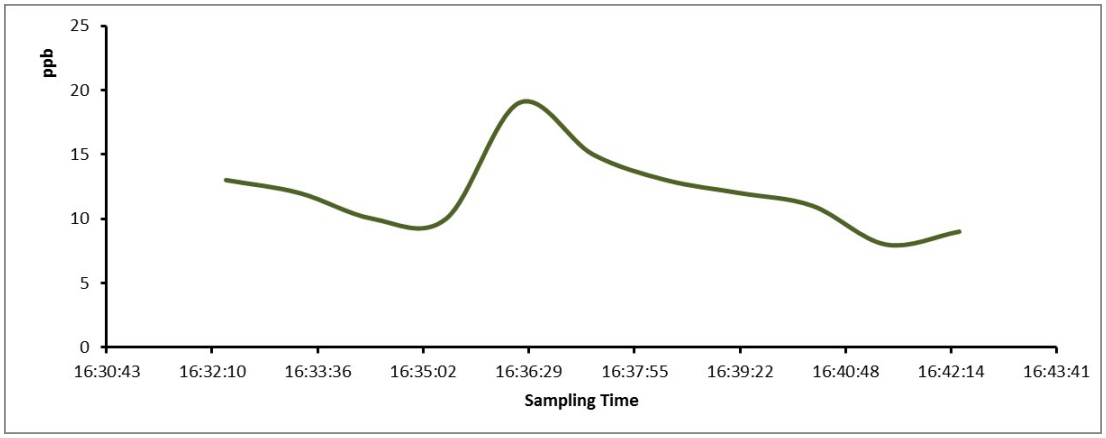

Figure 2.45: H_2S Concentration at the Fixed Site

At the fixed site, the average concentration of H_2S was 2 ppb higher than the whole dairy route average. Pulling over to the dairy fenceline did not dramatically affect the concentration.

Contents / Date	Range (μg/m³)	Average (μg/m³)	Maximum (μg/m³)	Standard Deviation	Peak Value Location
Na^+-2015/09/11 Route 1(PCH)	0-1.91	0.47	1.91	0.36	Near Huntington Beach
2012	0.05-8.01	0.72	8.01	1.15	Anaheim Monitoring Station AQMD
August 2012	0.46-8.01	1.84	8.01	2.73	
September 2012	0.34-1.08	0.64	1.08	0.28	
October 2012	0.21-0.83	0.43	0.83	0.23	
2013	0.22-12.5	1.79	12.5	3.18	
NH_4^+-2015/09/17 Route 2(Dairy Farm)	0.005-0.136	0.05	0.136	0.027	Adjacent to a dairy farm
2012	0.23-8.97	1.52	8.97	1.38	Anaheim Monitoring Station AQMD
August 2012	0.54-2.18	1.36	2.18	0.65	
September 2012	0.64-1.87	0.99	1.87	0.53	
October 2012	0.51-2.71	1.42	2.71	1.01	
2013	0.36-4.33	1.53	4.33	1.26	

Table 2.1: Hydrogen Ion Displacement Contamination (Na^+ & NH_4^+)

2.5 Executive Summary

2.5.1 H^+ Displacement Contamination (Na^+ & $NH_4{}^+$)

The highest concentration of Na^+ (around 2 µg/m^3) was observed near Huntington Beach. Sea spray is the major source of Na^+ in the ambient (Vignati et al., 2010), while Huntington Beach is famous for being a surfing site of Southern California due to yearlong strong wind coming from the Pacific Ocean with huge waves. The nearest AQMD site for Na^+ is the Anaheim monitoring station. According to the AQMD data (Highlighted in Table 2.1), year average of 2012 was 0.72 µg/m^3 and the highest concentration was 8.01 µg/m^3. Na^+ concentration of August, September and October can be found in the table.

Agricultural emission is one of the major source of $NH_4{}^+$ (Bouwman et al., 1997). In our observation, the average concentration of ammonium on the farm route was 0.047 µg/m^3. The two major peaks appeared right next to the dairy farm and the highest peak was 0.136 µg/m^3.

2.5.2 Platinum Anode Contamination (NO_2 & SO_2)

NO_2 mainly comes from heavy duty diesel vehicles on the Southern California Freeways (Halonen et al., 1997). The maximum value (101 ppb) was observed on freeways when following heavy duty diesel vehicles. Also, freeway intersections have highly elevated NO_2 level due to large traffic volume. The standard deviation is close to the average concentration, which means NO_2 distribution varies dramatically and spatially on freeways.

The NO_2 concentration on Long Beach Route is around 10 ppb higher than the freeway average (Table 2.2). This could be attributed to large traffic volume of semi-trucks

Contents / Date	Range (ppb)	Average (ppb)	Maximum (ppb)	Standard Deviation	Peak Value Location
NO_2-2016/09/08 Freeways	0.3 - 101.5	16.8	101.5	14.6	When following a Semi-Truck
NO_2-2015/09/11 Route 3(Long Beach)	9.7 - 84.1	25.5	84.1	7.57	Intersection of I-710 and PCH
AQMD 2015/09/11	4.9- 62.9	24.7	62.9	13.3	I-710 Long Beach
AQMD 2015/09/11	2.9-20.6	8.9	20.6	5.24	Costa Mesa
AQMD 2015/09/11	7.9-41.8	21.8	41.8	9.80	Los Angeles
AQMD 2016/01/22	16.2-47.1	32.5	47.1	8.93	I-710 Long Beach
AQMD 2016/01/22	12.8-37.2	27.6	37.2	6.16	Costa Mesa
AQMD 2016/01/22	10.7-53.7	32.0	53.7	13.4	Los Angeles
SO_2-2016/01/21 Freeways	2.1 - 7.6	4.5	7.6	1.73	No obvious events
SO_2-2016/01/22 Route 2(Dairy Farm)	3.5 - 11.7	7.5	11.7	1.40	When following cars at intersection
SO_2-2016/01/21 Route 3 Long Beach	4.1 - 33.8	7.8	33.8	3.00	Vincent Thomas Bridge
SO_2-2016/01/22 Route 3 Long Beach	1.6 - 20.8	6.4	20.8	2.29	Vincent Thomas Bridge
AQMD 2016/01/22	0.02 - 0.81	0.24	0.81	0.23	Costa Mesa
AQMD 2016/01/22	0.17 - 1.91	0.85	1.91	0.53	Los Angeles

Table 2.2: Platinum Anode Contamination (NO_2 & SO_2)

and industrial emissions. The much low standard deviation indicates NO_2 distribution in Long Beach area is more even and relatively higher.

According to NO_2 data from AQMD monitoring station near I-710 freeway in Long Beach on the same day (2015/09/11), the average concentration of 24.7 ppb was very close to our observation of 25.5 ppb. The highest concentration from AQMD was 62.9 ppb, which was lower than our value of 84.1 ppb. Standard deviation from AQMD data was 13.3 while ours was 7.57, indicating that our test values were less fluctuating. More NO_2 data from Los Angeles, Long Beach and Costa Mesa on different days and location can also be seen in the chart.

In regular California vehicle gasoline and diesel, sulfur is no long a major pollutant (Kirchstetter et al., 1999). Therefore, on freeways the SO_2 concentration is very low. The highest SO_2 concentrations were observed at the same spot-Vincent Thomas Bridge (Table 2.2). The Vincent Thomas Bridge was originally designed to allow ships to sail under it. Most SO_2 emissions in California come from ocean transportation near ports (Maes et al., 2007). The standard deviation stayed low on freeways and farms, while in Long Beach the standard deviation is higher. This means SO_2 are more controlled and evenly distributed in California except the ports where ships contributed most of the SO_2 emissions.

According to SO_2 data from AQMD monitoring station in Costa Mesa and Los Angeles, SO_2 concentration stayed very low all the time, with an average concentration of 0.24 ppb and 0.85 ppb, respectively.

Contents / Date	Range (ppb)	Average (ppb)	Maximum (ppb)	Standard Deviation	Peak Value Location
NH_3-2016/01/21 Freeways	3.4 - 207.3	65.5	207.3	56.70	Construction zone on CA-91
NH_3-2016/01/21 Route 3 Long Beach	10.7 - 185.4	67.3	185.4	29.82	Next to heavy duty warehouse
NH_3-2016/01/22 Dairy Farm	0 - 1173.0	204.4	1173.0	148.11	Adjacent to a dairy farm
NH_3-2016/01/22 Fixed Site	270.0 -1173.0	407.0	1173.0	183.62	Adjacent to a dairy farm
H_2S -2015/09/17 Freeway & Route 3	0 – 14.0	5.0	14.0	2.66	No obvious events
H_2S -2015/09/17 Dairy Farm	7.0 - 34.0	10.2	34.0	4.78	No obvious events
H_2S-2015/09/17 Fixed Site	8.0 - 19.0	11.8	19.0	2.98	No obvious events

Table 2.3: Agricultural Emissions NH_3 & H_2S

2.5.3 Agricultural Emissions NH_3 & H_2S

In the United States, the largest source of ammonia (NH_3) emissions is livestock, estimated to account for 70–90% of total emissions, and dairy cows are one of the largest livestock sources (Battye et al., 1994). Another important source of ammonia is old vehicles that are not properly maintained of emission regulated (Kean et al., 2000) and ammonia slip for SCR equipped vehicles. It is anticipated that NH_3 concentration near the dairy farms will be higher than that of the California roadways.

In our observation, the average NH_3 concentration on freeways was 65.5 ppb (Table 2.3) with a standard deviation of 56.7, which means on the freeways NH_3 concentration varies spatially likely due to a locally significant source such as a vehicle with high-ammonia slip. The highest concentration recorded on the freeway is 207.3 ppb near a construction area on CA-91 freeway in Corona. On Route 3 in Long Beach, both the average concentration (67.3 ppb) and peak value (185.4 ppb) were close to the freeway concentration, except for the standard deviation. On the Dairy Farm Route, NH_3 concentration climbed up to 1173 ppb when the test vehicle pulled over to a fixed site that was 10 ft away from the cows and the average was around 204.4 ppb. Due to the transient highly elevated level of NH_3, the standard deviation was relatively high during the whole route.

Commercial farm operation is also a major source of H_2S (Lin et al., 2012)). During our test, the average concentration of H_2S was 5 ppb (Table 2.3) on the freeways and twice higher on the farm route (10.2 ppb). The highest concentration observed (34 ppb) was also on the farm route. The standard deviation of H_2S concentration remained low all the time, indicating an evenly distribution on the routes we covered.

Chapter 3

Establishment and Characterization of a Multi-Purpose Large Animal Exposure Chamber for Investigating Health Effects

3.1 Introduction

Air pollution is the presence in the outdoor atmosphere of one or more contaminants, which include particulates, gases, vapors, compounds, or biological materials in

quantities, characteristics and durations that are either damaging to property or injurious to human, plant or animal life. Particulate matter (PM), including PM2.5 (particulate matter with aerodynamic diameter less than 2.5 µm) and coarser particles like dust and pollens, are major atmospheric air contaminants that continue to a pose significant threat to human health (Ziska and Caulfield, 2000; Traidl-Hoffmann et al., 2003; Onishi et al., 2012). In recent years, extensive studies have investigated the resultant health effects of exposure to PM on human and model organisms. Numerous epidemiological studies have consistently demonstrated that air pollution is strongly associated with the morbidity and mortality from multiple cardiopulmonary and lung diseases; results indicate that PM2.5 has far more impacts on health than heretofore recognized (Li et al., 2003, 2008; Pope III and Dockery, 2006; Gehring et al., 2006; Hoek et al., 2013; Raaschou-Nielsen et al., 2013). One major factor is the relatively high deposition fraction of particles smaller than 2.5 µm in all regions of the lungs. The smaller the size of particulate matter, the deeper they travel into the lung; PM2.5 will even reach the alveoli. Inhaled nanoparticles can pass from the lungs into the bloodstream and extrapulmonary organs. Studies in mice have demonstrated an accumulation in the blood and liver following pulmonary exposure to a broader size range of 2∼200 nm (Miller et al., 2017).

This chamber system allows for a route of exposure that simulates naturally occurring inhalation, as opposed to the most common method to study mouse exposures to environmental challenges. In fact, intranasal delivery may not be representative of common exposures. During an intranasal treatment, a mouse is held in a supine position while a micropipette is placed at the external nares and a concentrated solution is trickled in

Chamber Systems	Chamber Type/Size **(L)**	Exposure Duration **(Hrs/day)**
Ye et al., 2017	Nose Only	1 ~ 2
Mainelis et al., 2013	Nose Only	1
Ko et al., 2015	1	0.2
Kang et al., 2004	6.3	6
Hougaard et al., 2008	18	1
Peng et al., 2018	**540**	**24**

Table 3.1: Comparison of Existing Chamber Systems

slowly (Doherty et al., 2012; Zhou et al., 2016). Heightened concerns regarding the use of intranasal treatment, and its lack of relevance to common human exposure modes, has motivated our research aimed at exposing mice via inhalation in this study.

For better understanding the health impacts of air pollution exposure, we constructed a large-scale chamber for exposure to multiple pollutants. Featuring on whole-body exposure, this chamber houses up to 18 mice in separate cages for each experiment (Figure 1) with its large dimension of 540 L, which is much larger than other chambers (Ko et al., 2015; Barnewall et al., 2015). Compared to other chronic exposure chambers featuring nose-only exposures that limits the animal activities and only allow short term exposure for each test (Mauderly, 1986; Kaur et al., 2008), our chamber frees the mice in a natural way of inhalation and delivers 7 consecutive days of exposure until the need of changing beddings or adding food supplies. Using our chamber system, we are capable of uniformly dispersing particles with sizes ranging from coarse mode particles (e.g., dust) to fine particulate matters (nano-size particles) at controlled size distributions and concentrations, while maintaining stability.

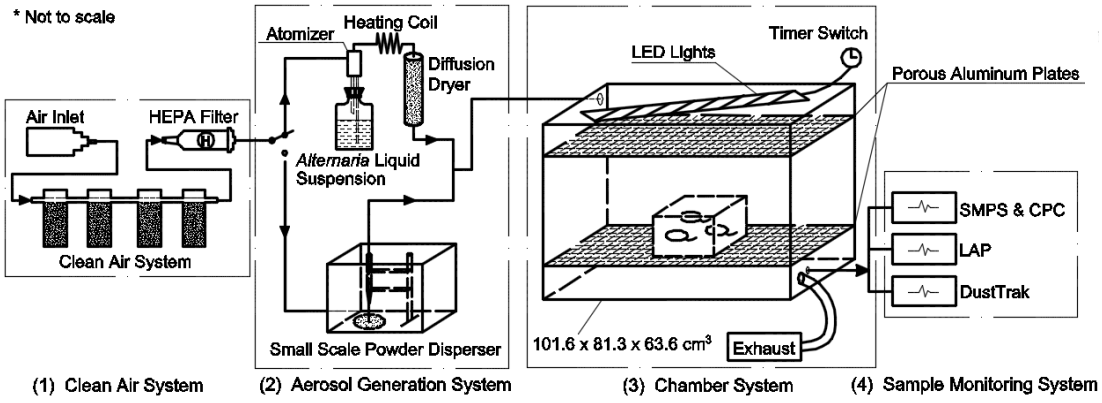

Figure 3.1: Schematic of the chamber system

The chamber system includes four main components: (1) Clean air system; (2) Aerosol generation system; (3) Chamber system; (4) Sample monitoring system.

3.2 Chamber description

3.2.1 Clean air system

Lab compressed air is passed through a filter system prior to entering an Atomizer/Particle Disperser (Figure 1). The filter system consists of silica gel (absorbs water moisture), activated carbon (absorbs organics), hopcalite (absorbs CO), purafil (absorbs NOx) and a HEPA Filter (absorbs 99.97% of airborne particles). The total flowrate of the nebulizer injection system is 6L/min while the SSPD injection system flowrate ranges from 12 to 20 L/min. When flushing the chamber with clean air before/after each experiment, Organics, CO and NOx concentration were below the detection limit of the Hydrocarbon/CO/NOx gas analyzer.

3.2.2 Aerosol generation system

The aerosol generation system consists of two parts, including a house-built atomizer for generating aerosol sprays from multiple liquid solutions and a Small Scale Powder Disperser for dispersing dry powder from the surface of a turntable.

Atomizer for nanoparticles

A stainless-steel atomizer generates aerosol from an ultrapure water solution of target pollutants. Compressed air passes through an orifice that creates an air jet which breaks up the solution, which is then sucked up via reduction of static pressure, generating a continuous wet aerosol spray from the solution(May, 1973). The wet aerosol is then routed through a heated copper coil at 127 $^{\circ}F$ to transform water moisture into vapor, which is absorbed when passed through a diffuser dryer filled with indicator silica gel, replaced daily. This is to provide a pure particle dose in nano-size range since the nebulizer aerosol spray produces a particle size at micron level. The dried aerosols are subsequently injected into the second component, the mouse chamber. The atomizer design continuously delivers nano-size aerosol with consistent size distribution and mass concentration throughout the exposure period. Mass concentration is controlled through the concentration of aqueous solution.

Small Scale Powder Disperser (SSPD)

An SSPD from TSI (Model 3433, TSI, Minnesota, USA) was used to disperse target pollutants in powder forms, which are insoluble in water, as well as micron-size particles from 0.5 µm to 50 µm efficiently. Powders were loaded on a turntable that rotates

at speeds ranging from 0.25 to 3.3 rev/hour. A stainless-steel capillary positioned just above the turntable removes powder from the surface of a turntable; the shear forces created by two flows deagglomerates the powder, which enters an expansion cone and is exhausted from the instrument and then enters the chamber. In this design, the SSPD delivers a continuous powder aerosol dose for four hours for each loading of powder on the turntable. Exposure times and mass concentrations are controlled by changing the rotation speed of the turntable.

3.2.3 Chamber system

The mouse chamber is made of 6 clear acrylic sheets with a thickness of ¼ inch. The total chamber volume is approximately 540 L with external dimensions of 101.6 x 81.3 x 63.6 cm^3 (length x width x height). Two porous aluminum plates were used to help deliver uniform dispersion by separating the aerosol inlet (upper left) and sampling ports (lower right). The large size of the chamber allows up to six mouse cages (carrying up to three mice each under normal laboratory conditions) to fit in simultaneously for exposure tests. An LED warm light string attached to a timer switch simulates a light cycle for experimental mice daily by switching on at 7 a.m. and off at 7 p.m.

To avoid light contamination, the whole chamber is covered with a customized blackout cloth and a small detachable window allows observance of mice during the exposure tests. A ¼ inch inlet from the upper left of the chamber was used for injection while four ½ inch exhaust ports located in the lower right chamber ensured that the in-chamber pressure would not build up during aerosol injection. Another ¼ inch outlet located below the exhaust tubes was used for sampling monitoring. Before and after each test, the chamber

was flushed with particle free air of at least ten chamber volumes to avoid contamination.

3.2.4 Sample monitoring systems

Three instruments were attached to the chamber sample port to monitor the experiments.

Size Distribution and concentration measurements

Aerosol size distribution and concentration during the experiments are recorded by two different instrument systems. The Scanning Mobility Particle Sizer (SMPS) (Series 3080, TSI, Minnesota, USA) and Condensation Particle Counter (CPC) (Model 3776, TSI, Minnesota, USA) system is used to measure particles in the range of 2 nm to 1000 nm while the Laser Aerosol Particle Size Spectrometer (LAP) (TOPAS, Germany) provides information of particle size ranging from 0.2 µm to 40 µm. The SMPS-CPC system is widely used as a standard method for characterization of particles smaller than 1 µm in diameter with high resolution of up to 167 channels (Wang and Flagan, 1990; Mulholland et al., 2006). The LAP served as a supplemental instrument for detecting micron size particles with high resolution of up to 128 channels.

Total PM mass concentration measurements

The DustTrak^{TM} (TSI, Minnesota, USA) Aerosol Monitor provides real-time aerosol mass readings using a light-scattering laser photometer. When equipped with different size impactors, the DustTrak measures aerosol concentrations corresponding to PM1, PM2.5 or PM10, ranging from 0.001 to 400 mg/m^3.

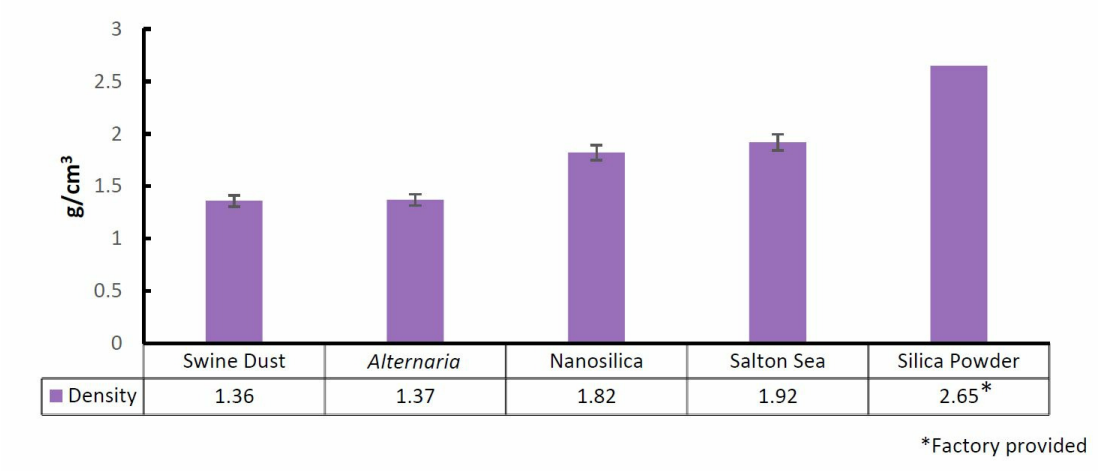

Figure 3.2: Densities of five target particle suspension

Density data was obtained using an Aerosol Particle Mass Analyzer (APM)/Scanning Mobility Particle Spectrometer (SMPS) setup, which has been modified to achieve higher transmission of particles and improved sampling frequency (Malloy et al., 2009).

3.3 Target Pollutants

Multiple target pollutants, either field collected samples (swine dust/Salton Sea samples) or industrial products (Nanosilica/*Alternaria*/Silica powder), were injected into the chamber through the aerosol generation system. While the dry silica powder with the highest density (Figure 2) was dispersed using the SSPD 3433, other targets were nebulized from aqueous solutions and their size distributions can be found in Figure 6. The purpose of nebulizing targets that are soluble in water was to consistently produce nano-size particles with stable size distribution and mass concentration regardless of their density, instead of reproducing environmental particles in their original physical properties. All five particle suspensions in the chamber were of a size distribution to allow deep penetration into the

lungs and even potential penetration into the bloodstream and extrapulmonary organs.

Fungal extract solution

The fungus *Alternaria* alternata is a common allergen, widespread in many indoor and outdoor habitats, found to thrive on various types of vegetation. Contact with this fungus is unavoidable, given that *Alternaria* produces thousands of spores per cubic meter of air (Gabriel et al., 2016; Knutsen et al., 2012). *Alternaria* poses a general health threat as one of the most abundant sources of aeroallergens known to trigger immune sensitization and as a primary risk factor for the development of asthma. Furthermore, exposure to *Alternaria* alternata in previously sensitized individuals is correlated with a severe increased risk of morbidity and a higher risk of fatal asthma attacks (Bush and Prochnau, 2004; Gabriel et al., 2016; Knutsen et al., 2012; Vianello et al., 2016). In children raised in desert environments, natural exposure to *Alternaria* spores induces allergic rhinitis symptoms and serves as a major allergen causing juvenile allergic asthma (Andersson et al., 2003; Bush and Prochnau, 2004; Gabriel et al., 2016; Halonen et al., 1997; Knutsen et al., 2012). In this study, we nebulized an *Alternaria* extract solution and monitored the size distribution of *Alternaria* aerosol using the SMPS.

Salton Sea dust

Salton Sea-adjacent airborne particles we obtained by using passive collectors consisting of Teflon-coated round pans (25.4 cm in diameter) filled with quartz marbles suspended from the pan bottom with Teflon mesh, and capped with two overarching crossbraces covered in Tanglefoot to discourage roosting by birds(Aciego et al., 2017). All ma-

terials in contact with dust (i.e., pan, marbles, and Teflon mesh) were pre-washed prior to installation using first bleach, then distilled 2 M HCl, and finally distilled 3 M HNO_3 with rinses of >18.2 MΩ·cm water between each reagent cleaning step. The collectors were deployed on 2.4 m tall wooden posts in open areas at each on the field sites to minimize local contributions of material from wind-suspended soil (i.e., from saltation) and nearby trees. Collectors were deployed continuously from December 2015 through March 2017 at the Dos Palmas Preserve, at 33°29'22.1"N 115°50'06.3"W. To recover dust samples from each collector in March 2017, we rinsed the marbles with >18.2 MΩ·cm water into the Teflon-coated pan, removing the marbles and mesh, then transferring the water and dust suspension to pre-cleaned 1 L LDPE Nalgene bottles. The samples were frozen and stored either at -20 or 4 $°C$ until use.

Swine facility dust

Dusts were also collected from swine concentrated animal feeding operations and prepared into a sterile aqueous extract solution(Romberger et al., 2002). Briefly, settled surface dusts were collected off horizontal surfaces within swine confinement facilities (500 $\sim$ 700 animals per facility). Collections were obtained from surfaces located approximately three feet above the floor of the facilities. Dusts obtained in this manner are routinely characterized for major determinants, including endotoxin and muramic acid concentrations to determine relative uniformity of samples across collection facilities and seasons. Detailed analyses of these and other determinants have been previously published(Poole et al., 2008, 2010; Boissy et al., 2014). Following collection, dust samples were placed in a buffered

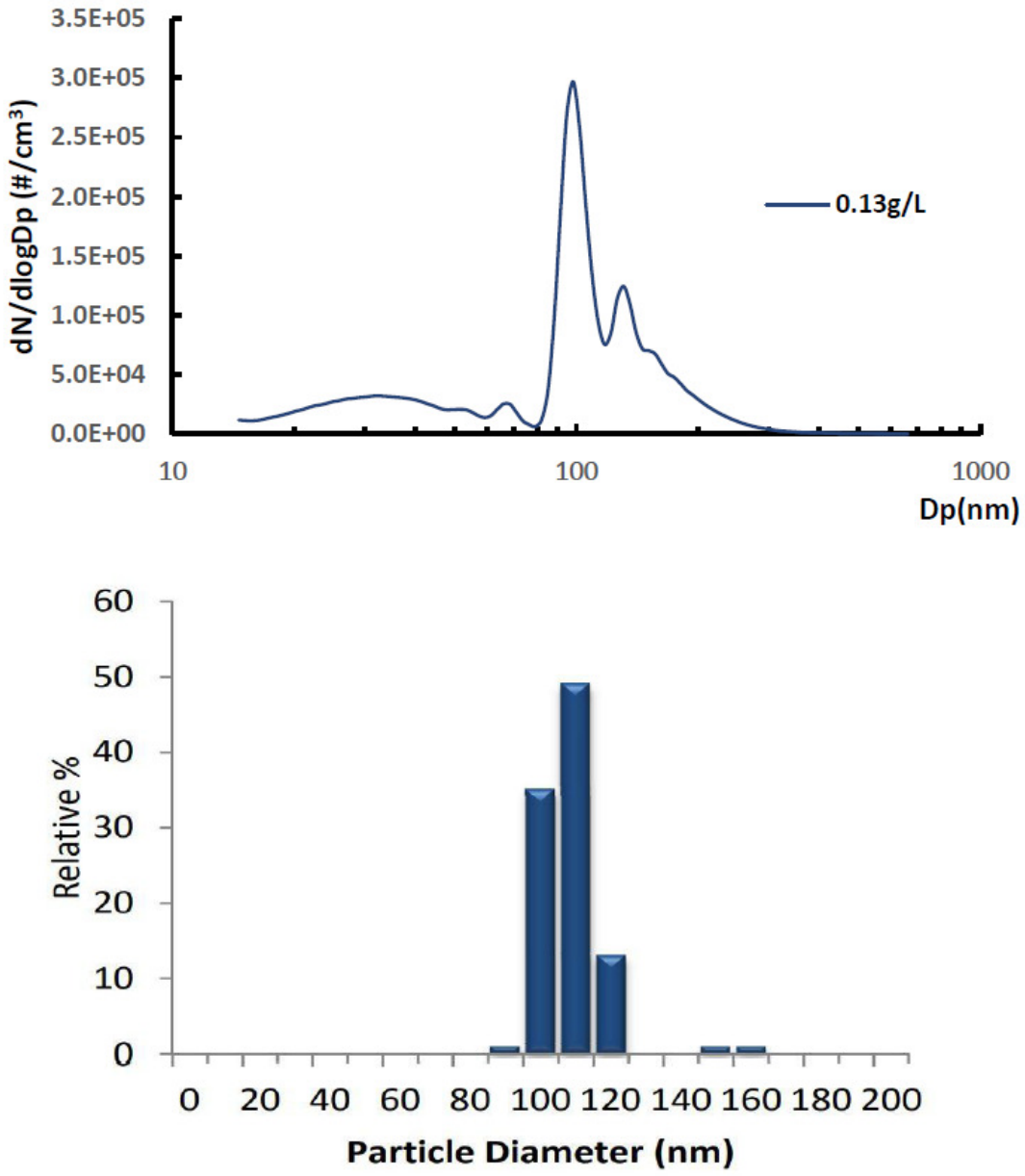

Figure 3.3: Factory provided and lab nebulized nano-silica

Size distribution comparison of factory provided and lab nebulized nano-silica size distribution.

saline solution at 100 mg/mL concentration. Following a 1-hour incubation, samples were centrifuged to pellet all course particles and the supernatant fractions were filtered through a 0.22 micrometer pore filter. Aqueous extracts obtained following filtration were considered a 100% stock concentration and were frozen at -20 $°C$ until use.

Nanosilica and ground silica powder

The 100 nm Non-Functionalized NanoXact^{TM} Silica (nanoComposix Inc, California, USA) are produced via the condensation of silanes form nanoparticles that consists of an amorphous network of silicon and oxygen and the particles are monodisperse with narrow size distributions. The particles are readily suspended in polar solvents such as water and ethanol.

The MIN-U-SIL 5 GROUND SILICA powder (Western Reserve Chemical, Ohio, USA) is a natural, fine ground silica with high purity. The consistent pH and narrow size distributions allow very high loading with minimal effect on viscosity and cure rate versus synthetic silicas. The high quality, inert, white crystalline silica is available in five size distributions (5, 10, 15, 30, and 40 µm topsize). The comparison of the factory provided silica particle distribution and the lab nebulized distribution can be found in Figure 3.

3.4 Results and Discussions

3.4.1 Mass concentration across the chamber

Figure 4 shows the PM2.5 concentration of aerosolized ammonium nitrate (NH_4NO_3) solution in six different locations of the chamber plate with a standard deviation of 1.97.

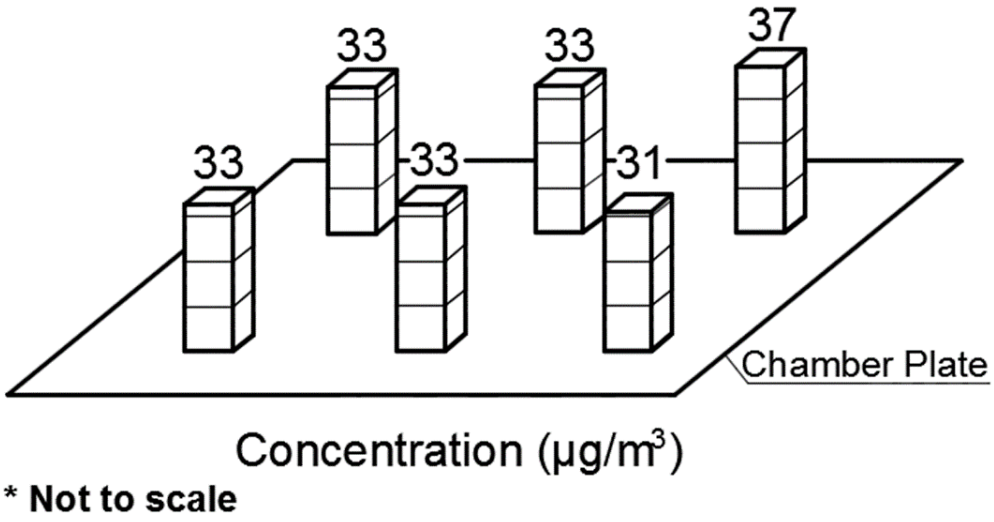

Figure 3.4: Mass concentration across the chamber (Peng et al., 2018)

Mass concentration across the chamber (Peng et al., 2018). Reproduced with permission from Peng, X., Madany, A. M., Jang, J. C., Valdez, J. M., Rivas, Z., Burr, A. C., ... Lo, D. D. (2018). Continuous Inhalation Exposure to Fungal Allergen Particulates Induces Lung Inflammation While Reducing Innate Immune Molecule Expression in the Brainstem. ASN Neuro. https://doi.org/10.1177/1759091418782304. Copyright 2018 ASN Neuro.

The DustTrak was placed inside the chamber at six locations, with the sampling port at the height of ∼10 cm to simulate mouse breathing conditions in the cages. Overall, the chamber could deliver uniform dispersion within the two porous aluminum plates that separated the aerosol inlet and the exhaust.

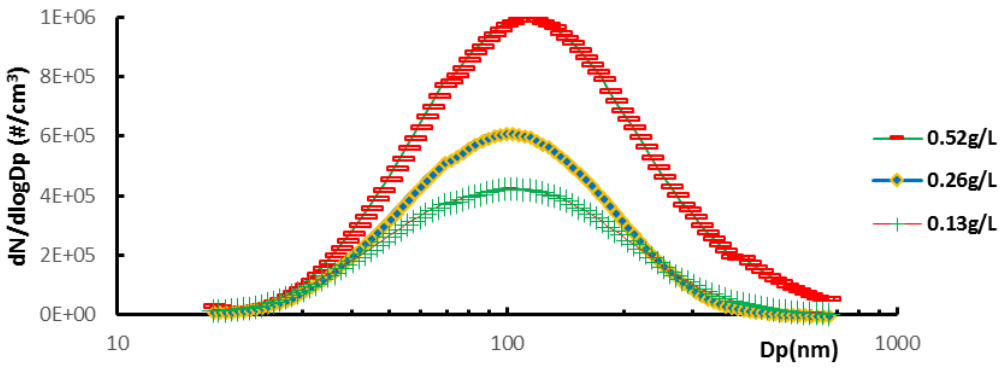

Figure 3.5: Size distribution of *Alternaria* aerosol in three different levels

The Y axis stands for particle number concentration dN/dlogDp (#/cm^3) while the X axis represents particle size on a logarithmic scale.

3.4.2 Nebulized aerosol suspension in different levels

The concentration of aerosol suspension in the chamber (Figure 5) could be controlled through changing the aqueous solution concentration, resulting in different levels of mass concentration. Three different aqueous solution concentrations of *Alternaria* extract of 0.13 g/L, 0.26 g/L and 0.52 g/L were nebulized into the chamber through an atomizer. The size distribution was acquired through the SMPS. The higher solution concentration leads to higher total number concentration in the chamber aerosol suspension without significantly changing the particle mode diameter of 100 nm.

Four different types of target pollutants were nebulized into the chamber at a controlled number/mass concentration (Figure 6 & Figure 7). While the mode diameters of these aerosol range from 53 nm to 109 nm, all of them can pass from the lungs into the bloodstream and extra-pulmonary organs. Higher number concentration does not always result in higher mass concentration since larger size particles dominate the total mass

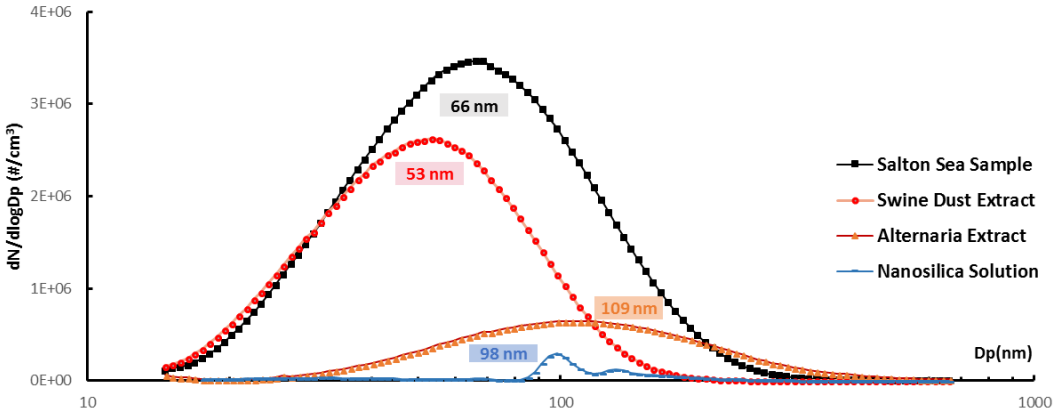

Figure 3.6: Multiple size distribution comparison

Size distribution comparison of four different nebulized target pollutants from SMPS.

concentration. For example, the swine dust extract had a much lower total mass concentration than that of the *Alternaria* extract (Figure 7) even though it had significantly higher number concentration (Figure 6).

Mass concentration could be controlled from the micro gram per cubic meter range to milligram per cubic meter range (Figure 7). The chamber was saturated with continuous aerosol injection and remain consistent throughout the whole experiment, providing a much more effective and protracted dose delivery than the intranasal method. We have conducted separate tests with animal subjects for a full week exposure. For the 3 exposure tests where target concentration was $1.5\,\mathrm{mg/m^3}$, we measured an average concentration of $1.47 \pm 0.03\,\mathrm{mg/m^3}$; For the 8 exposure tests where target concentration was $1.3\,\mathrm{mg/m^3}$, we measured an average concentration of $1.2 \pm 0.13\,\mathrm{mg/m^3}$.

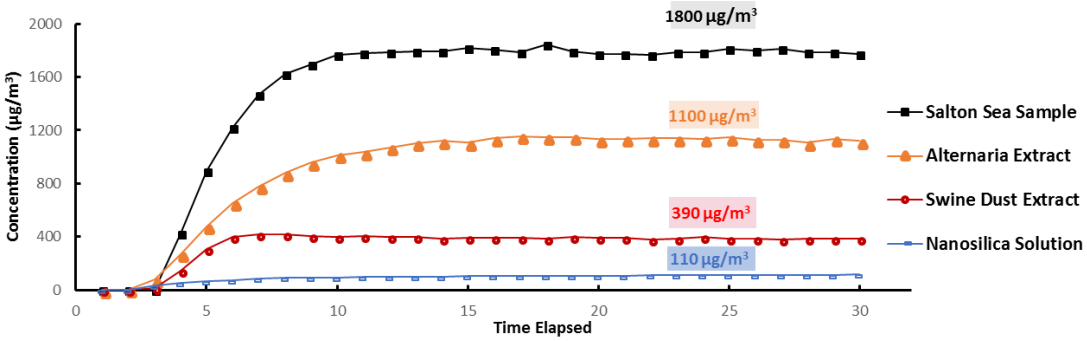

Figure 3.7: Mass concentration of target pollutants in nanosize

Consistent mass concentration of target pollutants over time.

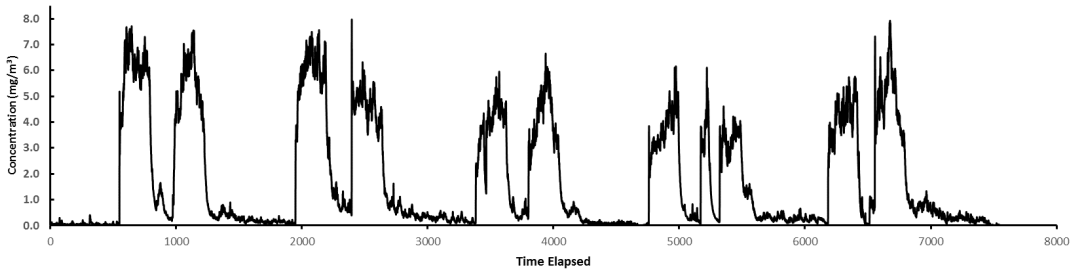

Figure 3.8: Mass concentration of powder silica aerosol

Mass concentration of powder silica aerosol throughout the five-day exposure.

3.4.3 Powder-silica aerosol from SSPD 3433

Occupational exposures in different trades range from the lowest on operation engineers (0.075∼0.720 mg/m^3) to the highest on painters (1.28∼13.5 mg/m^3)(Rappaport et al., 2003), which significantly exceeds the US Occupational Exposure Limit (OEL) of 0.05 mg/m^3 for respirable silica(Linch et al., 1998).

To simulate exposures to respirable silica among construction sites in the USA, two 4-hour silica doses were injected into the chamber each day (Figure 8). The first dose

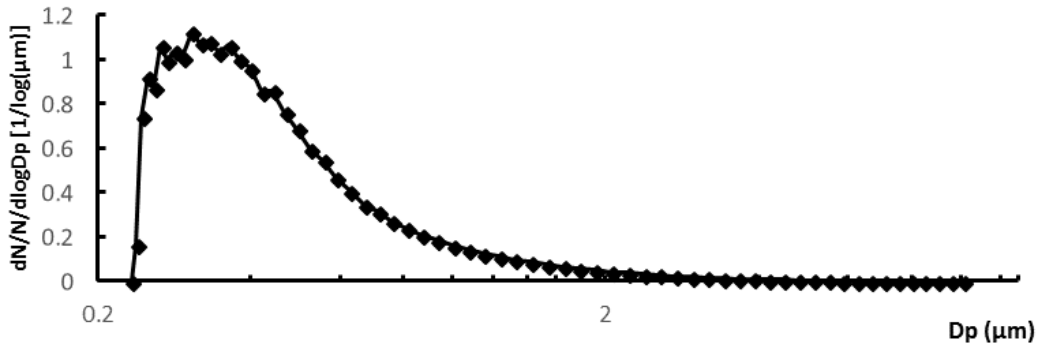

Figure 3.9: Size distribution of powder silica aerosol

The vertical axis stands for particle number distribution dN/N/dlogDp [1/log(µm)] while the horizontal axis represents particle size on a logarithmic scale.

was given from 8 a.m. to 12 p.m. while the second dose was given from 4 p.m. to 8 p.m. Figure 8 shows ten doses injected over 5 days with average dose concentration of around $5\,\mathrm{mg/m^3}$ and the overall average concentration was $1.43\,\mathrm{mg/m^3}$. Figure 9 shows the size distribution of dispersed silica powder with a mode of around 306 nm.

3.5 Conclusion

Here we developed a large-scale multipurpose animal exposure chamber for health effects investigation of air pollutants. Compared to other chamber systems featuring nose-only or activity-limited whole-body exposure, this system provides continuous exposure through the natural inhalation route at controlled concentration, size distribution and duration for both chronic, sub-chronic and acute epidemiological studies. Our method is also

easily reproducible and has the potential to mimic the real atmospheric environment by adding multiple air contaminants at the same time for health investigations.

Chapter 4

Continuous inhalation exposure to fungal allergen particulates induces lung inflammation while reducing innate immune molecule expression in the brainstem

4.1 Introduction

For much of the 20th century, the brain was viewed as immunologically separate from the rest of the body (Carson et al., 2006; Cunningham, 2013; Czirr and Wyss-Coray, 2012; Perry, 2010). However, triggering acute or chronic systemic inflammation with viral,

bacterial and manmade toxicants is now well described to induce innate immune responses within the central nervous system (CNS) (Bilbo et al., 2018; Calderón-Garcidueñas et al., 2016; Cole et al., 2016; Cunningham, 2013; Jayaraj et al., 2017; Ljubimova et al., 2018; Mumaw et al., 2016; Perry, 2010). Less studied are the neuroinflammatory consequences of airborne allergens (Klein et al., 2016).

Airborne allergens trigger both acute and chronic pulmonary inflammation and rhinitis in a large proportion of the human population at times in which the brain is still developing (childhood) through times in which the brain is at increased susceptibility for neurodegenerative disease (for example, as with advancing age; Croston et al., 2018; Ghosh et al., 2013; Kader et al., 2018; Klein et al., 2016). Indeed, in animal model systems, chronic exposure to allergens has revealed consequences for altered behavior including impaired learning and memory in the Morris water maze, disturbed long-term potentiation in the hippocampal CA1 region and reduced cell proliferation in the hippocampal neurogenic niche (Guo et al., 2013; Klein et al., 2016). As yet, it is unknown to what extent altered behavior might be due to innate (non-lymphocyte) immune responses versus adaptive (lymphocyte) immune responses in the CNS.

Because systemic (non-CNS) exposure to bacterial components triggers an innate (non-T cell) immune response in the CNS, it is expected pulmonary that innate immune responses to allergens would similarly trigger innate inflammation in the CNS. However, immune responses to antigens including allergens are dependent on the route of administration, the composition of the antigen and whether antigens are administered in the presence or absence of immune activating adjuvants. In the case of antigens administered via inhala-

tion, the size of the aerosolized particulates also can modulate the immune response (Jayaraj et al., 2017; Ljubimova et al., 2018; Kumar et al., 2014). Most studies examining the CNS consequences of allergic inflammation use neither natural allergens nor an inhalation route of exposure. Instead they most often use repetitive injections of non-allergen antigens often in the presence of adjuvants. The repetitive treatment with adjuvant associated antigens is especially confounding because adjuvants by themselves can trigger neuroinflammatory responses in the CNS (Cunningham, 2013; Czirr and Wyss-Coray, 2012; Perry, 2010).

Natural allergens are characterized by multiple characteristics (Kumar et al., 2014). They are proteins often stably desiccated and delivered as part of a larger particle. They are low molecular weight, able to be eluted from the larger particle in the "wet" environment of the lung, are recognized by pathogen associated molecular pattern (PAMP) receptors on innate immune cells and often have protease activity. However, many studies focusing on the consequences of allergic inflammation use model systems in which the adaptive immune system (T cells) are primed to respond to a non-allergen antigen such as ovalbumin (OVA) by repetitive intravenous, intraperitoneal or subcutaneous injections in the presence of adjuvant over a period of one to three months. The allergic adaptive immune response is triggered in these model systems by subsequent acute or chronic intranasal administration of the antigen in solution (Doherty et al., 2012; Klein et al., 2016; Ploix et al., 2009; Zhou et al., 2016). Natural allergen exposure usually occurs by continuous low dose exposure in the absence of adjuvant based priming. Substantially different inflammatory mechanisms are known to be triggered by this type of administration frequency than by single or multiple discrete deliveries of high antigen doses (Bonam et al., 2017; Kumar et al., 2014). Furthermore,

with an intranasal treatment, the mouse is subjected to either the stress of restraint or anesthesia while held in a supine position as a micropipette is placed at the external nares and a concentrated solution is trickled in slowly (Doherty et al., 2012; Ploix et al., 2009; Zhou et al., 2016). Thus, it is likely that pathologic mechanisms elicited by intranasal application (+/- sensitization) may not be representative of natural inhalation exposure to environmental airborne allergens.

Several studies have examined the consequences of inhalation exposure to natural allergens, including plant pollens, fungal allergens, and arthropod antigens but the focus of these studies has primarily been on induction of pulmonary inflammation (Gabriel et al., 2016; Gold et al., 2017; Knutsen et al., 2012; Kubo, 2017). By contrast, most studies examining the CNS consequences of inhalation exposure have focused on the effects of airborne pollutants instead of allergens (Bilbo et al., 2018; Calderón-Garcidueñas et al., 2016; Cole et al., 2016; Gackière et al., 2011; Heusinkveld et al., 2016; Jayaraj et al., 2017; Levesque et al., 2011; Ljubimova et al., 2018; Mumaw et al., 2016). These studies demonstrate that in the absence of priming, the inhalation route of exposure is effective at inducing both systemic and CNS inflammatory responses. While the composition of these airborne toxicants is an important determinant in triggering inflammation, particle size is also an important determinant. In animal models as well as in human epidemiological studies, it is apparent that pollutants in the ultrafine (particle size < 2.5 µm) and ultrafine (particle size < 0.1 µm) size range are highly implicated in contributing to observed effects on the CNS.

Taken together, these types of studies have clearly demonstrated the potential for allergic responses to modify the inflammatory environment and potentially the function of

the CNS. However, as yet, the CNS consequences of natural airborne allergens administered via inhalation are infrequently examined. Therefore, here we chose to test the consequences of continuous inhalation exposure to fungal Alternaria alternata particulates. Alternaria alternata is a known common allergen found to thrive on various type of vegetation. It is virtually impossible to avoid contact with Alternaria alternata since its spores can reach levels of thousands of spores per cubic meter of air and can be found both indoors and outdoors (Gabriel et al., 2016; Knutsen et al., 2012). As a general health risk, Alternaria alternata is considered one of the most abundant sources of airborne allergens, readily triggers immune sensitization and is a primary risk factor for development of asthma. Furthermore, Alternaria alternata exposure in previously sensitized individuals is correlated with severe increased risk of morbidity and a higher risk of fatal asthma attacks (Bush and Prochnau, 2004; Gabriel et al., 2016; Knutsen et al., 2012; Vianello et al., 2016). It is also a major allergen for asthma in children raised in desert environments and natural exposure to Alternaria alternata spores also induces allergic rhinitis symptoms (Anderson et al., 2003; Bush and Prochnau, 2004; Gabriel et al., 2016; Halonen et al., 1997; Knutsen et al., 2012).

Finally, studies examining the consequences of airborne exposure to manmade toxicants have demonstrated that CNS inflammation is triggered prior to the development of a mature adaptive immune response (occurring >96 hours of exposure). By contrast, studies focusing on the CNS consequences to allergens have focused primarily on the consequences of chronic or long term inflammation comprised of ongoing adaptive immune responses driving innate immune responses (Doherty et al., 2012; Ghosh et al., 2013; Kubo, 2017; Kumar et al., 2014). The type of innate inflammation induced by the initial exposure to

an immune stimulant, shapes qualitatively and quantitatively the subsequent T cell, B cell and antibody responses to the initial immune stimulant (Kumar et al., 2014).

Therefore, in this study, we designed and constructed a new whole body exposure chamber that allows us to conduct in vivo continuous exposure studies for inhaled toxicants. Exposure times in other model systems are often limited to repetitive short term exposures (example, 4-5 hours per day for 3-5 days per week for a periods up to several months; Barnewall et al., 2015; McDonald et al., 2010; Roy et al., 2003; Roy and Pitt, 2006; Ye et al., 2017). By contrast, whole body exposures could be continuous over days because the construction parameters of our new whole body chamber system maintained ammonia levels well below levels required for optimal murine husbandry (Rosenbaum et al., 2009). Using this model system, we can investigate health effects of aerosolized materials without restricting animal movement or feeding behavior. The system provides controlled and well characterized whole animal exposures where dosage is by inhalation of particle suspensions that more closely mimics natural airborne exposure in contrast to the more commonly used intranasal applications of dilute solutions of particulate material or movement restricting nose cone administration of inhaled particulates (Barnewall et al., 2015; McDonald et al., 2010; Roy et al., 2003; Roy and Pitt, 2006; Ye et al., 2017). Using this chamber, we describe the effects of continuous extended exposure to fine particle Alternaria allergen aerosol suspensions on inflammation in the lung and CNS. To our knowledge, this study is the first to test the consequences of this prevalent health related airborne allergen on the brain's innate immune status. Strikingly we find that despite inducing overt lung inflammation with eosinophilia characteristic of innate immunity preceding allergic (hypersensitivity type

1) lymphocyte responses, we did not induce pro-inflammatory innate immune activation with the brain (Doherty et al., 2012; Ghosh et al., 2013; Kubo, 2017; Kumar et al., 2014). Instead, we observed a decrease in basal expression of select innate immune molecules in the region of the brain regulating respiration reminiscent of the phenomenon associated with endotoxin tolerance (Collins and Carmody, 2015; Nomura et al., 2000; Pena et al., 2011; Rajaiah et al., 2013).

4.2 Material and Methods

4.2.1 Animals

Male C57Bl/6J mice (8-12 weeks old) were maintained in standard mouse cages with fresh bedding and standard Purina food chow for the duration of each experimental exposure. All experiments were performed in compliance with University of California IACUC regulations and review.

4.2.2 Mouse Chamber

The chamber was made of clear acrylic sheets with internal dimensions of 40 x 32 x 25 $inch^3$ (length x width x height) for approximately 540 liter in volume (Figure 4.1). Inside the chamber, two perforated aluminum plates separated the inlet (upper left) and the outlet (lower right) to enable uniform dispersion of injected aerosols. The large size of the chamber accommodates up to six mouse cages simultaneously for exposure tests. On the top of the chamber, an LED warm light string was attached to a timer switch to provide a 12:12 hour light cycle. The whole chamber was covered with black-out cloth to

ensure zero light contamination from outside. A ¼ inch inlet from the upper left of the chamber was used for injection while four ½ inch exhaust ports located in the lower right chamber ensured that the in-chamber pressure remained the same as atmospheric. Another ¼ inch outlet located in the lower right of the chamber was used for instrument sampling and monitoring. The chamber was flushed with clean air with at least ten chamber volumes before and after each test to avoid contamination.

4.2.3 Aerosol Generation

Lab compressed air passed through a clean air system consisting of silica gel (to absorb water moisture), activated carbon (to absorb organics), hopcalite (to absorb CO) and purafil (to absorb NOx). Pressure at both the inlet and outlet of the clean air system were monitored and controlled by a pressure regulator. During the test, the inlet pressure remained controlled at 60 psi while the outlet pressured was 25 psi, resulting in an aerosol flow at 6 L/min (monitored by a mass flow controller) coming out of the nebulizer. The nebulizer converted Alternaria liquid particulate solution into an aerosol spray (May, 1973) and the spray went through a diffusion dryer for physical absorption of water vapor.

4.2.4 Sample Monitoring System

Four instruments were attached from the sample port of the chamber. Aerosol concentration and size distribution were monitored by a Scanning Mobility Particle Sizer (SMPS). The SMPS is widely used as a standard method for characterization of particles smaller than 1 µm in diameter (Wang and Flagan, 1990; Mulholland et al., 2006). It

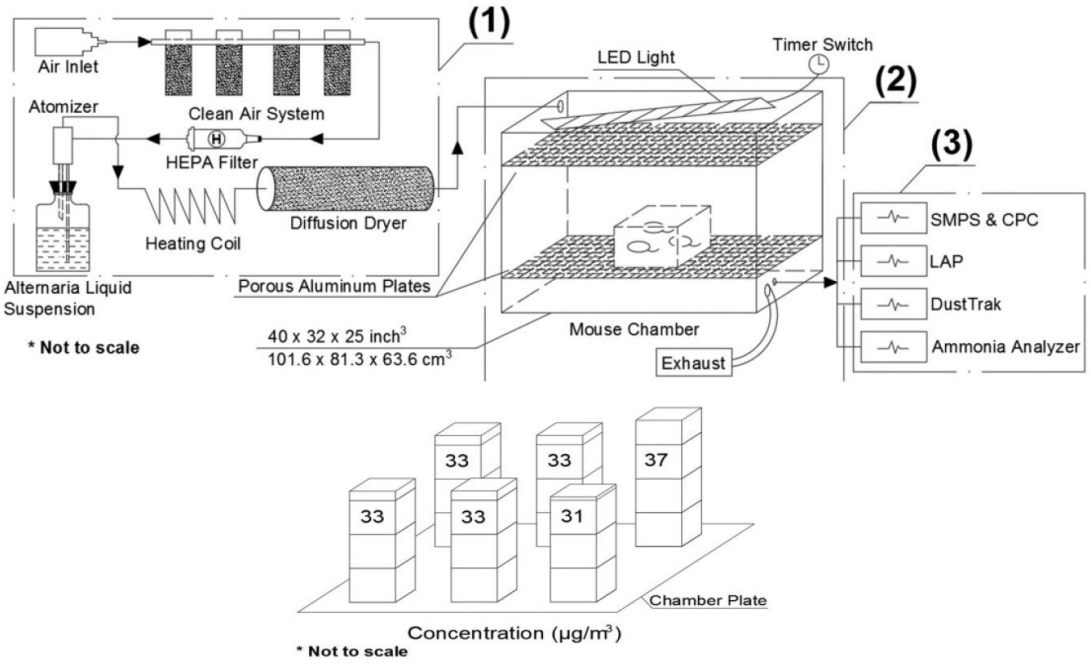

Figure 4.1: Exposure chamber design

Exposure chamber design. (a) Schematic design of the mouse chamber system. The system includes three main components of the mouse chamber system: (1) the aerosol generation system, (2) the exposure chamber, and (3) the aerosol monitoring system. (b) Chamber characterization data: SMPS data showing distribution of particle concentrations across the chamber. HEPA = High Efficiency Particulate Air; SMPS = Scanning Mobility Particle Sizer; CPC = Condensation Particle Counter; LAP = Laser Aerosol Particle Sizer.

provides size from 2 to 1000 nm with high resolution (107 channels). A Condensation Particle Counter (CPC) was used to measure airborne particle number concentration for the SMPS to provide overall particle size distribution. The Laser Aerosol Particle sizer (LAP) served as a supplemental instrument for monitoring particle size ranging from 200 nm to 40 µm with high resolution of up to 128 channels. A DustTrak (TSI) provided information about the total PM2.5 concentration. A modified ammonia (NH_3) analyzer provided measurements of the NH_3 level inside the chamber.

4.2.5 Operation of the Chamber: Biological Material Introduction and Dose Preparation

Lab compressed air passed through a clean air system before entering an atomizer. A stainless-steel atomizer generated aerosols from a 0.26 g/mL solution of Alternaria particulate in ultrapure water. The wet aerosol passed through a heated copper coil at 52°C to transform water moisture into vapor and the water vapor was absorbed by passing through a diffuser dryer filled with indicating silica gel, which was replaced daily. The dry aerosol was subsequently injected into the mouse chamber. The chamber held mice in conventional mouse cages with wire tops to hold food as well as enable free flow of air into the cages, and hydrogel containers in the bottom to provide water along with conventional wood shaving bedding. Injected aerosols were shown to saturate the chamber with Alternaria particulates by 2 hours of continuous injection. In this study, tests continued for 96 hours with continuous aerosol injection. During the injection period, instruments monitored the aerosol concentration and size distribution, as well as the overall Particulate Matter (PM) concentration. To ensure that mice would not be affected by lung irritation

from ammonia accumulation within the chamber during the time of the experiment, we used continuous air injection at a rate greater than 1 full volume change per hour. At the end of the exposure period, ammonia levels were monitored to ensure that the mice were under a non-toxic environment. The chamber was flushed with clean air of at least ten chamber volumes before and after each test to avoid contamination.

4.2.6 Lung Histology and Bronchio-Alveolar Lavage Cell Counts

Bronchio-alveolar lavage (BAL) cells and fluid were recovered through intra-tracheal washing with 2x 0.75mL of ice cold PBS as previously described (Chen et al., 2016). Cells were recovered by centrifugation followed by red blood cell lysis. BAL cells were then counted, cytocentrifuged (1,000 RPM, 5 minutes) onto a glass microscope slide, stained with hematoxylin and eosin, and differential counts performed based on cell morphology and stain. For each sample, >150 cells were counted from five total frames of view spread throughout the microscope slide at 40x magnification. Following BAL washing, lungs were inflated with 0.75 mL 1 part 4% PFA/30% sucrose and 2 parts OCT and stored overnight in 4% PFA at 4°C for lung histology and immunofluorescence. After 24 hours, lungs were removed from 4% PFA and incubated another 24 hours in 30% sucrose. Lungs were then blocked in OCT and sectioned at 10 µm. H&E-stained lung sections were blindly scored at 20x magnification on a 1-5 scale with 5 being the most severe score of pathology using criteria of leukocyte infiltration and aggregation of leukocytes into the bronchioles (1-5) and vascular inflammation/endothelial cell hyperplasia (1-5) visualized by thickening of endothelial cells surrounding the vasculature for a total score out of 10 as previously described. Scoring of the lung section was based on the total area affected: 1 – absent, 2 – slight, 3

– moderate (covering up to 5% of total area), 4 – marked (>5% and <10% of total area), and 5 – severe (covering ≥10% of total area). For immunofluorescence staining, sections were incubated with rabbit anti-RELMα (0.5mg/mL Peprotech), at room temperature for 2 hours. Then sections were incubated with the appropriate fluorochrome-conjugated secondary antibody for 2 hours at room temperature and counterstained with DAPI. Sections were visualized under a Leica microscope (DM5500 B).

4.2.7 Enzyme-Linked Immunosorbent Assay

Greiner 96-well plates were coated with primary antibodies to RELMα (Peprotech, 1µg/mL) overnight at room temperature. After blocking the plates with 5% newborn calf serum in PBS for 1 hour, sera, BAL fluid or tissue homogenates were added at various dilutions and incubated at room temperature for 2 hr. Detection of RELMα was done with biotinylated antibodies (Peprotech, 2.5µg/mL) for 1 hour, followed by incubation with streptavidin-peroxidase (Jackson Immunobiology) for 1 hour in the dark. The peroxidase substrate tetramethylbenzidine (TMB; BD Biosciences) was added followed by addition of 2N H_2SO_4 as a substrate stop, and the optical density (OD) was captured at 450 nm. Samples were compared to a serial-fold dilution of recombinant protein.

4.2.8 Quantitative Polymerase Chain Reaction Analysis

In brief, the medulla and the rest of the brain from each mouse were separately homogenized and total RNA was extracted using Trizol (Invitrogen, Carlsbad, CA, USA) as previously described (Hernandez et al., 2016). Following RNA extraction, first strand cDNA was synthesized per the conditions outlined in the cDNA synthesis kit (GE health-

care, Pittsburgh, PA, USA). Only samples with RNA and cDNA quality verified by presence of ribosomal bands and appropriate levels of HPRT per ug cDNA were used for subsequent qPCR analysis. qPCR analysis was performed as previously described using a CFX96 Real Time PCR Detection System (Bio-Rad Laboratories, Hercules, CA, USA). The relative number of transcripts per hypoxanthine guanine phosphoribosyl transferase (HPRT) transcripts was determined using calibration standards for each of the tested molecules. For each molecule being assayed, a qPCR standard curve was also generated to define the correspondence of transcript numbers to the cycle threshold (Ct value) for qPCR detection. Specifically, standards for HPRT and each molecule being assayed, were diluted to obtain standard curves of 50 pg, 5 pg, 0.5 pg, 0.05 pg, 0.005 pg, 0.0005 pg and 0 pg (no template control) for qPCR determination of transcript levels in each sample. The transcript copy number of each molecule per sample was normalized to the expression of HPRT per sample to account for minor variations in sample aliquots. Primers for HPRT: (forward) CCCTCTGGTAGATTGTCGCTTA and (reverse) AGATGCTGTTACTGATAGGAAATCGA; Arginase I: (forward) CAGAAGAATGGAAGAGTCAG and (reverse) CAGATATGCAGGGAGTCACC;; IL-6: (forward) CCCCAATTTCCAATGCTCTCC and (reverse) CGCACTAGGTTTGCCGAGTA; iNOS) (forward) GGCAGCCTGTGAGACCTTTG and (reverse) GCATTGGAAGTGAAGCGTTTC; NOX2 (gp91-phox subunit): (forward) CCAACTGGGATAACGAGTTCA and (reverse) GAGAGTTTCAGCCAAGGCTTC; TNFα (forward) CTGTGAAGGGAATGGGTGTT and (reverse) GGTCACTGTCCCAGCATCTT.

4.2.9 Flow Cytometry

Microglia and CNS-infiltrating macrophages were isolated from the brains and medulla oblongata of mice immediately following euthanasia as previously described (Hernandez et al., 2016). In brief, the brain with cerebellum was separated from the brainstem at the level of the border between the pons and the medulla (medulla region containing the dorsal respiratory group, the ventral respiratory group, the Bötzinger and preBötzinger complexes; Feldman and Kam, 2015; Smith et al., 2013). Both brain regions (the whole brain without medulla and the medulla) from each mouse were mechanically dissociated as separate samples. Samples were not pooled and were not treated with DNAse or collagenase. The resulting cell suspensions were separated on a discontinuous 1.03/1.088 percoll gradient and microglia/macrophages/infiltrating immune cells were collected from the interface as well as from the 1.03 percoll fraction. Microglial activation was analyzed by flow cytometry using a Cell Quest equipped FACSCalibur (BD Scientific) and fluorescently conjugated antibodies: Allophycocyanin (APC)-conjugated CD45, fluorescein (FITC)-conjugated FcR and phycoerythrin (PE)-conjugated antibodies against Triggering Receptor Expressed on Myeloid cells-2 (TREM2), Fc Receptor (FcR), CD11b and Toll-like receptor 2 (TLR2) (BD Biosciences, San Diego, CA, USA). Microglia were defined as CD45lo, FcR+ cells. Flow cytometric data was quantified using FloJo software using standard methodologies for identifying gated populations and mean fluorescence intensity values (MFI) (Allan and Keeney, 2010). Because baseline fluorescence values are not absolute values between experiments, all MFI values were normalized to untreated male mice. MFI values for the CD45lo, FcR+ cell population were calculated for each activation marker using FloJo software.

4.2.10 Histology

Brain tissue collected at dissection was immediately incubated at 4°C for 24 hours in 4% paraformaldehyde, followed by 48 hours in 4% paraformaldehyde/30% sucrose solution. Tissue was cryopreserved, cryosectioned (25µm) onto Fischer Superfrost plus slides and exposed to rabbit anti-Iba1 antibodies (Wako) and murine anti-GFAP antibodies (Invitrogen Thermofisher), followed by incubation with Alex-680 conjugated goat anti-rabbit and Alexa-488 conjugated goat anti-mouse antibodies (Invitrogen Thermofisher) as previously described (Ploix et al., 2011). Tissue sections were mounted in Prolong Gold containing DAPI and subsequently imaged on a Yokogawa spinning disc confocal microscopy system. Immunofluorescence was quantified (6 mice per condition, 2 brain sections per mouse) with NIH Image J (version 1.5K) using the Mean Grey Value tool (sum of the grey values of all pixels in specific fluorescent channel divided by the number of pixels in the specific fluorescent channel in the total image). Specifically, the CA1 region of the hippocampus in the stratum radiatum (-1.5 to -2.5mm past bregma on a sagittal plane) and the dorsal medulla, ventral to the 4th ventricle (-5.5 to -6.5mm past bregma on a sagittal plane).

4.2.11 Statistical Analysis

Values are reported as means ± standard error of the mean (SEM), with sample size as reported in each assay. Student's t-test or Analysis of Variance (ANOVA) with post-hoc Dunnett's multiple comparison test were used to analyze data as indicated using Prism7 (Graphpad Software, La Jolla, CA). No significant differences were detected in the standard deviation (SD) of populations being compared by ANOVA (Brown-Forsythe test

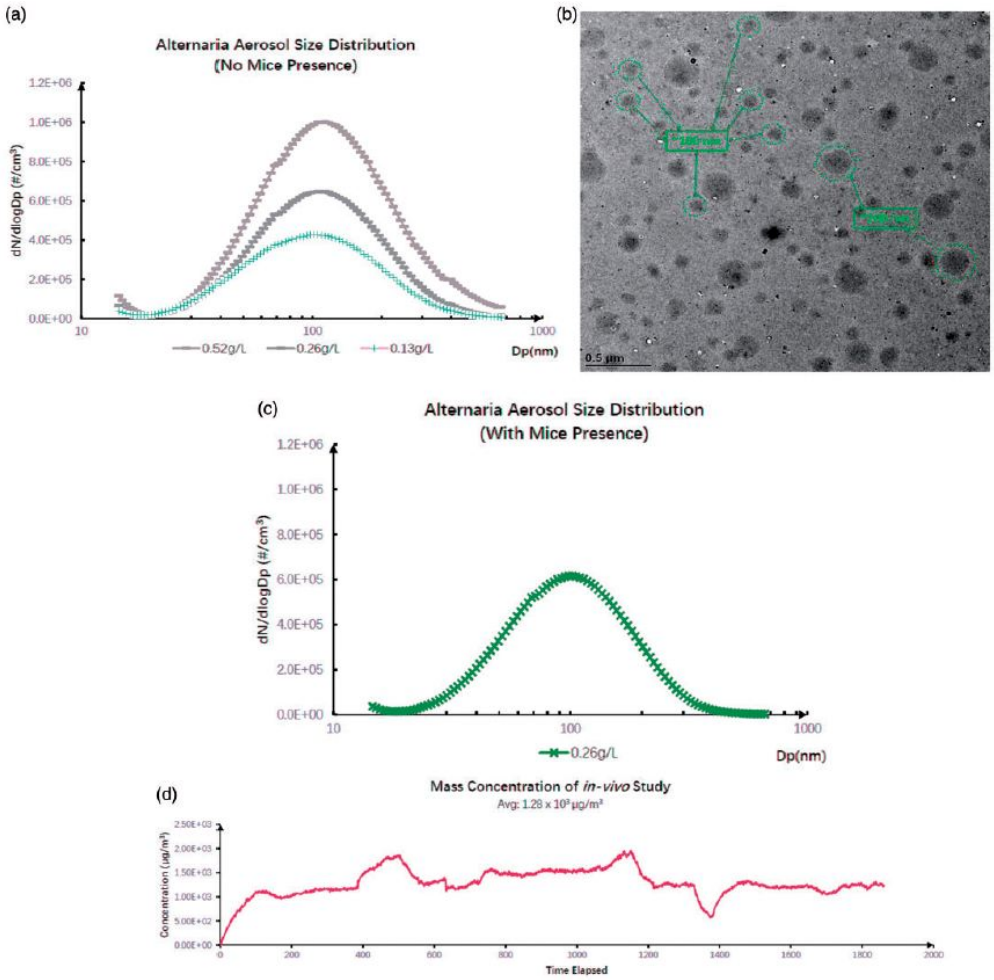

Figure 4.2: *Alternaria* Aerosol Suspension

P=0.9516). In all data sets, sample comparisons with P values less than 0.05 were considered statistically significant.

Figure 4.2: Alternaria aerosol particle size distribution (with and without mice) in the chamber. (a) Illustration of Alternaria aerosol particle size distribution and concentration at bottle solution of 0.13 g/L, 0.26 g/L, and 0.52 g/L, respectively. The vertical axis for represents particle number concentration dN/dlogDp (#/cm3), while the horizontal

axis represents particle size on a logarithmic scale. (b) The overall size distribution during the test with mice presence over 96 hr. (c) Illustration of the mass concentration over the 96-hr exposure. (d) TEM image of the distribution of nebulized Alternaria aerosol particles (sampled through a low-pressure impactor that collects particles ranging from 50 nm to 4 mm) on a carbon-coated copper grid (Hering et al., 1978). TEM = transmission electron microscopy.

4.3 Results

4.3.1 Production of Stable Aerosol Suspensions of Alternaria Nanoparticles in an Environmental Chamber

Here we report a mouse environmental chamber able to provide continuous air injection with the capability to inject a stable suspension of particulates or other aerosol components over an extended period (Figure 4.1). Figure 1A depicts the chamber system and Figure 1B depicts representative TSI DustTrak data showing relatively even distribution of test particles across the chamber. The chamber and injection characteristics were subsequently characterized along several parameters, including aerosolized particle size and concentration, stability in aerosol suspension within the chamber, and ammonia levels (Figure 4.2 and 4.3). Specifically, aqueous solutions of Alternaria particulate at different concentrations were injected through an atomizer and the resulting aerosolized particle suspension was analyzed. The concentration of particles in the chamber were dependent on the Alternaria solution concentration (Figure 4.2A).

To characterize the stability of the particle suspension, several studies were con-

ducted with no mice present in the chamber while particle concentration and distribution were monitored using the SMPS system. Particles in the chamber were found to show an average peak particle size of approximately 100 nm regardless of the concentration of aqueous solutions of Alternaria particulate (Figure 4.2A) or the presence of mice in the chamber (Figure 4.2B). Figure 4.2A and 4.2B also show that the average particle number concentration of two separate injections of aqueous solution (0.26g/L) in the chamber were nearly identical with or without the presence of mice. The mass concentration of the particles in the chamber under continuous injections conditions remained relatively stable overtime with the slight variations possibly reflecting minor variation in air pressure in the injection system (Figure 4.2C). While there was a range of particle sizes (Figures 4.2A and 4.2D), the average particle size appeared to be a property of the Alternaria particulate rather than the concentration of the protein. Thus, as with the comparisons between empty chamber and the chamber with mice, the chamber conditions did not affect the particle size, concentration, nor stability.

To confirm that appropriately low ammonia levels were maintained for the duration of an experimental exposure treatment, we measured ammonia within the chamber at the end of a full 96-hour exposure (Figure 4.3). Although precise upper limits for murine exposure are debated, it has been generally accepted that human exposure limits should not be exceeded for laboratory-housed rodents with 25 parts per million being the recommended exposure limit as an 8-hr time-weighted average according to NIOSH guidelines (Rosenbaum et al., 2009). Here, we found that ammonia levels were significantly lower than the recommended 25 parts per million even with six mice in the chamber.

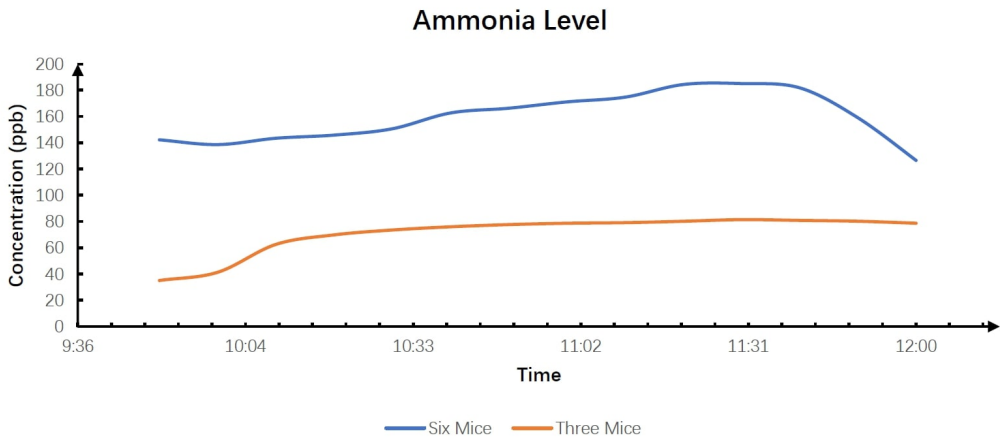

Figure 4.3: Ammonia level in the chamber

Figure 4.3: Ammonia level in the end of the 96-hr exposure. The ammonia gas (NH_3) concentration in the chamber was acquired at the end of each 96-hr exposure experiment. The figure shows two different ammonia (NH_3) levels during the last 3 hr of an exposure study with either three (dashed black line) or six (solid blue line) mice in the chamber.

4.3.2 Continuous Exposure to Alternaria Particulate Nanoparticles Induces Overt Pulmonary Inflammation

We initially quantified lung inflammation by standard bronchio-alveolar lavage (BAL) and histology as the first site of allergen exposure (Figure 4.4). We found that 96 hours of treatment was insufficient to trigger a statistically significant increase in numbers of immune infiltrates in BAL with a standard regimen of daily intranasal dosing of the Alternaria particulate solution (Figure 4.4A-C, blue bars). By contrast, 96 hours of continuous chamber exposure to aerosolized Alternaria particulates was sufficient to cause significant (∼60%) increases in the numbers of total lavage cells (Figure 4.4A, red bar; F=8.853, p= 0.0162) and in total alveolar macrophages (Figure 4B, red bar; F=9.314, P=0.0145). While inhalation exposure was more effective at triggering immune cell influx into the lung, histological analysis revealed that both the intranasal dosing regimen and continuous chamber exposure to aerosolized Alternaria particulates triggered similar degrees of total lung pathology (Figure 4.4D and E). Specifically, blinded scoring of histology confirmed inhalation exposure to Alternaria particulates induced airway and endothelial thickening equivalent to that induced by conventional intranasal administration (F=14.54, P=0.0003). Immunofluorescent staining for RELMα, a highly-expressed protein in asthmatic inflammation (Doherty et al., 2012), revealed that both intranasal and inhalation exposure to Alternaria induced modest expression in the airway and in the lung parenchyma (Figure 4.4C). Quantification of RELMα induction in lavage isolated cells by ELISA revealed no significant differences between treated and untreated groups (Figure 4D). Together, these

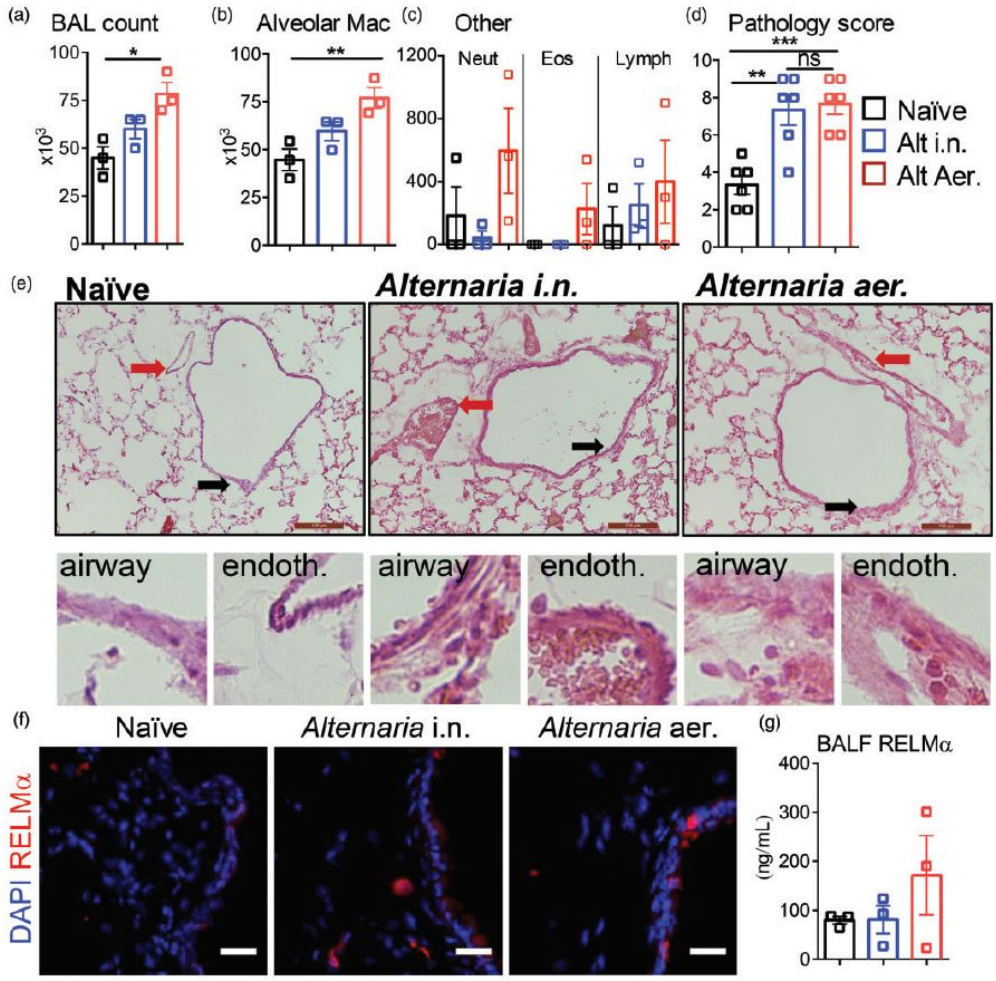

Figure 4.4: *Alternaria* promotes lung inflammation

studies show that physiological exposure to Alternaria particles in the form of aerosols in an atmospheric chamber is sufficient to produce pulmonary inflammation exhibiting early signs of allergic type innate immune responses.

Figure 4.4: Alternaria aerosol exposure in the environmental chamber promotes lung inflammation. Bronchio-alveolar lavage (BAL) of the lungs reveal Alternaria-induced cell numbers (a); alveolar macrophages (b); neutrophils (Neut), eosinophils (Eos), and

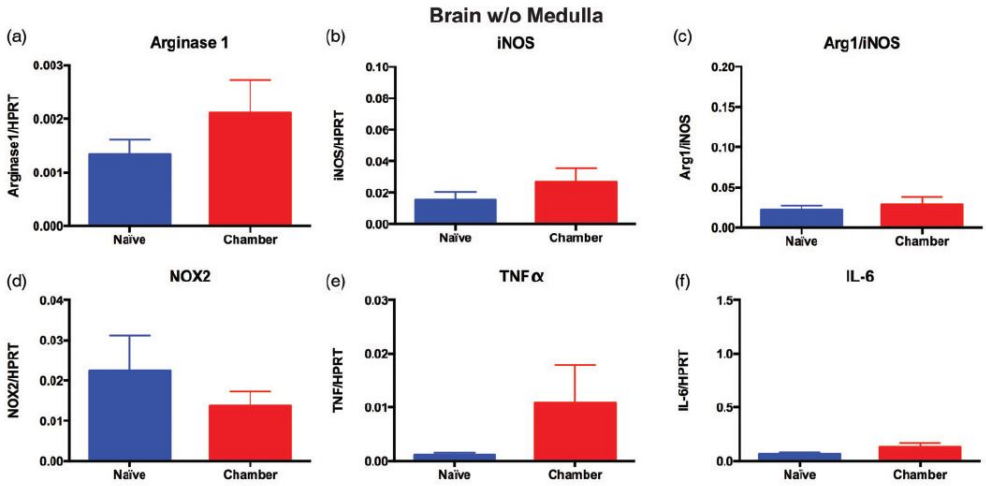

Figure 4.5: qPCR analysis of neuroinflammatory molecules in brain cDNA

lymphocytes (Lymph) (c); and lung pathology scores (d). (d) Representative H&E-stained lung sections reveal Alternaria-induced airway (black arrow) thickening and endothelial (red arrow) thickening and inflammation (scale, 100 µm). (f) Immunofluorescence labeling reveals increased expression of RELMα following Alternaria exposure (scale, 25 µm). (g) BAL Enzyme-Linked Immunosorbent Assay for RELMα. Three biologic replicates per experiment (total of two experiments) were analyzed for each condition depicted. Data are presented as mean SEM. Statistical differences were calculated by one-way ANOVA with post hoc Dunnett's multiple comparison test using GraphPad Prism. *p $<$0.05. BAL = bronchio-alveolar lavage.

Figure 4.5: qPCR analysis of neuroinflammatory molecules in brain cDNA from mice exposed for 96 hr to aerosolized Alternaria particulates or ambient air. (a–f) Data from samples of whole brain with the medulla removed. Data are presented as the mean SEM of three independent experiments with a total sample size of naive n = 15 and chamber

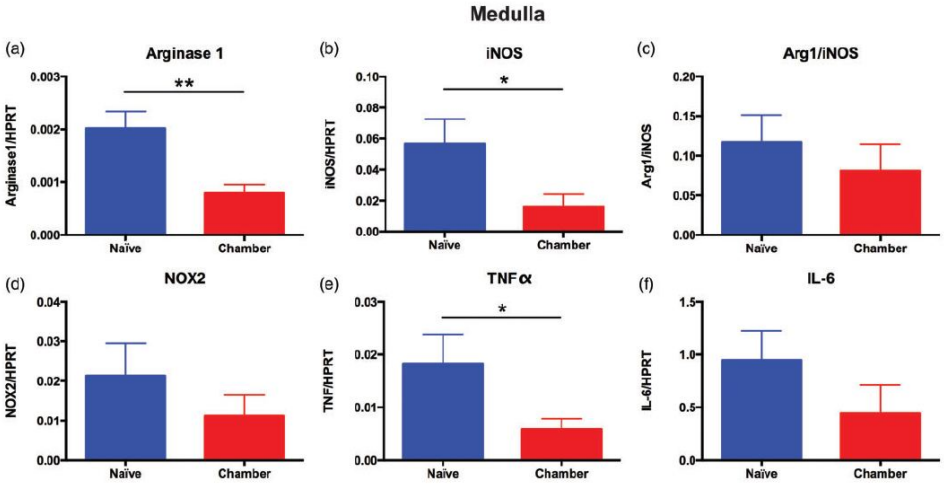

Figure 4.6: qPCR analysis of neuroinflammatory molecules in brain medulla cDNA

(Alternaria-exposed) n = 15. Statistical differences were calculated by unpaired Student's t test using GraphPad Prism. *p <0.05. iNOS = inducible nitric oxide synthase; NOX2 = NADPH oxidase; TNFα = tumor necrosis factor alpha; IL-6 = interleukin-6.

Figure 4.6: qPCR analysis of neuroinflammatory molecules in brain medulla cDNA from mice exposed for 96-hours to aerosolized Alternaria particulates or ambient air. Panels A-I depict data from samples of brain medulla (containing the dorsal respiratory group, the ventral respiratory group, the Bötzinger and preBötzinger complexes implicated in regulating lung respiration). Data is presented as the mean ± SEM of three independent experiments with a total sample size of naive n=15 and chamber (Alternaria exposed) n=15. Statistical differences were calculated by unpaired Student's t-test using GraphPad Prism, *P $<$ 0.05.

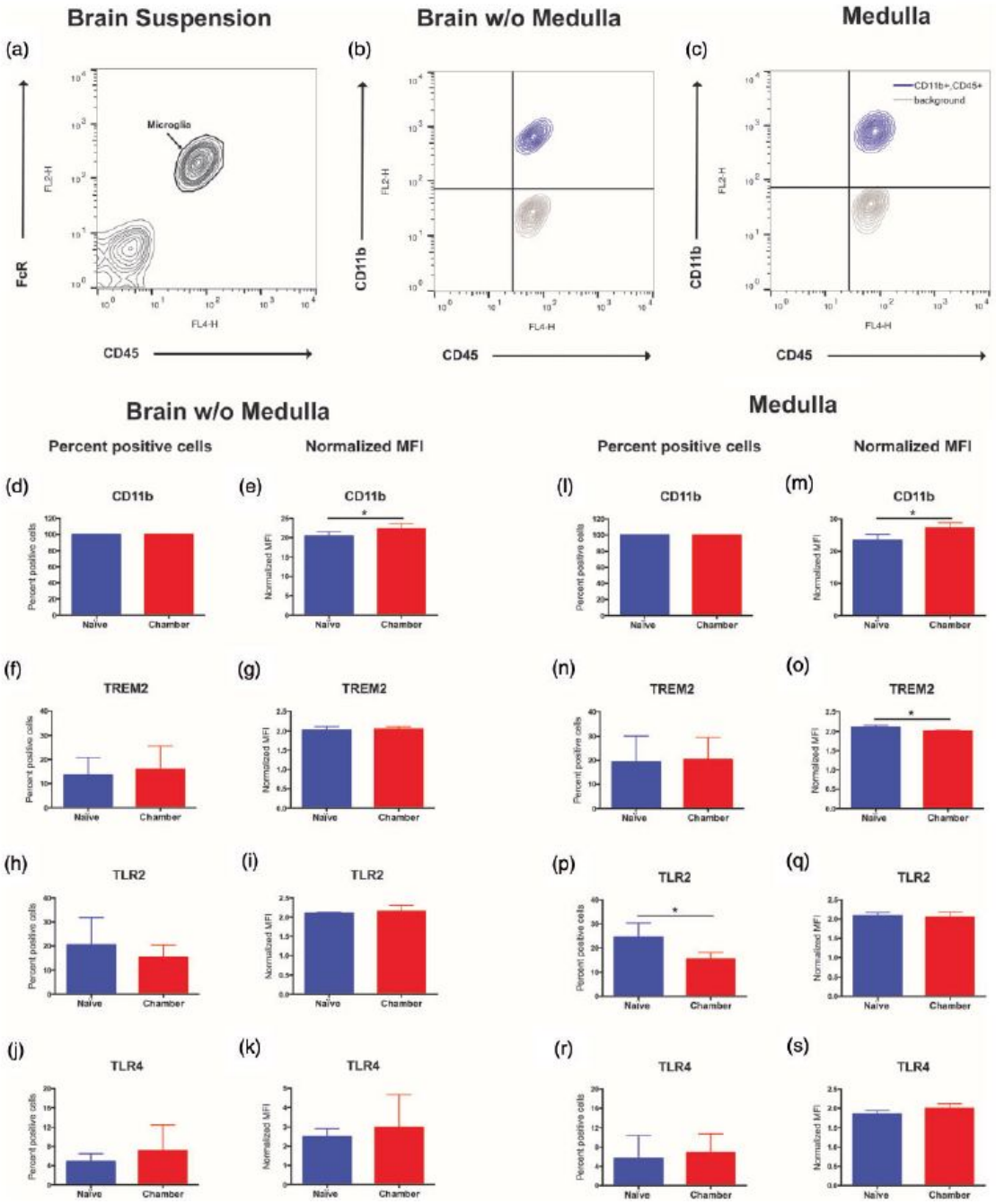

Figure 4.7: Flow cytometric analysis of microglial innate immune markers

Figure 4.7: Panel A depicts representative contour plot data of brain cell suspensions labeled with FITC-conjugated anti-FcR antibodies (FL1-H) and APC-conjugated anti-CD45 antibodies (FL4-H). The FcR+ and CD45lo microglial population is identified by the arrow. Representative contour plot data from brain cell suspensions labeled with are depicted from cell suspensions of brain w/o medulla (panel B) and of the medulla only (panel C). Cell suspensions labeled only with FITC-conjugated FcR antibodies and APC-conjugated anti-CD45 antibodies are depicted in grey and depict the relative level of autofluorescence in the FL-2 PE channel). Cell suspensions labeled additionally with PE-conjugated anti-CD11b antibodies are depicted in magenta. Cell suspensions from brain without medulla (panels D-E) and from only medulla (panels L-S) were similarly labeled with PE-conjugated antibodies against TREM2, TLR2 and TLR4. The percentages of microglia being immunoreactive for each molecule above background fluorescence (background: grey population in panels B and C) and the mean fluorescence intensity (relative expression level per microglia) were calculated in FlowJo and graphed in Graphpad Prism. Data is represented as mean ± SEM from a total sample size of n=6 (all parameters for brain without medulla) and n=4 (for all medulla samples). Statistical differences were calculated by unpaired Student's t-test using GraphPad Prism, *$P < 0.05$. Student t-test values: panel E t=0.5186 df=10; panel M t=3.246 df=6; panel P t=2.765 df=6.

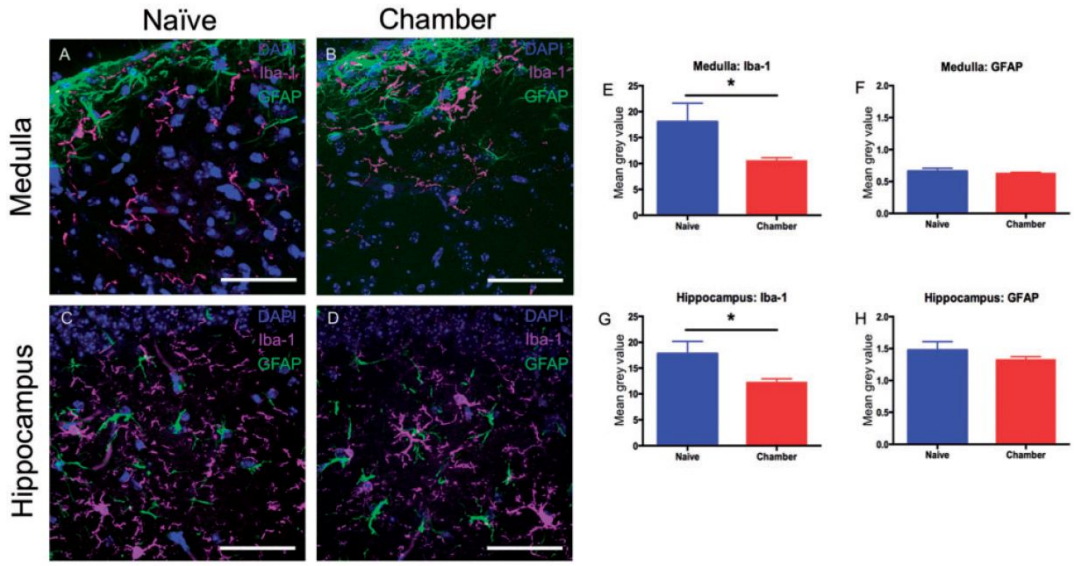

Figure 4.8: Histological analysis of microglia and astrocytes in tissue

Figure 4.8: Histological analysis of microglia and astrocytes in tissue from mice +/- exposure for 96-hours to aerosolized Alternaria particulates. Glial immunofluorescence was examined in medulla (panels A and B) and hippocampus (C and D) from mice exposed to ambient air (panels A and C) or aerosolized Alternaria particulates (B and D). In panels A-D, nuclei were labeled with DAPI (blue), microglia with iba1 antibodies (magenta) and astrocytes with-GFAP antibodies (green). Immunofluorescence was quantified using NIH image J (Panel E and J) and data are represented as mean ± SEM from a total sample size of n=6 (ambient air) and n=6 (Alternaria exposed). Statistical differences were calculated by unpaired Student's t-test using GraphPad Prism, *P < 0.05. Iba1 Student t-test values: hippocampus t=2.241 df=10; medulla t=2.270 df=10.

4.3.3 Inhaled Alternaria Exposure Decreases Basal Level of Innate Immune Molecules in Brain Medulla

We hypothesized that if continuous inhalation exposure to Alternaria particulates was sufficient to trigger lung inflammation, it should also be sufficient to trigger neuroinflammatory responses within the brain. Therefore, we surveyed expression of molecules previously implicated in systemic- and emission particle-induced innate immune responses: Arginase 1, iNOS, NOX, TNFα and IL-6 and (Figure 4.5 and 4.6). Surprisingly, an initial qPCR survey detected no significant differences in the expression of these molecules in cDNA prepared from total brain tissue of mice plus/minus Alternaria exposure (Figure 4.5). In the absence of global differences detectable in total brain samples, we speculated that any effects in the CNS might be localized to specific brain regions. We chose to examine the brain region involved in the direct innervation and regulation of respiration (Feldman and Kam, 2015; Smith et al., 2013). For all subsequent experiments, we dissected the medulla containing the "CNS respiratory circuit" (composed of the dorsal respiratory group, the ventral respiratory group, the Bötzinger and preBötzinger complexes) away from the rest of the brain (Figures 4.6).

While no significant difference in Arginase I and INOS expression levels were detected in cDNA from the whole brain samples of naïve and Alternaria exposed mice (Figure 4.5A and 4.5B), both Arginase I (Figure 6A; t=3.434 df=20) and INOS levels (figure 6B; t=2.293 df=20) were significantly decreased by $\sim$50% in cDNA from the medulla of Alternaria exposed mice as compared to cDNA from the medulla of naïve mice. Arginase I and iNOS both compete for the same substrate: arginine. Arginase converts arginine to

ornithine leading to the polyamine pathways while iNOS generates nitric oxide from arginine. Thus, the ratios of arginase I to iNOS are often used as a diagnostic marker of a shift in innate immune propensity for anti-inflammatory/tissue repair responses to a propensity for pro-inflammatory cytotoxicity responses (Cho et al., 2014; Gordon, 2003; Munder et al., 1998). Therefore, we also compared the ratios of Arginase 1/iNOS per mouse as a measure of altered polarization separate from the absolute levels of each transcript. Exposure to aerosolized Alternaria particulates did not cause significant changes in Arginase 1/iNOS ratios in either the brain as a whole or in the medulla (Figure 4.5C and 4.6C). NAPDH oxidase (gp91-phox subunit:NOX2), TNFα, and IL-6 are classic pro-inflammatory molecules induced in the CNS by systemic inflammatory challenges and by CNS injury (figure 4.6D-F). While no difference in NOX2 and IL-6 expression were observed between the Alternaria and ambient air exposed mice (Figure 4.6D and Figure 4.6F), the mean baseline levels of TNFα were reduced by nearly 2/3 in the medullas of Alternaria exposed mice (Figure 4.6E; t=2.090 df=20).

4.3.4 Inhaled Alternaria Exposure Decreases Percentage of Microglia Expressing Detectable TLR2

Systemic inflammation as well as inhaled pollutants can trigger infiltration of peripheral immune cells into the CNS with even small (fine and ultrafine) particulates in the size range, but with different composition than the Alternaria particulates used here (Jayaraj et al., 2017). The most quantitative method for characterizing the degree of immune cell influx is flow cytometric analysis of CD45+ cells (Carson et al., 2006. In brief, all nucleated cells of hematopoietic origin including microglia express CD45 (also known as

leukocyte common antigen). However, microglia express very low levels of CD45 (CD45lo) while all other differentiated immune cells in the adult express an order of magnitude higher CD45 levels (CD45hi). In cell suspensions of the brain and medulla, microglia are identified as FcR+ (Figure 4.7A, FL1-H) and CD45lo (Figure 4.7A, FL4-H). In all samples from naïve and Alternaria exposed mice (brain: Figure 7A, 7B and medulla: Figure 4.7C), no CD45hi cells were detected (Figure 4.7A-C). Thus, there was no overt peripheral immune cell infiltration in Alternaria exposed mice despite ongoing inflammation in the lung (Figure 4.4A).

By immunolabeling with PE-conjugated antibodies, we analyzed microglial surface expression of pathogen associated molecular pattern (PAMP) receptors (CD11b, TLR2 and TLR4) which have been implicated in neuroinflammatory responses to systemic inflammation and inhaled pollutants (Jayaraj et al., 2017). We also examined microglial expression of TREM2 as a marker of general microglial activation. TREM2 expression is often induced by brain injury while its expression is reduced by direct exposure to LPS and TNF (Schmid et al., 2009). In the brain (Figure 4.7B) and in the medulla (Figure 4.7C) of naïve mice, nearly 100% of microglia express CD11b (blue population is CD11b+, non-specific autofluorescence is grey population, Figure 4.7B and 4.7C). 96-hour treatment with aerosolized Alternaria particulates did not alter the percentage of microglia expressing CD11b, TLR4 or TREM2 in either brain or medulla cell suspensions (Figure 4.7D, F, J, L, M, R). By contrast, the percentage of TLR2+ microglia in medulla cell suspensions was decreased by ∼30% in Alternaria exposed mice as compared to naïve mice (Figure 7P). However, the level of TLR2 per TLR2+ microglia (mean fluorescence intensity per microglia) was not

altered by Alternaria exposure (Figure 4.7Q). While the percentage of CD11b+ cells was not altered by Alternaria exposure, CD11b levels per cell were increased by Alternaria exposure in both the whole brain (Figure 4.7E) and in the medulla (Figure 4. 7M). Although quite modest and of uncertain biologic significance, chamber exposure did reduce TREM2 levels per microglia in the medulla (Figure 4.7O).

4.3.5 Inhaled Alternaria Exposure Decreases Iba1 but Not GFAP Immunoreactivity

Within the CNS, Iba1 is expressed by microglia and glial fibrillary acidic protein (GFAP) by astrocytes. Prior to our studies, Klein et al. (2016) challenged mice with a natural allergen from timothy grass and observed a decrease in hippocampal microglial activation using histologic measures. However, they repetitively administered their natural allergen as a solubilized antigen preceded by adjuvant priming. Therefore, it is unclear whether the reduced microglial reactivity was due to a mature lymphocyte response that evolved over weeks and/or the repetitive route of administration. Here, we compared Iba1 and GFAP immunofluorescence in the medulla (Figure 4.8A and 4.8B) and hippocampus (Figure 4.8C and 4.8D) of mice exposed to ambient air (naïve, Figure 4.8A and 4.8C) or aerosolized Alternaria particulates (chamber, Figure 4.8B and 4.8D) for 96 hours. Microglia and astrocytes in Alternaria exposed mice retained the characteristic stellate morphology observed in ambient air exposed mice. However, the mean immunofluorescence of Iba1 per image was significantly reduced by nearly 50% in the hippocampus of Alternaria exposed mice and by nearly 30% in the medulla (Figure 4.8E and 4.8E). By contrast, mean immunofluorescence of GFAP per image was not significantly reduced.

4.4 Discussion

Exposure to airborne particulates (natural and manmade) is a major focus for understanding environmental contributions to the pathogenic mechanisms underlying asthma, cardiovascular disease, neurodevelopmental and neurodegenerative disorders (Dockery et al., 1993; Kodavanti et al., 2011, 2000; Pope III et al., 2002; Raaschou-Nielsen et al., 2013). A central theme in epidemiologic and mechanistic studies defining disease promoting contributions has been to define the links between air exposures and organ specific inflammatory responses likely to provoke maladaptive or disease predisposing conditions in lung, heart and brain (Bilbo et al., 2018; Calderón-Garcidueñas et al., 2016; Cole et al., 2016; Gackière et al., 2011; Heusinkveld et al., 2016; Jayaraj et al., 2017; Levesque et al., 2011; Mumaw et al., 2016). Allergic lung inflammation is known to cause systemic and organ specific inflammation (Xia et al., 2014). Therefore, based on studies defining the effects of ambient manmade airborne toxicants and systemic inflammation inducing activation of CNS innate immune responses, it is possible that natural allergens could also have detrimental effects predisposing the brain for disease predisposing conditions.

Studies examining the effects of natural allergens including plant pollens, fungal allergens, and arthropod antigens have focused primarily on defining mechanisms of allergic lung inflammation and propensity for chronic pulmonary diseases such as asthma (Doherty et al., 2012; Gabriel et al., 2016; Gold et al., 2017; Knutsen et al., 2012; Kubo, 2017). The few reports linking allergic lung inflammation and neuroinflammation have not examined ambient exposure of allergens. Instead, these reports have relied on immune sensitization protocols often in the presence of robust adjuvant based priming of allergic inflammation

using well characterized antigens such as ovalbumin which lack the defining features of an allergens (Xia et al., 2014; Yamasaki et al., 2016). Most studies with non-allergen antigens observed induction of pro-inflammatory innate immune responses in the brain (Sarlus et al., 2013; Yamasaki et al., 2016). However, one study that did examine the consequences of a natural allergen from Timothy grass looked at only the long term neuroinflammatory consequences of allergic inflammation stimulated by a solubilized antigen administered in a long-term injection priming/intranasal challenge model system. Striking in this system, microglial activation was reduced in specific regions of the brains from treated mice (Klein et al., 2016). These studies have been useful in defining the potential of allergic inflammation to drive neuroinflammation but have also provided potentially conflicting results. In part this may be because these studies rely on strategies that may induce hypersensitivity immune responses that are unrelated to natural allergens associated with unprimed exposure to allergens by continuous period of inhalation (Kumar et al., 2014). In addition, these studies have primarily examined long term allergic responses (>12 weeks of fully developed respiratory asthma with fully developed adaptive immune responses; Xia et al., 2014; Klein et al., 2016).

In our current studies, we sought to use an experimental system that mimics chronic environmental exposure to aerosolized particulates. Therefore, we generated and characterized a novel murine exposure chamber equipped to disperse a natural fungal allergen continuously and simultaneously to monitor sustained aerosolized dispersion of the natural allergen. Specifically, our chamber is much larger (540 L) than other reported chamber systems with (0.4 L or 16 L volumes) and thus able to house up to 18 mice at a single

time without accumulation of high ammonia levels (Ko et al., 2015; Barnewall et al., 2015). Our chamber system also uses multiple instruments to characterize particle sizes ranging from 2 nm to 40 µm, instead of using only one instrument to detect particles in the range of 500 nm to 20 µm (Barnewall et al., 2015). In contrast to nose-only exposure systems that limits the animal activities and only allow 2-hr exposed time for each test, our chamber system allows continuous exposure to occur under conditions of free mobility and normal access to food and water (Ye et al., 2017).

It is difficult to determine the actual absorbed dose of allergen in the lung, whether it is applied intranasally or intratracheally as a solution, or as a nebulized aerosol. In this study, we chose a stable aerosol suspension concentration, which we could set by using a fixed Alternaria particulate concentration at the atomizer (in this case, 0.26g/L). Thus, for each exposure study, mice were placed in the chamber and the aerosol injection was begun, and particle concentration and size was monitored to ensure a stable suspension. This exposure was continued for 96 hours because 96 hours encompasses the entire period of initial innate immune response to the allergen and after which lymphocytic responses to the allergen become apparent. The nebulized Alternaria aerosol particles were found to be an average size of approximately 100 nm. This size range is within the size ranges of ultra-fine PM0.1 and fine PM2.5 particles of airborne toxicants demonstrated to provoke potent inflammatory responses. Indeed, such fine aerosol particles are capable of penetrating deep into the alveolar spaces in the lung (Barnewall et al., 2015; Jayaraj et al., 2017). Therefore, continuous exposure to aerosolized Alternaria particulates ensured wide distribution throughout the lung, and avoided the known artefactual ingestion of a large proportion

of an allergen solutions when applied intranasally. In addition, continuous exposure over several days avoided the immunoregulatory effects of inducing multiple short term bursts of acute systemic allergic hypersensitivity responses.

Pro-inflammatory innate immune responses are triggered within the CNS by systemic inflammation induced by bacterial and viral stimuli as well as by sustained exposure to airborne emission particulates in the size range of the Alternaria particles used here (Jayaraj et al., 2017).

In our model system, we were struck by the ability of continuous inhalation of aerosolized Alternaria particulates to drive lung inflammation that was more robust than daily intranasal application of an Alternaria particulate solution. Furthermore, it was notable that simple continuous inhalation exposure without prior antigen sensitization and without inclusion of priming adjuvant was by itself sufficient to drive a large BAL inflammatory infiltrate comprised of a mixed population of macrophages, neutrophils and eosinophils characteristic of allergic responses. Therefore, it might be surprising or alternatively it might be comforting that broad spectrum proinflammatory responses were not observed in the brain after exposure to this common natural airborne fungal antigen in the presence of robust lung inflammation. However, the study by Klein et al. (2016) does suggest that natural allergens albeit using an adjuvant priming/challenge model resulted in decreased microglial activation as assayed by histologic measures. Because mature Th2/IgE lymphocyte responses were fully developed at the 12-week time point of their assay collection, the authors ascribed the reduction in microglial activation to the sustained actions of a fully mature adaptive immune response. Here we report observations in the brainstem and hippocampus

consistent with their study (decreased Iba1 immunofluorescence, decreased expression of a subset of innate immune markers) prior to the development of a fully mature lymphocyte and/or IgE allergy response.

When considering the apparent lack of pro-inflammatory responses in the brain, it is useful to place our observations in the context of endotoxin tolerance (also referred to as LPS preconditioning; Collins and Carmody, 2015; Nomura et al., 2000; Pena et al., 2011; Rajaiah et al., 2013). Endotoxin tolerance refers to the well described phenomena where pretreatment of immune cells or of an individual with a series of low dose endotoxin (lipopolysaccharide) treatments causes the cells or individual to become refractory to subsequent endotoxin challenge. Phenotypically, macrophages treated to become endotoxin tolerant express lower levels of many pro-inflammatory and PAMP receptor molecules at baseline prior to subsequent endotoxin challenge. Indeed, initial reports have ascribed endotoxin tolerance to the acquisition of an alternatively activated (M2) innate immune status. In our studies, we did indeed see decreased expression of TNFα, and INOS in brainstem tissue samples as well as decreased expression of TLR2 on brainstem microglia. While these are indicative of a lower propensity for a pro-inflammatory response to immune stimulants, a shift toward an alternative or M2 polarized phenotype should result in an altered ratio of key innate immune markers. Specifically, an alternative activation/M2 baseline polarization should have been reflected in an increased Arginase1/INOS ratio which we did not observe (Cho et al., 2014; Gordon, 2003; Munder et al., 1998). More recently, the association of endotoxin tolerance with acquisition of an alternative/M2 innate immune polarization is being revisited as in many paradigms Arginase 1 is decreased as observed in our studies (Rajaiah et al., 2013).

Changes in baseline innate immunity and baseline microglial activation states can have biological consequences for brain function and do have consequences for immune surveillance of the brain's cellular health, phagocytosis of cellular components and altered inflammatory responses to subsequent insults in many models (Ji et al., 2013; Tremblay and Majewska, 2011; Schafer et al., 2013). In the studies by Klein et al. (2016), decreased microglial activation correlated with decreased neurogenesis in the hippocampus. In our study, the consequences of modifying the baseline innate immune state in brain regions regulating respiratory control can only be speculated at this point (Feldman and Kam, 2015; Smith et al., 2013). However, the similarity of the changes in our study with those triggered by endotoxin tolerance may suggest that the changes observed here have a similar desensitizing function. Namely, to reduce the toxic effects of similar allergic challenges at subsequent time points on critical brain regions such as the brainstem regions controlling respiration.

Chapter 5

Thesis Summary

This Ph.D. thesis provides construction of two energy self-supported mobile laboratories and an environmental chamber for animal exposure experiments. The real-time field test mobile laboratories built in chapter 2 provides an excellent example for future field measurement projects and technical support for the construction of instrument platforms for a robust mobile laboratory. The abundant tests results of multiple atmospheric contaminants also serve as a great supplement for data comparison in addition to the air monitoring station data from South Coast Air Quality Management District. In Chapter 3, we developed a large-scale multipurpose animal exposure chamber for health effects investigation of air pollutants. Compared to other chamber systems featuring nose-only or activity-limited whole-body exposure, this system provides continuous exposure through the natural inhalation route at controlled concentration, size distribution and duration for both chronic, sub-chronic and acute epidemiological studies. Our method is also easily reproducible and has the potential to mimic the real atmospheric environment by adding

multiple air contaminants at the same time for health investigations. As a direct application of Chapter 3, Chapter 4 provides detailed *in-vivo* exposure test operations and health outcomes of fungal allergen particulates. Our research research discovered that continuous exposure to aerosolized fine (particle size < 2.5 µm) and ultrafine (particle size < 0.1 µm) particulates can trigger innate inflammatory responses in the lung and brain depending on particle composition.

Bibliography

S. Aciego, C. Riebe, S. Hart, M. Blakowski, C. Carey, S. Aarons, N. Dove, J. Botthoff, K. Sims, and E. Aronson. Dust outpaces bedrock in nutrient supply to montane forest ecosystems. *Nature communications*, 8:14800, 2017.

S. Aksoyoglu, G. Ciarelli, I. El-Haddad, U. Baltensperger, and A. S. Prévôt. Secondary inorganic aerosols in europe: sources and the significant influence of biogenic voc emissions, especially on ammonium nitrate. *Atmospheric Chemistry and Physics*, 17(12):7757, 2017.

A. L. Allan and M. Keeney. Circulating tumor cell analysis: technical and statistical considerations for application to the clinic. *Journal of oncology*, 2010, 2010.

B. Amon, V. Kryvoruchko, T. Amon, and S. Zechmeister-Boltenstern. Methane, nitrous oxide and ammonia emissions during storage and after application of dairy cattle slurry and influence of slurry treatment. *Agriculture, ecosystems & environment*, 112(2-3):153–162, 2006.

N. Anderson, R. Strader, and C. Davidson. Airborne reduced nitrogen: ammonia emissions from agriculture and other sources. *Environment International*, 29(2-3):277–286, 2003.

M. Andersson, S. Downs, T. Mitakakis, J. Leuppi, and G. Marks. Natural exposure to alternaria spores induces allergic rhinitis symptoms in sensitized children. *Pediatric Allergy and Immunology*, 14(2):100–105, 2003.

V. F. Assaad, J. C. Jofriet, S. C. Negi, and G. L. Hayward. Sulfide and sulfate attack on reinforced concrete of livestock buildings. In *2003 ASAE Annual Meeting*, page 1. American Society of Agricultural and Biological Engineers, 2003.

R. E. Barnewall, E. M. Benson, M. A. Brown, D. A. Fisher, A. S. Lindsay, A. A. Simmons, and M. S. Anderson. Characterization of a large animal aerosol exposure system for aerosolizing four strains of burkholderia pseudomallei. *Journal of Aerosol Science*, 84: 21–38, 2015.

R. Battye, W. Battye, C. Overcash, and S. Fudge. Development and selection of ammonia emission factors. 1994.

T. H. Bertram, R. E. Cochran, V. H. Grassian, and E. A. Stone. Sea spray aerosol chemical composition: elemental and molecular mimics for laboratory studies of heterogeneous and multiphase reactions. *Chemical Society Reviews*, 47(7):2374–2400, 2018.

S. D. Bilbo, C. L. Block, J. L. Bolton, R. Hanamsagar, and P. K. Tran. Beyond infection-maternal immune activation by environmental factors, microglial development, and relevance for autism spectrum disorders. *Experimental neurology*, 299:241–251, 2018.

G. A. Bishop, B. G. Schuchmann, D. H. Stedman, and D. R. Lawson. Emission changes resulting from the san pedro bay, california ports truck retirement program. *Environmental science & technology*, 46(1):551–558, 2011.

R. J. Boissy, D. J. Romberger, W. A. Roughead, L. Weissenburger-Moser, J. A. Poole, and T. D. LeVan. Shotgun pyrosequencing metagenomic analyses of dusts from swine confinement and grain facilities. *PloS one*, 9(4):e95578, 2014.

J. Bollen, S. Hers, and B. Van der Zwaan. An integrated assessment of climate change, air pollution, and energy security policy. *Energy Policy*, 38(8):4021–4030, 2010.

S. R. Bonam, C. D. Partidos, S. K. M. Halmuthur, and S. Muller. An overview of novel adjuvants designed for improving vaccine efficacy. *Trends in pharmacological sciences*, 38 (9):771–793, 2017.

A. Bouwman, D. Lee, W. Asman, F. Dentener, K. Van Der Hoek, and J. Olivier. A global high-resolution emission inventory for ammonia. *Global biogeochemical cycles*, 11(4):561–587, 1997.

R. K. Bush and J. J. Prochnau. Alternaria-induced asthma. *Journal of Allergy and Clinical Immunology*, 113(2):227–234, 2004.

L. Calderón-Garcidueñas, E. Leray, P. Heydarpour, R. Torres-Jardón, and J. Reis. Air pollution, a rising environmental risk factor for cognition, neuroinflammation and neurodegeneration: the clinical impact on children and beyond. *Revue neurologique*, 172(1): 69–80, 2016.

M. J. Carson, C. R. Reilly, J. G. Sutcliffe, and D. Lo. Mature microglia resemble immature antigen-presenting cells. *Glia*, 22(1):72–85, 1998.

M. J. Carson, J. M. Doose, B. Melchior, C. D. Schmid, and C. C. Ploix. Cns immune privilege: hiding in plain sight. *Immunological reviews*, 213(1):48–65, 2006.

C. C. Chan. The state of the art of electric, hybrid, and fuel cell vehicles. *Proceedings of the IEEE*, 95(4):704–718, 2007.

G. Chen, S. H. Wang, J. C. Jang, J. I. Odegaard, and M. G. Nair. Comparison of relmα and relmβ single and double deficient mice reveals that relmα expression dictates inflammation and worm expulsion in hookworm infection. *Infection and immunity*, pages IAI–01479, 2016.

D.-I. Cho, M. R. Kim, H.-y. Jeong, H. C. Jeong, M. H. Jeong, S. H. Yoon, Y. S. Kim, and Y. Ahn. Mesenchymal stem cells reciprocally regulate the m1/m2 balance in mouse bone marrow-derived macrophages. *Experimental & molecular medicine*, 46(1):e70, 2014.

S. K. Christianson, S. Lemay, C. Laguë, T. Bjarnason, M. Marshall, and L. Chénard. Engineering controls to reduce hydrogen sulphide exposure of workers in swine buildings. In *2004 ASAE Annual Meeting*, page 1. American Society of Agricultural and Biological Engineers, 2004.

S. COAST. Mates-iv. 2014.

T. B. Cole, J. Coburn, K. Dao, P. Roqué, Y.-C. Chang, V. Kalia, T. R. Guilarte, J. Dziedzic, and L. G. Costa. Sex and genetic differences in the effects of acute diesel exhaust exposure on inflammation and oxidative stress in mouse brain. *Toxicology*, 374:1–9, 2016.

P. E. Collins and R. J. Carmody. The regulation of endotoxin tolerance and its impact on macrophage activation. *Critical Reviews™ in Immunology*, 35(4), 2015.

T. L. Croston, A. R. Lemons, D. H. Beezhold, and B. J. Green. Microrna regulation of host immune responses following fungal exposure. *Frontiers in immunology*, 9:170, 2018.

C. Cunningham. Microglia and neurodegeneration: the role of systemic inflammation. *Glia*, 61(1):71–90, 2013.

E. Czirr and T. Wyss-Coray. The immunology of neurodegeneration. *The Journal of clinical investigation*, 122(4):1156–1163, 2012.

P. F. DeCarlo, J. R. Kimmel, A. Trimborn, M. J. Northway, J. T. Jayne, A. C. Aiken, M. Gonin, K. Fuhrer, T. Horvath, K. S. Docherty, et al. Field-deployable, high-resolution, time-of-flight aerosol mass spectrometer. *Analytical chemistry*, 78(24):8281–8289, 2006.

I. Dincer. Renewable energy and sustainable development: a crucial review. *Renewable and sustainable energy reviews*, 4(2):157–175, 2000.

D. W. Dockery, C. A. Pope, X. Xu, J. D. Spengler, J. H. Ware, M. E. Fay, B. G. Ferris Jr, and F. E. Speizer. An association between air pollution and mortality in six us cities. *New England journal of medicine*, 329(24):1753–1759, 1993.

T. A. Doherty, N. Khorram, K. Sugimoto, D. Sheppard, P. Rosenthal, J. Y. Cho, A. Pham, M. Miller, M. Croft, and D. H. Broide. Alternaria induces stat6-dependent acute airway eosinophilia and epithelial fizz1 expression that promotes airway fibrosis and epithelial thickness. *The Journal of Immunology*, 188(6):2622–2629, 2012.

M. Ehsani, Y. Gao, S. Longo, and K. Ebrahimi. *Modern electric, hybrid electric, and fuel cell vehicles*. CRC press, 2018.

J. L. Feldman and K. Kam. Facing the challenge of mammalian neural microcircuits: taking a few breaths may help. *The Journal of physiology*, 593(1):3–23, 2015.

M. F. Gabriel, I. Postigo, C. T. Tomaz, and J. Martínez. Alternaria alternata allergens: markers of exposure, phylogeny and risk of fungi-induced respiratory allergy. *Environment international*, 89:71–80, 2016.

F. Gackière, L. Saliba, A. Baude, O. Bosler, and C. Strube. Ozone inhalation activates stress-responsive regions of the cns. *Journal of neurochemistry*, 117(6):961–972, 2011.

B. Gantt, J. Kelly, and J. Bash. Updating sea spray aerosol emissions in the community multiscale air quality (cmaq) model version 5.0. 2. *Geoscientific Model Development*, 8 (11):3733–3746, 2015.

U. Gehring, J. Heinrich, U. Krämer, V. Grote, M. Hochadel, D. Sugiri, M. Kraft, K. Rauchfuss, H. G. Eberwein, H.-E. Wichmann, et al. Long-term exposure to ambient air pollution and cardiopulmonary mortality in women. *Epidemiology*, 17(5):545–551, 2006.

S. Ghosh, S. A. Hoselton, G. P. Dorsam, and J. M. Schuh. Eosinophils in fungus-associated allergic pulmonary disease. *Frontiers in pharmacology*, 4:8, 2013.

D. R. Gold, G. Adamkiewicz, S. H. Arshad, J. C. Celedón, M. D. Chapman, G. L. Chew, D. N. Cook, A. Custovic, U. Gehring, J. E. Gern, et al. Niaid, niehs, nhlbi, and mcan workshop report: the indoor environment and childhood asthma—implications for home environmental intervention in asthma prevention and management. *Journal of Allergy and Clinical Immunology*, 140(4):933–949, 2017.

S. Gordon. Alternative activation of macrophages. *Nature reviews immunology*, 3(1):23, 2003.

H. Guo, A. Nenes, and R. J. Weber. The underappreciated role of nonvolatile cations in aerosol ammonium-sulfate molar ratios. *Atmospheric Chemistry and Physics*, 18(23): 17307–17323, 2018.

R.-B. Guo, P.-L. Sun, A.-P. Zhao, J. Gu, X. Ding, J. Qi, X.-L. Sun, and G. Hu. Chronic asthma results in cognitive dysfunction in immature mice. *Experimental neurology*, 247: 209–217, 2013.

M. Halonen, D. A. Stern, A. L. Wright, L. M. Taussig, and F. D. Martinez. Alternaria as a major allergen for asthma in children raised in a desert environment. *American journal of respiratory and critical care medicine*, 155(4):1356–1361, 1997.

P. Hari, T. Raunemaa, and A. Hautojärvi. The effects on forest growth of air pollution from energy production. *Atmospheric Environment (1967)*, 20(1):129–137, 1986.

S. V. Hering, R. C. Flagan, and S. K. Friedlander. Design and evaluation of new low-pressure impactor. i. *Environmental Science & Technology*, 12(6):667–673, 1978.

A. Hernandez, V. Donovan, Y. Y. Grinberg, A. Obenaus, and M. J. Carson. Differential detection of impact site versus rotational site injury by magnetic resonance imaging and microglial morphology in an unrestrained mild closed head injury model. *Journal of neurochemistry*, 136:18–28, 2016.

H. J. Heusinkveld, T. Wahle, A. Campbell, R. H. Westerink, L. Tran, H. Johnston, V. Stone, F. R. Cassee, and R. P. Schins. Neurodegenerative and neurological disorders by small inhaled particles. *Neurotoxicology*, 56:94–106, 2016.

G. Hoek, R. M. Krishnan, R. Beelen, A. Peters, B. Ostro, B. Brunekreef, and J. D. Kaufman. Long-term air pollution exposure and cardio-respiratory mortality: a review. *Environmental Health*, 12(1):43, 2013.

R. L. Jayaraj, E. A. Rodriguez, Y. Wang, and M. L. Block. Outdoor ambient air pollution and neurodegenerative diseases: the neuroinflammation hypothesis. *Current environmental health reports*, 4(2):166–179, 2017.

K. Ji, J. Miyauchi, and S. E. Tsirka. Microglia: an active player in the regulation of synaptic activity. *Neural plasticity*, 2013, 2013.

B. Jourdain and M. Legrand. Year-round records of bulk and size-segregated aerosol composition and hcl and hno3 levels in the dumont d'urville (coastal antarctica) atmosphere: Implications for sea-salt aerosol fractionation in the winter and summer. *Journal of Geophysical Research: Atmospheres*, 107(D22):ACH–20, 2002.

A. C. Just, R. O. Wright, J. Schwartz, B. A. Coull, A. A. Baccarelli, M. M. Tellez-Rojo, E. Moody, Y. Wang, A. Lyapustin, and I. Kloog. Using high-resolution satellite aerosol optical depth to estimate daily pm2. 5 geographical distribution in mexico city. *Environmental science & technology*, 49(14):8576–8584, 2015.

R. Kader, K. Kennedy, and J. M. Portnoy. Indoor environmental interventions and their effect on asthma outcomes. *Current allergy and asthma reports*, 18(3):17, 2018.

J. Kaur, P. Muttil, R. K. Verma, K. Kumar, A. B. Yadav, R. Sharma, and A. Misra. A hand-held apparatus for "nose-only" exposure of mice to inhalable microparticles as a dry powder inhalation targeting lung and airway macrophages. *european journal of pharmaceutical sciences*, 34(1):56–65, 2008.

A. J. Kean, R. A. Harley, D. Littlejohn, and G. R. Kendall. On-road measurement of ammonia and other motor vehicle exhaust emissions. *Environmental Science & Technology*, 34(17):3535–3539, 2000.

T. W. Kirchstetter, B. C. Singer, R. A. Harley, G. R. Kendall, and M. Traverse. Impact of california reformulated gasoline on motor vehicle emissions. 1. mass emission rates. *Environmental Science & Technology*, 33(2):318–328, 1999.

B. Klein, H. Mrowetz, J. Thalhamer, S. Scheiblhofer, R. Weiss, and L. Aigner. Allergy enhances neurogenesis and modulates microglial activation in the hippocampus. *Frontiers in cellular neuroscience*, 10:169, 2016.

A. P. Knutsen, R. K. Bush, J. G. Demain, D. W. Denning, A. Dixit, A. Fairs, P. A. Greenberger, B. Kariuki, H. Kita, V. P. Kurup, et al. Fungi and allergic lower respiratory tract diseases. *Journal of Allergy and Clinical Immunology*, 129(2):280–291, 2012.

M.-T. Ko, S.-C. Huang, and H.-Y. Kang. Establishment and characterization of an experimental mouse model of allergic rhinitis. *European Archives of Oto-Rhino-Laryngology*, 272(5):1149–1155, 2015.

P. R. S. Kodavanti, J. E. Royland, J. E. Richards, J. Besas, and R. C. MacPhail. Toluene effects on oxidative stress in brain regions of young-adult, middle-age, and senescent brown norway rats. *Toxicology and applied pharmacology*, 256(3):386–398, 2011.

U. P. Kodavanti, M. C. Schladweiler, A. D. Ledbetter, W. P. Watkinson, M. J. Campen, D. W. Winsett, J. R. Richards, K. M. Crissman, G. E. Hatch, and D. L. Costa. The spontaneously hypertensive rat as a model of human cardiovascular disease: evidence of exacerbated cardiopulmonary injury and oxidative stress from inhaled emission particulate matter. *Toxicology and applied pharmacology*, 164(3):250–263, 2000.

M. Kubo. Innate and adaptive type 2 immunity in lung allergic inflammation. *Immunological reviews*, 278(1):162–172, 2017.

V. Kumar, A. K. Abbas, N. Fausto, and J. C. Aster. *Robbins and Cotran pathologic basis of disease, professional edition e-book*. elsevier health sciences, 2014.

S. Levesque, T. Taetzsch, M. E. Lull, U. Kodavanti, K. Stadler, A. Wagner, J. A. Johnson, L. Duke, P. Kodavanti, M. J. Surace, et al. Diesel exhaust activates and primes microglia: air pollution, neuroinflammation, and regulation of dopaminergic neurotoxicity. *Environmental health perspectives*, 119(8):1149, 2011.

N. Li, M. Hao, R. F. Phalen, W. C. Hinds, and A. E. Nel. Particulate air pollutants and asthma: a paradigm for the role of oxidative stress in pm-induced adverse health effects. *Clinical Immunology*, 109(3):250–265, 2003.

N. Li, T. Xia, and A. E. Nel. The role of oxidative stress in ambient particulate matter-induced lung diseases and its implications in the toxicity of engineered nanoparticles. *Free Radical Biology and Medicine*, 44(9):1689–1699, 2008.

X.-J. Lin, E. Cortus, R. Zhang, S. Jiang, and A. Heber. Ammonia, hydrogen sulfide, carbon dioxide and particulate matter emissions from california high-rise layer houses. *Atmospheric Environment*, 46:81–91, 2012.

K. D. Linch, W. E. Miller, R. B. Althouse, D. W. Groce, and J. M. Hale. Surveillance of respirable crystalline silica dust using osha compliance data (1979–1995). *American journal of industrial medicine*, 34(6):547–558, 1998.

J. Y. Ljubimova, O. Braubach, R. Patil, A. Chiechi, J. Tang, A. Galstyan, E. S. Shatalova, M. T. Kleinman, K. L. Black, and E. Holler. Coarse particulate matter (pm 2.5–10) in los angeles basin air induces expression of inflammation and cancer biomarkers in rat brains. *Scientific reports*, 8(1):5708, 2018.

F. Maes, J. Coene, F. Goerlandt, P. De Meyer, A. Volckaert, D. Le Roy, J. VAN YPERSELE, and P. Marbaix. Emissions from co2, so2 and nox from ships (ecosonos). 2007.

Q. G. Malloy, S. Nakao, L. Qi, R. Austin, C. Stothers, H. Hagino, and D. R. Cocker III. Real-time aerosol density determination utilizing a modified scanning mobility particle sizer—aerosol particle mass analyzer system. *Aerosol Science and Technology*, 43(7): 673–678, 2009.

J. L. Mauderly. Respiration of f344 rats in nose-only inhalation exposure tubes. *Journal of Applied Toxicology*, 6(1):25–30, 1986.

K. May. The collison nebulizer: description, performance and application. *Journal of Aerosol Science*, 4(3):235–243, 1973.

R. L. McCormick, J. D. Ross, and M. S. Graboski. Effect of several oxygenates on regulated emissions from heavy-duty diesel engines. *Environmental Science & Technology*, 31(4): 1144–1150, 1997.

J. D. McDonald, M. Doyle-Eisele, M. J. Campen, J. Seagrave, T. Holmes, A. Lund, J. D. Surratt, J. H. Seinfeld, A. C. Rohr, and E. M. Knipping. Cardiopulmonary response to inhalation of biogenic secondary organic aerosol. *Inhalation toxicology*, 22(3):253–265, 2010.

M. R. Miller, J. B. Raftis, J. P. Langrish, S. G. McLean, P. Samutrtai, S. P. Connell, S. Wilson, A. T. Vesey, P. H. Fokkens, A. J. F. Boere, et al. Inhaled nanoparticles accumulate at sites of vascular disease. *ACS nano*, 11(5):4542–4552, 2017.

C. S. Moore, A. R. Ase, A. Kinsara, V. T. Rao, M. Michell-Robinson, S. Y. Leong, O. Butovsky, S. K. Ludwin, P. Séguéla, A. Bar-Or, et al. P2y12 expression and function in alternatively activated human microglia. *Neurology-Neuroimmunology Neuroinflammation*, 2(2):e80, 2015.

G. W. Mulholland, M. K. Donnelly, C. R. Hagwood, S. R. Kukuck, V. A. Hackley, and D. Y. Pui. Measurement of 100 nm and 60 nm particle standards by differential mobility analysis. *Journal of research of the National Institute of Standards and Technology*, 111 (4):257, 2006.

C. L. Mumaw, S. Levesque, C. McGraw, S. Robertson, S. Lucas, J. E. Stafflinger, M. J. Campen, P. Hall, J. P. Norenberg, T. Anderson, et al. Microglial priming through the lung–brain axis: the role of air pollution–induced circulating factors. *The FASEB Journal*, 30(5):1880–1891, 2016.

M. Munder, K. Eichmann, and M. Modolell. Alternative metabolic states in murine macrophages reflected by the nitric oxide synthase/arginase balance: competitive regulation by cd4+ t cells correlates with th1/th2 phenotype. *The Journal of Immunology*, 160(11):5347–5354, 1998.

F. Nomura, S. Akashi, Y. Sakao, S. Sato, T. Kawai, M. Matsumoto, K. Nakanishi, M. Kimoto, K. Miyake, K. Takeda, et al. Cutting edge: endotoxin tolerance in mouse peritoneal macrophages correlates with down-regulation of surface toll-like receptor 4 expression. *The Journal of Immunology*, 164(7):3476–3479, 2000.

K. Onishi, Y. Kurosaki, S. Otani, A. Yoshida, N. Sugimoto, and Y. Kurozawa. Atmospheric transport route determines components of asian dust and health effects in japan. *Atmospheric Environment*, 49:94–102, 2012.

J. Ovadnevaite, D. Ceburnis, M. Canagaratna, H. Berresheim, J. Bialek, G. Martucci, D. R. Worsnop, and C. O'Dowd. On the effect of wind speed on submicron sea salt mass concentrations and source fluxes. *Journal of Geophysical Research: Atmospheres*, 117 (D16), 2012.

N. Panwar, S. Kaushik, and S. Kothari. Role of renewable energy sources in environmental protection: a review. *Renewable and Sustainable Energy Reviews*, 15(3):1513–1524, 2011.

O. M. Pena, J. Pistolic, D. Raj, C. D. Fjell, and R. E. Hancock. Endotoxin tolerance represents a distinctive state of alternative polarization (m2) in human mononuclear cells. *The Journal of Immunology*, page 1001952, 2011.

X. Peng, A. M. Madany, J. C. Jang, J. M. Valdez, Z. Rivas, A. C. Burr, Y. Y. Grinberg, T. M. Nordgren, M. G. Nair, D. Cocker, et al. Continuous inhalation exposure to fungal allergen particulates induces lung inflammation while reducing innate immune molecule expression in the brainstem. *ASN neuro*, 10:1759091418782304, 2018.

V. H. Perry. Contribution of systemic inflammation to chronic neurodegeneration. *Acta neuropathologica*, 120(3):277–286, 2010.

C. Ploix, R. I. Zuberi, F.-T. Liu, M. J. Carson, and D. D. Lo. Induction and effector phase of allergic lung inflammation is independent of ccl21/ccl19 and lt-beta. *International journal of medical sciences*, 6(2):85, 2009.

C. C. Ploix, S. Noor, J. Crane, K. Masek, W. Carter, D. D. Lo, E. H. Wilson, and M. J. Carson. Cns-derived ccl21 is both sufficient to drive homeostatic cd4+ t cell proliferation and necessary for efficient cd4+ t cell migration into the cns parenchyma following toxoplasma gondii infection. *Brain, behavior, and immunity*, 25(5):883–896, 2011.

J. A. Poole, N. E. Alexis, C. Parks, A. K. MacInnes, M. J. Gentry-Nielsen, P. D. Fey, L. Larsson, D. Allen-Gipson, S. G. Von Essen, and D. J. Romberger. Repetitive organic dust exposure in vitro impairs macrophage differentiation and function. *Journal of Allergy and Clinical Immunology*, 122(2):375–382, 2008.

J. A. Poole, G. M. Thiele, N. E. Alexis, A. M. Burrell, C. Parks, and D. J. Romberger. Organic dust exposure alters monocyte-derived dendritic cell differentiation and maturation. *American Journal of Physiology-Lung Cellular and Molecular Physiology*, 297(4): L767–L776, 2009.

J. A. Poole, G. P. Dooley, R. Saito, A. M. Burrell, K. L. Bailey, D. J. Romberger, J. Mehaffy, and S. J. Reynolds. Muramic acid, endotoxin, 3-hydroxy fatty acids, and ergosterol content explain monocyte and epithelial cell inflammatory responses to agricultural dusts. *Journal of Toxicology and Environmental Health, Part A*, 73(10):684–700, 2010.

C. A. Pope III and D. W. Dockery. Health effects of fine particulate air pollution: lines that connect. *Journal of the air & waste management association*, 56(6):709–742, 2006.

C. A. Pope III, R. T. Burnett, M. J. Thun, E. E. Calle, D. Krewski, K. Ito, and G. D. Thurston. Lung cancer, cardiopulmonary mortality, and long-term exposure to fine particulate air pollution. *Jama*, 287(9):1132–1141, 2002.

O. Raaschou-Nielsen, Z. J. Andersen, R. Beelen, E. Samoli, M. Stafoggia, G. Weinmayr, B. Hoffmann, P. Fischer, M. J. Nieuwenhuijsen, B. Brunekreef, et al. Air pollution and lung cancer incidence in 17 european cohorts: prospective analyses from the european study of cohorts for air pollution effects (escape). *The lancet oncology*, 14(9):813–822, 2013.

R. Rajaiah, D. J. Perkins, S. K. Polumuri, A. Zhao, A. D. Keegan, and S. N. Vogel. Dissociation of endotoxin tolerance and differentiation of alternatively activated macrophages. *The Journal of Immunology*, page 1202407, 2013.

S. Rappaport, M. Goldberg, P. Susi, and R. F. Herrick. Excessive exposure to silica in the us construction industry. *Annals of Occupational Hygiene*, 47(2):111–122, 2003.

D. Romberger, V. Bodlak, S. Von Essen, T. Mathisen, and T. Wyatt. Hog barn dust extract stimulates il-8 and il-6 release in human bronchial epithelial cells via pkc activation. *Journal of Applied Physiology*, 93(1):289–296, 2002.

M. D. Rosenbaum, S. VandeWoude, and T. E. Johnson. Effects of cage-change frequency and bedding volume on mice and their microenvironment. *Journal of the American Association for Laboratory Animal Science*, 48(6):763–773, 2009.

C. Roy and L. Pitt. Infectious disease aerobiology. In *Biodefense Research Methodology and Animal Models*. Taylor & Francis Group, 2006.

C. J. Roy, M. Hale, J. M. Hartings, L. Pitt, and S. Duniho. Impact of inhalation exposure modality and particle size on the respiratory deposition of ricin in balb/c mice. *Inhalation toxicology*, 15(6):619–638, 2003.

G. Sancini, F. Farina, C. Battaglia, I. Cifola, E. Mangano, P. Mantecca, M. Camatini, and P. Palestini. Health risk assessment for air pollutants: alterations in lung and cardiac gene expression in mice exposed to milano winter fine particulate matter (pm2. 5). *PLoS One*, 9(10):e109685, 2014.

H. Sarlus, X. Wang, A. Cedazo-Minguez, M. Schultzberg, and M. Oprica. Chronic airway-induced allergy in mice modifies gene expression in the brain toward insulin resistance and inflammatory responses. *Journal of neuroinflammation*, 10(1):866, 2013.

D. P. Schafer, E. K. Lehrman, and B. Stevens. The "quad-partite" synapse: Microglia-synapse interactions in the developing and mature cns. *Glia*, 61(1):24–36, 2013.

C. D. Schmid, B. Melchior, K. Masek, S. S. Puntambekar, P. E. Danielson, D. D. Lo, J. Gregor Sutcliffe, and M. J. Carson. Differential gene expression in lps/ifnγ activated microglia and macrophages: in vitro versus in vivo. *Journal of neurochemistry*, 109: 117–125, 2009.

D. Smith and P. Španěl. Selected ion flow tube mass spectrometry (sift-ms) for on-line trace gas analysis. *Mass spectrometry reviews*, 24(5):661–700, 2005.

J. C. Smith, A. P. Abdala, A. Borgmann, I. A. Rybak, and J. F. Paton. Brainstem respiratory networks: building blocks and microcircuits. *Trends in neurosciences*, 36(3): 152–162, 2013.

G. Snider, C. L. Weagle, K. K. Murdymootoo, A. Ring, Y. Ritchie, E. Stone, A. Walsh, C. Akoshile, N. X. Anh, R. Balasubramanian, et al. Variation in global chemical composition of pm 2.5: emerging results from spartan. *Atmospheric Chemistry and Physics*, 16 (15):9629–9653, 2016.

M. Sutton, U. Dragosits, Y. Tang, and D. Fowler. Ammonia emissions from non-agricultural sources in the uk. *Atmospheric Environment*, 34(6):855–869, 2000.

C. Traidl-Hoffmann, A. Kasche, A. Menzel, T. Jakob, M. Thiel, J. Ring, and H. Behrendt. Impact of pollen on human health: more than allergen carriers? *International archives of allergy and immunology*, 131(1):1–13, 2003.

M.-È. Tremblay and A. K. Majewska. A role for microglia in synaptic plasticity? *Communicative & integrative biology*, 4(2):220–222, 2011.

G. Velthof, C. Van Bruggen, C. Groenestein, B. De Haan, M. Hoogeveen, and J. Huijsmans. A model for inventory of ammonia emissions from agriculture in the netherlands. *Atmospheric environment*, 46:248–255, 2012.

A. Vianello, M. Caminati, M. Crivellaro, R. El Mazloum, R. Snenghi, M. Schiappoli, A. Dama, A. Rossi, G. Festi, M. R. Marchi, et al. Fatal asthma; is it still an epidemic? *World Allergy Organization Journal*, 9(1):42, 2016.

E. Vignati, M. Facchini, M. Rinaldi, C. Scannell, D. Ceburnis, J. Sciare, M. Kanakidou, S. Myriokefalitakis, F. Dentener, and C. O'Dowd. Global scale emission and distribution of sea-spray aerosol: Sea-salt and organic enrichment. *Atmospheric Environment*, 44(5): 670–677, 2010.

S. Vutukuru and D. Dabdub. Modeling the effects of ship emissions on coastal air quality: A case study of southern california. *Atmospheric Environment*, 42(16):3751–3764, 2008.

S. C. Wang and R. C. Flagan. Scanning electrical mobility spectrometer. *Aerosol Science and Technology*, 13(2):230–240, 1990.

M.-X. Xia, X. Ding, J. Qi, J. Gu, G. Hu, and X.-L. Sun. Inhaled budesonide protects against chronic asthma-induced neuroinflammation in mouse brain. *Journal of neuroimmunology*, 273(1-2):53–57, 2014.

R. Yamasaki, T. Fujii, B. Wang, K. Masaki, M. A. Kido, M. Yoshida, T. Matsushita, and J.-i. Kira. Allergic inflammation leads to neuropathic pain via glial cell activation. *Journal of Neuroscience*, 36(47):11929–11945, 2016.

J. Ye, S. Salehi, M. L. North, A. M. Portelli, C.-W. Chow, and A. W. Chan. Development of a novel simulation reactor for chronic exposure to atmospheric particulate matter. *Scientific reports*, 7:42317, 2017.

D. E. Young, H. Kim, C. Parworth, S. Zhou, X. Zhang, C. D. Cappa, R. Seco, S. Kim, and Q. Zhang. Influences of emission sources and meteorology on aerosol chemistry in a polluted urban environment: results from discover-aq california. *Atmospheric Chemistry and Physics*, 16(8):5427–5451, 2016.

R. Zhang, J. Jing, J. Tao, S.-C. Hsu, G. Wang, J. Cao, C. S. L. Lee, L. Zhu, Z. Chen, Y. Zhao, et al. Chemical characterization and source apportionment of pm 2.5 in beijing: seasonal perspective. *Atmospheric Chemistry and Physics*, 13(14):7053–7074, 2013.

W. Zhou, S. Toki, J. Zhang, K. Goleniewksa, D. C. Newcomb, J. Y. Cephus, D. E. Dulek, M. H. Bloodworth, M. T. Stier, V. Polosuhkin, et al. Prostaglandin i2 signaling and inhibition of group 2 innate lymphoid cell responses. *American journal of respiratory and critical care medicine*, 193(1):31–42, 2016.

L. H. Ziska and F. A. Caulfield. Rising co2 and pollen production of common ragweed (ambrosia artemisiifolia l.), a known allergy-inducing species: implications for public health. *Functional Plant Biology*, 27(10):893–898, 2000.

T. Zrzavy, S. Hametner, I. Wimmer, O. Butovsky, H. L. Weiner, and H. Lassmann. Loss of 'homeostatic'microglia and patterns of their activation in active multiple sclerosis. *Brain*, 140(7):1900–1913, 2017.